

POLITECNICO DI TORINO

Master's Degree in Mechatronic Engineering



**Politecnico
di Torino**

Master's Degree Thesis

SimRod E-Powertrain Modelling and Identification

Supervisors

Prof. Stefano Alberto Malan

Dr. Eng. Bart Forrier

Candidate

Giovanni D'Eredità

302431

April 2024

Abstract

Nowadays, mechatronic systems modelling and identification methods are going towards more challenging and complex scenarios. Practically, model based testing (MBT) approaches are mostly employed in order to face several kind of requirements and features of specific systems designs. Moreover, generally, the development of these techniques allows to move to new testing methodologies, such as X-in-the-Loop (XiL).

Moving to the automotive world and, specifically, to modern electric vehicle (EV) powertrain systems, advanced and complex methods are continuously designed and developed for centering goals in terms of safety and production requirements. Indeed, high reliability with a reduced amount of costs, efforts and time are increasingly widespread requirements. Physical vehicle prototypes testing is an expensive and time consuming process and the instrumentation needed for multi-physical acquisitions is not always easy to implement in on-road test scenarios so that, obviously, virtual approaches are becoming increasingly preferable.

This thesis project, carried out with the collaboration of Politecnico di Torino and Siemens Digital Industries Software (DISW), presents a specific Model based approach for the development of a software simulation model of an EV powertrain test setup in order to reproduce specific behaviors of the real test setup in a virtual environment.

This classical powertrain test setup is upgraded for the implementation of an XiL setup preserving all the safety features of the starting test bench.

The main purpose of this thesis project, indeed, is starting the creation of a reliable predictive model capable to perform a preventive system simulation before the real commission of advanced test campaigns. In order to get this objective, the experimental activity starts with the general analysis of the test setup, then it moves to the implementation of a test/measurements campaign exploited for the latter identification and/or modelling activity. The identified test setup features are implemented on the software model and, at the end, simulated results are validated.

Table of Contents

Abstract	ii
1 Introduction	1
1.1 XiL testing	1
1.2 SimRod E-Powertrain system	3
1.3 Goal of the thesis	5
1.4 Thesis outline	6
2 Multi-physical System-level Modelling	8
2.1 Model prediction	8
2.2 Modelling approach	9
2.2.1 Port-based (bond graph) modelling	10
2.2.2 SimRod E-Powertrain setup model design	11
2.3 Operating modes of the test setup	12
3 Model description	15
3.1 System inputs	16
3.1.1 SuT Motor Throttle	16
3.1.2 Load Motors Current	18
3.2 System outputs	20
3.2.1 Mechanical domain outputs	20
3.2.2 Electrical domain outputs	20
3.3 System Parameters	21
3.3.1 Mechanical domain parameters	21
3.3.2 Electrical domain parameters	21
3.3.3 Signal domain - SuT Inverter parameters	22
4 Test campaign definition and instrumentation	23
4.1 Test profiles	23
4.1.1 Test Profile 11 - TP11	24
4.1.2 Test Profile 14 - TP14	27
4.2 Instrumentation	28

4.2.1	Setup changes	31
5	Test campaign implementation and Model identification	33
5.1	Test campaign	33
5.2	System Mapping	35
5.2.1	SuT Motor Map	37
5.2.2	Load Motors Maps	39
5.2.3	Secondary results from System Mapping	44
5.3	Friction and Inertia Identification	46
5.3.1	SuT Axle Friction Model	48
5.3.2	System Moments of Inertia	54
5.4	Mechanical Stiffness of the Couplings Identification	59
5.5	Electrical Power Flow Mapping and Resistance Identification	65
5.6	SuT Inverter Transient Analysis	73
6	Model validation	81
6.1	TP11 Simulation	83
6.1.1	TP07 Validation	88
6.1.2	Simulation Time Performances	93
7	Conclusions	95
A	SimRod E-Powertrain test setup <i>Amesim</i> draft model	98
A.1	SuT Motor+Inverter <i>Supercomponent</i>	100
A.2	Load Motor <i>Supercomponent</i>	101
	List of Tables	105
	List of Figures	106
	Bibliography	109
	Acknowledgements	110

Chapter 1

Introduction

1.1 XiL testing

The automotive systems design is becoming increasingly complex and technologically advanced. For this reason, new challenges are faced and new ways for improving these methodologies are developed. New multi-actuated electric vehicles and new automated driving technologies need a relevant number of complex experimental processes and a relevant number of road tests.

Siemens DISW commitment in the testing field and, specifically for what concerns this thesis topic, in the automotive system testing is to develop and propose new and advanced solutions for costumers accordingly to the technological environment requests. In response to the main market drivers which are energy efficiency, safety and performance, many products now include controllers and electronic components that help optimize the product performance or refine its brand character. The widespread use of advanced control systems increases the complexity of product development, simulation and testing [1]. To accelerate system testing at any development stage of the model-based development process, *Simcenter* (the software tools proposed by Siemens DISW) extends its portfolio with model-based system testing capabilities [1].

The conventional and classical testing approach consists in trying to implement on vehicles a specific instrumentation made of sensors, on-board processors and electronic control units for performing real and safe road tests. Of course, this process can be time consuming and extremely expensive. This last important cause is suggesting researchers to follow different and more efficient prototyping and validation routes in order to reduce time and costs efforts. Traditionally, the development of vehicles and automotive systems is successively implementing

Software-in-the-Loop (SiL), Model-in-the-Loop (MiL), and Hardware-in-the-Loop (HiL) tools, which together can be concisely referred as "X-in-the-Loop" or "XiL", [2]. A general overview is given in fig.1.1.

An XiL setup imposes realistic test scenarios onto the System under Test (SuT) by emulating the environment(s) in which the latter will operate during its operational life, [3]. The benefits of XiL testing include early performance assessments on vehicle-level, laboratory instrumentation capabilities and extensive what-if testing possibilities, [4]. A main hurdle is the intrinsically high complexity, causing significant investment costs and safety concerns due to possibly unstable closed-loop model-driven operation[3].

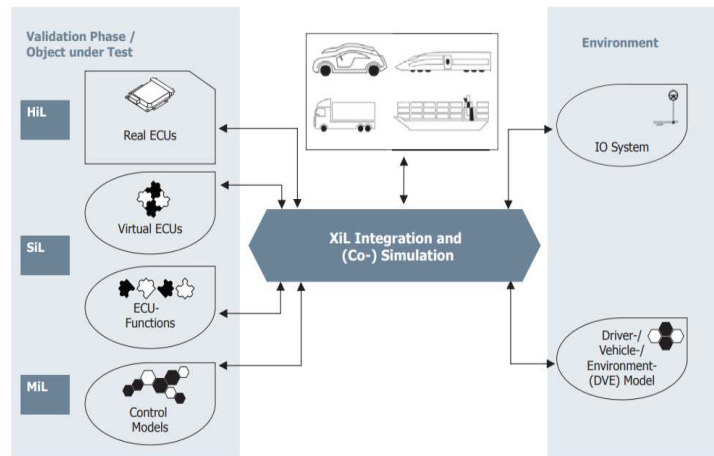


Figure 1.1: XiL in embedded software and system development [5].

Generally, it is possible to state that these XiL solutions can speed-up and improve the sub-systems testing and validation in a lab.

In this thesis activity, these XiL test setups were implemented by exploiting crucial tools such as *Simcenter Testlab* RT and simulators using Executable Digital Twins (xDT). *Simcenter Testlab* RT provides a software and hardware real-time environment that allows a physical system to be connected to virtual representations (aka xDTs) of its operating environments. For example, a physical braking system or a physical powertrain system can be tested as if they were operating in any of the vehicle variants it will be used in. The XiL approach thus shifts

the physical system test program earlier in the development cycle by reducing dependency on the availability of other physical systems. It also supports the evaluation of many system-level variants for a wide range of operating loads. The XiL tests will reveal potential issues far earlier in the overall system development program for the system-under test [6].

Of course, it is also possible to state that xDTs have a central role in these implemented solutions: they try to emulate, practically, what happens in the real environment and, specifically in this research case, they replicate the driver behavior, the environment external conditions, the road profile etc.

The digital twin is inclusive, holistic (in the sense of consistently representing all available data) and dynamic as it will continuously be updated along the product lifecycle and enriched with new datasets and models as these become available [7].

1.2 SimRod E-Powertrain system

This section presents a brief introduction and description of the test setup system whose model is the central protagonist of the thesis project. The system is reported in the figure 1.2.

The SuT is the full E-powertrain of the commercially available battery electric *Kyburz DXP* delivery vehicle [3]. Because its layout is the same as that of the SimRod sports car [4], the setup is called the SimRod E-powertrain test setup.

The *SimRod E-Powertrain SuT* is composed by a main motor and inverter. These latter components are connected through a gearbox and a differential to the two system drive shafts (L,R) which are both coupled to a brushless DC load motor. The SuT inverter and the two load motors are fed by a power supply. The low nominal voltage levels, of 24 V DC and 15 V AC, and rated motor power (0.9 kW continuous, 3.5 kW peak) of this SuT contribute to a high inherent safety level [3]. The brushless DC load motors with integrated inverters are selected to operate at 24 V DC as well. Thus, no DC/DC converter is required and a safe DC bus voltage level is maintained, at the expense of not covering the full operational envelope of the SuT [3]. The SuT motor is speed controlled, the load motors are current controlled. In view of XiL testing with battery emulation, the DC power supply supports voltage setpoint tracking in a range from 12 to 30 V DC [3]. Finally, the system is coupled through a real time platform (RT) to an executable Digital Twin (xDT) for operating in XiL mode.

Fig.1.3 also shows the multi-physical signal conditioning and data acquisition system (SCADAS) and the real time (RT) platform.

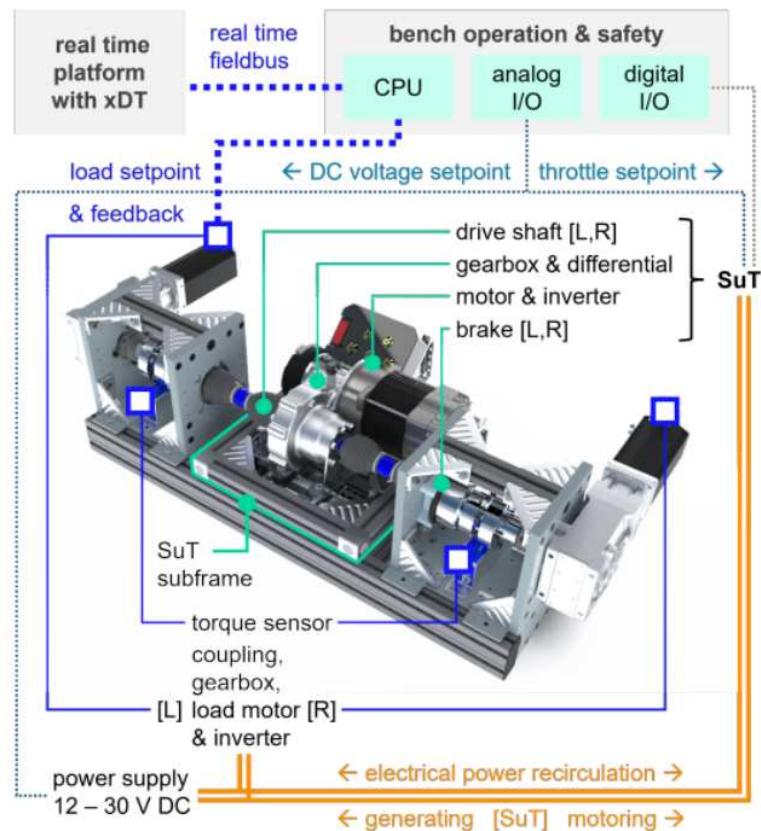


Figure 1.2: SimRod E-powertrain test setup: overview of the mechanical, electrical and communication layout [3].

To validate research linked to NVH analysis, e.g., the effect of electro-magnetic forces on vibration responses, the SuT is ideally mounted like it is in the vehicle and otherwise vibration-isolated from the rest of the setup. The SuT is therefore mounted onto the SuT subframe via the bushings of the DXP vehicle, and isolated from the load motors by flexible shaft couplings. Another set of rubber mounts isolates the SuT subframe from its support structure. The latter is integrated, via a third set of rubber mounts, into the complete setup of Fig.1.3 [3].

NVH analysis, indeed, even if it is not a treated thesis topic, is one of the main analysed features of Siemens DISW research: the NVH and acoustic performance of a vehicle strongly impacts the driving experience and hence the perception of quality. Impacted by regulations and low-emission and zero-emission strategies, car manufacturers and suppliers seek solutions to design for optimal NVH comfort

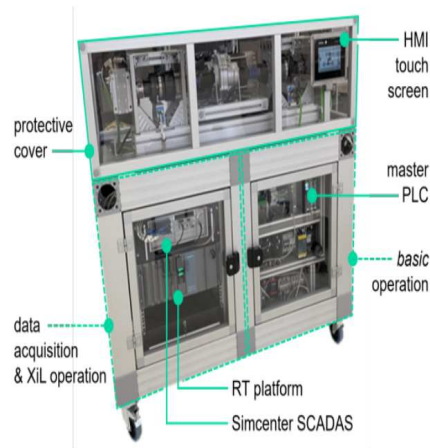


Figure 1.3: SimRod E-powertrain test setup: complete assembly - including permanent equipment only [3].

to adhere to their brand identity [8]. To design for premium NVH and acoustic quality, an integrated approach is required. Whether dealing with interior or exterior acoustics, intake or exhaust noise, engine acoustics, brake noise, noises from auxiliaries such as HVAC, batteries or inverters, or noise related to system integration, Siemens Digital Industries Software provides solutions for all stages of the development process [8].

At the end, the main novelty of this test setup is the possibility to switch between two different operating modes: the basic mode and the advanced one (XiL), however, they will be better discussed later.

1.3 Goal of the thesis

This thesis research is intended to start the building-up of the predictive simulation model of the SimRod E-powertrain system by employing a specific *Bond graph* (BG) modelling approach via *SimCenter Amesim* software. This model needs to be capable to replicate the physical setup behavior in terms of mechanical and electrical power flows responses with respect to specific input setpoints.

The offline simulation model is a needed setup integration for the implementation of the XiL operating mode.

Indeed, the main simulation role is the de-risking of closed-loop real-time testing when applying realistic test scenarios through the xDT and the RT platform on the SuT when the system is operating in XiL mode.

In order to get this objective, the following path is followed:

1. **Modelling methodologies definition** → A modelling approach is defined and every main model component modelling and identification is established in order to follow a general procedure for the replication of the test bench on the software side.
2. **Test scenarios definition** → Defining specific test scenarios to be implemented in the basic mode test setup in order to exploit the acquired results for the identification of the several investigated setup features.
3. **Test campaign and instrumentation definition** → Definition and commission of the test campaign and definition of the instrumentation needed for the acquisition of the related data from the real test setup.
4. **Data elaboration and identification** → Signals post-processing and data elaboration for modelling purposes.
5. **Model elaboration** → Building up of the model with related identified features and parameters.
6. **Model validation** → Validation of the model results.

1.4 Thesis outline

Here, a brief introduction of the general outline of this document is presented. The chapters' content is briefly described in the following lines:

- **1 Introduction** → General introduction to the research activity and to the test setup.
- **2 Multi-physical System-level Modelling** → Theoretical overview of the modelling methodologies employed in the thesis experimental project.
- **3 Model inputs, outputs and parameters** → Description of the reference quantities involved in the research work and introduction to the designed and employed test profiles.
- **4 Test campaign for model identification** → Description of the instrumentation setup and description of the practical test sessions. Moreover, description of the identification process for the several analysed features.

- **5 Model validation** → Report and comment of the validation results.
- **6 Conclusions** → General comment of the research activity and comments on the obtained results.
- **Appendix A** → *SimCenter Amesim* model detailed description.

Chapter 2

Multi-physical System-level Modelling

2.1 Model prediction

The *Simcenter Amesim* software model replication of the SimRod E-Powertrain SuT has been generated from the overall purpose to emulate the real system responses given specific inputs, in particular this research project mainly focuses on mechanical and electrical power responses.

Previously, Model Based Testing (MBT) has been mentioned, it is important to have a clear idea of these methodologies in order to understand the starting point of this reported activity.

The Model Based System Testing (MBST) is defined as the discipline combining physical testing and simulation models with the aim to study, identify, validate and improve the behavior of multiphysical and mechatronic systems. It deals not only with structural tests and/or 3D simulation models, but also with multiphysical systems and 1D simulation models. MBST can be divided into 3 categories: “Testing for Simulation”, “Simulation for Testing” and “Testing with Simulation”, with the first two being cases where test and simulation are decoupled, and in the latter, test and simulation are tightly coupled. The first category is an expansion of one of the main roles in modal analysis - obtaining test parameters to create and/or improve simulation models, but in this case also including multiphysics systems. It also involves the use of test post-processing tools with simulation data. The “Simulation for Testing” category is related to the use of simulation models to improve or accelerate the testing process - this includes well known procedures, such as optimal sensor and excitation placement, but contains also more recent

methodologies, such as virtual testing or human-in-the-loop applications. Finally, the last category contains the cases in which test and simulation are tightly coupled. Such is the case with hardware-in the-loop, system-in-the-loop, virtual sensing and hybrid testing, mostly involving real-time processing capabilities [9]. Fig.2.1 shows the MBT diagram.

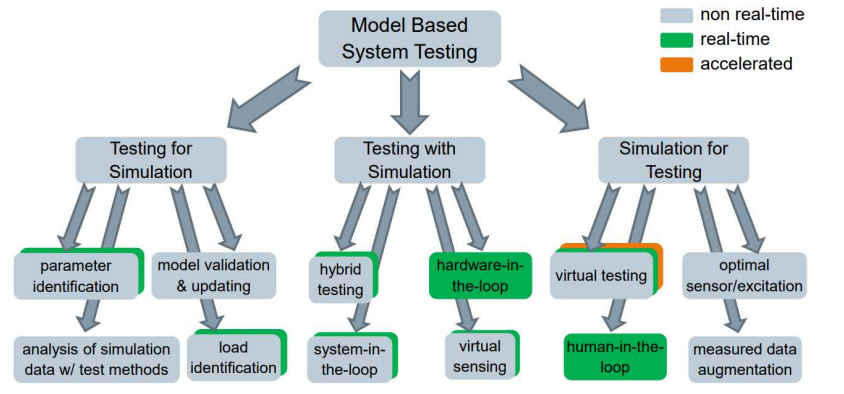


Figure 2.1: Model Based System Testing application tree [9].

This powertrain simulation model, of course, in its future perspective is employed for the development of the XiL mode of the SimRod E-Powertrain SuT. Indeed, the research work, subject of this experimental thesis, involves test and simulation phases.

The main capability and utility of the software model pretends to be the reliable prediction of the test setup outputs in both transient and steady-state behaviors. These simulations are then exploited for estimating several features which can be encountered during real test on the physical SuT, for avoiding any risks and for predicting possible anomalies.

Besides, SuT Power flow is the protagonist of this work and, for this reason, the main investigated SuT features and variables/parameters are related to rotating speed signals, torque signals, current and voltage signals.

2.2 Modelling approach

The routes which can be followed for modeling a mechatronic system can be different and each of them is characterised by some peculiarities.

For example, input-output-based method is mostly employed in specific environment in which the involved variables are connected to each other in a defined direction: each modeling component has an input signal and a related output signal. Indeed, input-output-based modelling is common practice in the field of control engineering [10].

Instead, bond graph's reasoning method is completely different: it follows the particular energy relationships between components and the general power flow of the analysed system.

In the previous section, it was explicitly mentioned that the model replication's purpose is mostly to emulate the power behavior inside the SuT so that the bond graph approach is surely the most suited method for this research case.

2.2.1 Port-based (bond graph) modelling

As it has been previously stated, the port-based modelling approach is particularly interesting for mechatronic system modelling [10], and it has been surely very appropriate for this activity.

It is argued that port-based modeling is ideally suited for the description of the energetic part of a multidomain, sometimes also called multi-physics, system or subsystem. This means that the approach by definition deals with mechatronic systems and even beyond those [11].

Port-based physical system modeling aims at providing insight, not only in the behavior of systems that an engineer working on multidisciplinary problems wishes to design, build, troubleshoot or modify, but also in the behavior of the environment of that system [11].

Complex system dynamic behaviour can be studied as the result of energetic interactions between elementary components. These energetic interactions are described by a component's static relations between so-called *effort*(e) or *flow*(f) variables [10]. The instantaneous power is nothing else than the product between these two kind of variables so that they are labeled as *power* variables. The behavior of a single-domain component is defined by a relationship between effort or flow variables at the ports and their related time-integrated values, called *momentum*(p) and *displacement*(q), labeled as *energy* variables.

The word "bond" indicates the direct connection and communication between different ports: it is possible to deal with a *power* bond or with an *active* bond. The first one states that there is a specific power flow between the related ports,

the latter one denotes an external influence on a component which does not change the power flow, but it works as an input for tuning some component parameters.

Elements in port-based modelling approach can be classified as:

- **Elementary 1-port elements** → dissipate, store or release energy. *Resistors* are characterized by a static relation between effort and flow ($e = R \times f$), *Compliance* elements rely effort to displacement ($e = q/C$) and *Inertia* elements rely momentum to flow ($p = I \times f$). Linear cases are indicated between brackets, but non-linear relationships are also possible. Effort and flow sources serve to describe idealized boundary conditions [10];
- **Elementary 2-port elements** → describe lossless energy transfer between two ports ($e_1 \times f_1 = e_2 \times f_2$) and possibly in different physical domains. In doing so, a *Transformer* further expresses the static relation between two effort variables ($e_1 = T \times e_2$) and a *Gyrator* relates the effort at one port to the flow at the other port ($e_1 = G \times f_2$) [10].

Junctions between more than two elements are classified as:

- **0-junctions** → *flow junctions* enforce the effort at their three ports to be equal and the algebraic sum of the three flows to be zero [10];
- **1-junctions** → *effort junction* enforce the flow at their three ports to be equal and the algebraic sum of the three efforts to be zero [10].

Besides, there are some specific component sources, $e(t)$ effort sources and $f(t)$ flow sources that are needed by the user to impose certain input variables. For energy-storing two-port elements, the preferred causality is integral: the output of a compliance element is the effort (specified as function of the time-integrated flow input) and the output of an inertia element is the flow (specified as function of the time-integrated effort input) [10].

Starting from this theoretical background approach, the practical modelling of the system consists in a graphic diagram (which can be obtained by specific softwares such as *Simcenter Amesim*) that corresponds to a related bond graph which states the specific kind of interconnection between each elementary component.

The causality may be assigned automatically, defining a set of state variables (for which initial values have to be assumed) [10].

System equations are derived automatically in first-order state space form [12].

2.2.2 SimRod E-Powertrain setup model design

In the following lines a more detailed description of the starting model design is presented. By exploiting the just introduced theoretical modeling approach, it was

clearly crucial to understand how to define the different system components and to have an idea of the energetic relations between them. The fig.2.2 shows a synthesis of the starting model idea.

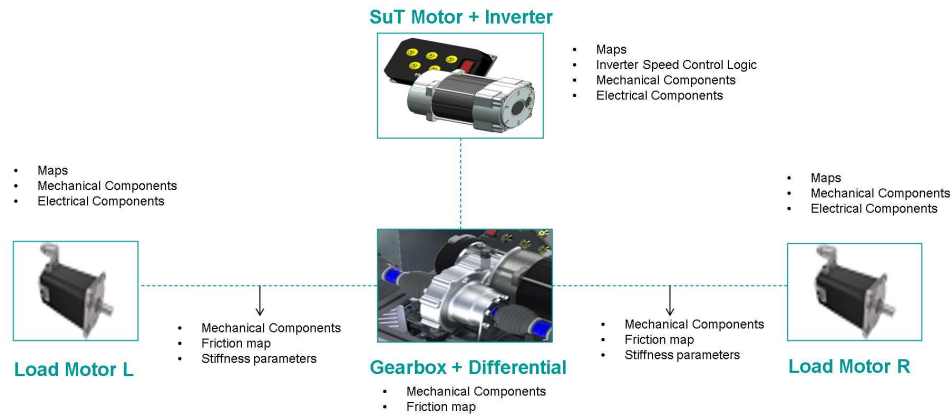


Figure 2.2: SimRod E-powertrain model starting design scheme.

The four main subsystems are the SuT motor (with the inverter), the two load motors and, finally, the gearbox with the differential. Each of them is emulated by exploiting specific *elementary elements*, mainly belonging to mechanical and electrical domain. In some regions, specific *1-D* or *2-D maps* are employed to reproduce some peculiar setup responses (mainly to relate some variables, e.g. speed to related torque for the friction maps, or to turn some specific input profiles into system variables). Plus there are, of course, modeled control logic which has been built up with signal domain components.

Moreover, in **Appendix A** the final obtained software model is presented in a detailed way and it corresponds exactly to the bond graph representation of the system.

2.3 Operating modes of the test setup

This section is primary for the comprehension of the real action of the test setup. Indeed, as previously mentioned, the real test setup is designed with the possibility to switch between two operating modes: the basic and the advanced (XiL).

The model has been entirely developed considering acquired data from testing SuT in its basic operating mode (the test campaign was entirely commissioned for basic test setup operations) because of the fact that it is intended to be an integration of the entire system in order to develop and improve the advanced

mode. An explanation of the two modes is given in the following lines.

A basic test scenario is pre-determined by a throttle setpoint table, and two (possibly but not necessarily identical) phase current setpoint tables for the load motors [3]. A scheme is presented in fig.2.3. This working mode is now shortly exemplified by employing also a basic scenario showed in fig.2.4 characterised by SuT throttle full acceleration and partial/neutral deceleration, and by deactivated load motors current setpoints.

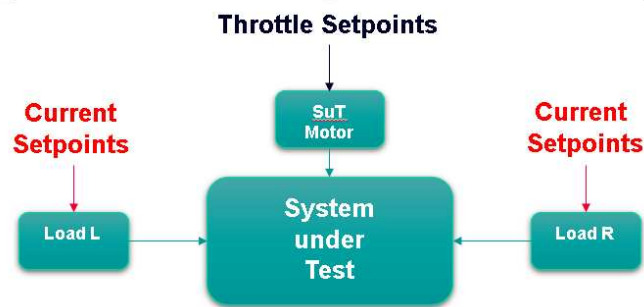


Figure 2.3: Basic mode inputs scheme.

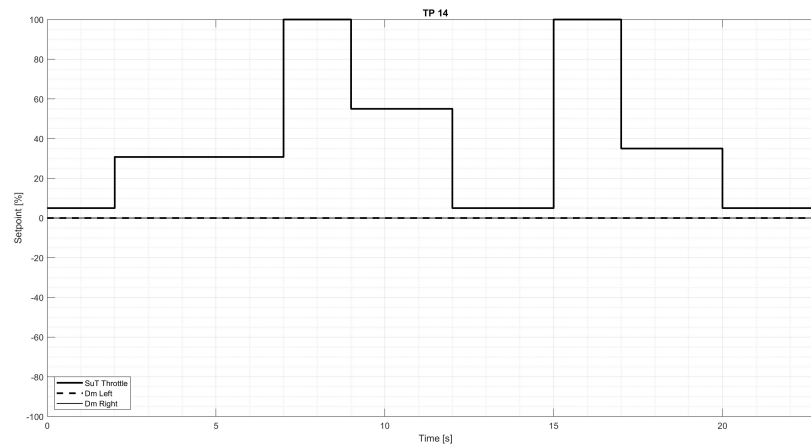


Figure 2.4: Setpoint profiles for SuT throttle and load motor currents, specifying the ‘TP14’ basic test scenario.

During the execution of a basic test scenario the CPU of the programmable logic controller (PLC) implements a specific algorithm [3] for inputting the setpoint test profile for the SuT motor and for the load motors. Doing so, the PLC communicates with the load motors and torque sensors via the RT fieldbus network, indicated by the thick dotted line in Fig.1.2.

In an advanced (XiL) test scenario, the main change to this scheme is that an xDT generates the setpoints. The latter runs on the RT platform and interacts only with the master PLC, which remains the bench controller. Such separation of concerns is safer than dismissing the PLC and controlling the test setup directly from a RT platform because it requires no adaptation of already tested and proven safety measures [3].

Chapter 3

Model description

The SimRod E-Powertrain setup model emulates the real test bench while working in basic operation mode. This chapter describes in detail the inputs/outputs system variables, their real practical operation method and the related model replication method.

Domain	Inputs	Outputs	Parameters
Electrical	<ol style="list-style-type: none">1. SuT Throttle Voltage Signal2. Load Motors Current Signal	<ol style="list-style-type: none">1. SuT Inverter Electrical Power2. Load Motors Electrical Power	<ol style="list-style-type: none">1. Electrical Subsystem Resistance
Mechanical	–	<ol style="list-style-type: none">1. SuT Motor Speed2. Drive Shaft Speeds3. Drive shaft Torques	<ol style="list-style-type: none">1. Motors Reduction Ratios2. Motors & Flanges Moments of Inertia3. Couplings & Flanges Stiffness Coefficients
Signal	–	–	<ol style="list-style-type: none">1. SuT Inverter rates

Table 3.1: Resume table for Model I/O & Parameters

In table 3.1 an overview of the analysed variables of this research activity is showed. They will be described in details in the following sections.

Moreover, the following paragraphs define and explain the interested mechanical and electrical parameters of the research activity and their related model

implementation way.

3.1 System inputs

System inputs are basically the setpoints imposed onto the three system motors:

- **SuT Motor** → **Throttle setpoints**, defined *SuT Throttle*;
- **Load Motor L** → **Phase current setpoints**, defined *Dm Left*;
- **Load Motor R** → **Phase current setpoints**, defined *Dm Right*;

Note that 'Dm' indicates just the Load Motor manufacturing company *Dunker-motoren*.

As showed in fig.2.4 and in the first graph of fig.3.1, the setpoints are imposed in the form of percentage test profiles. Instead, the second graph represented in fig.3.1 shows some acquired real-time signal responses via *Simcenter Testlab*: in particular,

- *C1/C2 Kistler L/R* are the torque signals acquired at the two drive shafts (L/R);
- *T3/T4 Kistler L/R* are the speed signals acquired at the two drive shafts;
- *C24 Throttle* is the throttle voltage signal imposed on the SuT inverter.

Note that 'C' indicates 'Channel' and 'T' indicates 'Tachometer' referring to the instrumentation of the multi-acquisition system. Moreover, *Kistler* is the torque flanges manufacturing company.

Looking at the second picture, indeed, it is possible to clearly see that *C24 Throttle* is the exact related signal to the imposed SuT throttle setpoint. Instead, the direct effect of load motors setpoint is not visible because the related input current signals are not measured in this commissioned run example. Moreover, looking at the torque and speed signals, it is possible to see the complete effect of the employed setpoints for the three motors on the mechanical response of the system.

3.1.1 SuT Motor Throttle

The *SuT Throttle* input is a percentage setpoint signal which is directly related to the voltage signal imposed to the SuT inverter, the *Curtis 1232SE AC controller*.

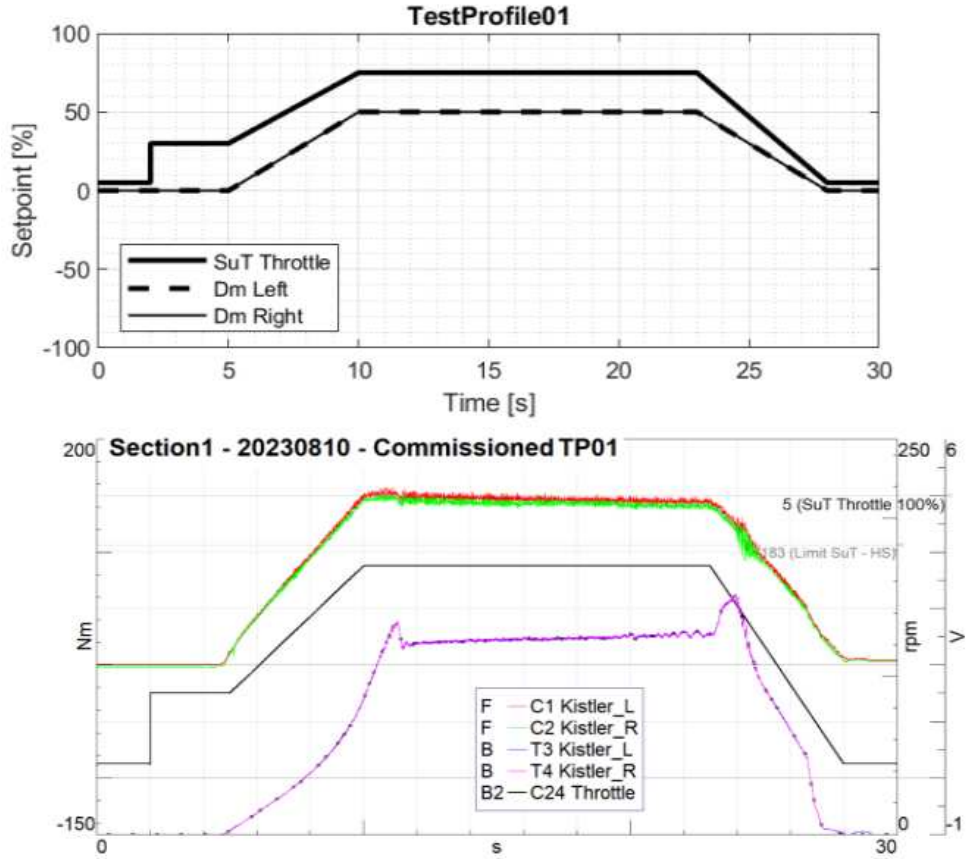


Figure 3.1: Test profile 01 → run-up and run-down/SuT motoring

This relation is:

$$Throttle[V] = \frac{setpoint[\%]}{20} \quad (3.1)$$

The relation is linear and "20" is due to the fact that the operating range of the throttle voltage signal goes from 0 to 5 V.

The SuT inverter acts in speed control mode. The AC controller (SuT inverter) reads the input throttle voltage signal and maps it in a percentage amount in order to select the reference speed of the SuT motor and the increase/decrease rate of the speed. The map is depicted in fig.3.2. This map is obtained by looking at the previously programmed parameters of the AC controller and looking at its datasheet (it explains the effect of programmed parameters on the inverter map).

By looking at fig.3.2, it is important to highlight that this operational region is characterised by:

- **Deadband** region (0 V → 1.5 V) in which the voltage signal has no effect on

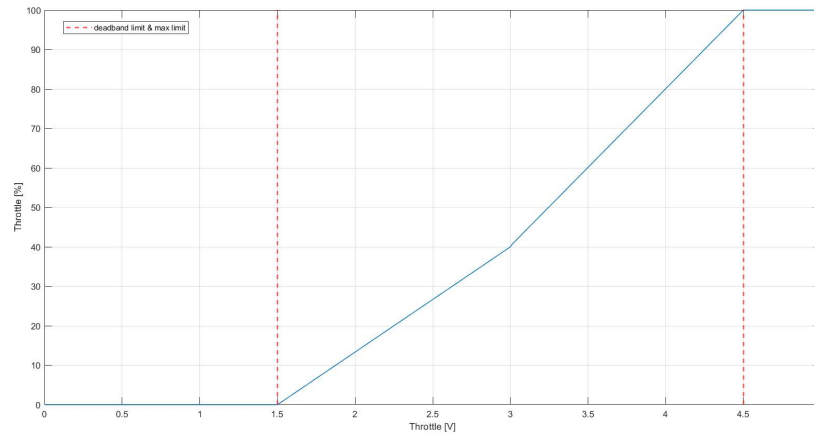


Figure 3.2: Relation between Voltage inverter input and effective related Throttle

the inverter mapped throttle.

- **Maximum Limit** region (4.5 V \rightarrow 5 V) in which the amount of inverter mapped throttle reaches its limit.

Obviously, this particular feature has been identified and then reproduced with defined 1-D maps onto the software model.

3.1.2 Load Motors Current

Before introducing the operating input method of the load motors, it is crucial to underline the fact that during this research activity the investigation has not been really focused on the current control system of these motors.

For this reason, the real system behavior and its emulation methodology is different and it will be now briefly explained.

DC brushless load motors are current controlled. The identified relation between the setpoints and the related amount of input current depends on both Load Motors setpoint and on SuT throttle setpoint. This relation is represented by a 2-D map, figure 3.3 and figure 3.4, that is then also employed in the software model.

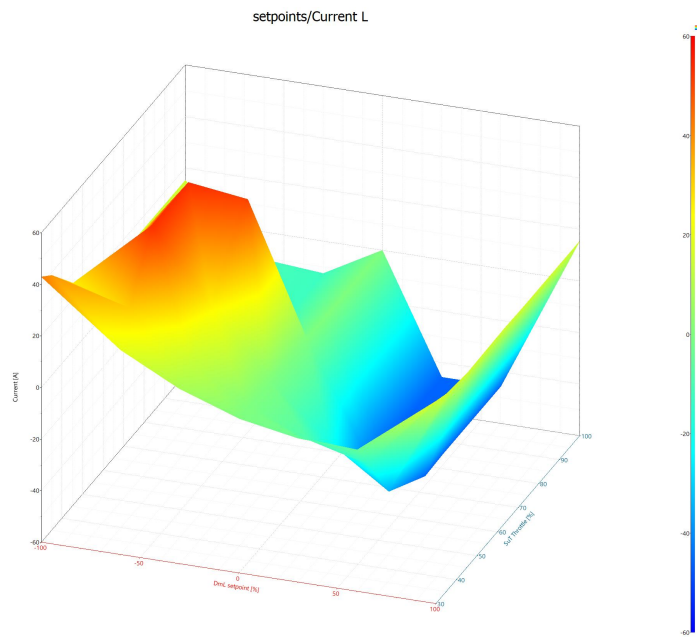


Figure 3.3: Load Motor L 2-D map input setpoints \rightarrow Current

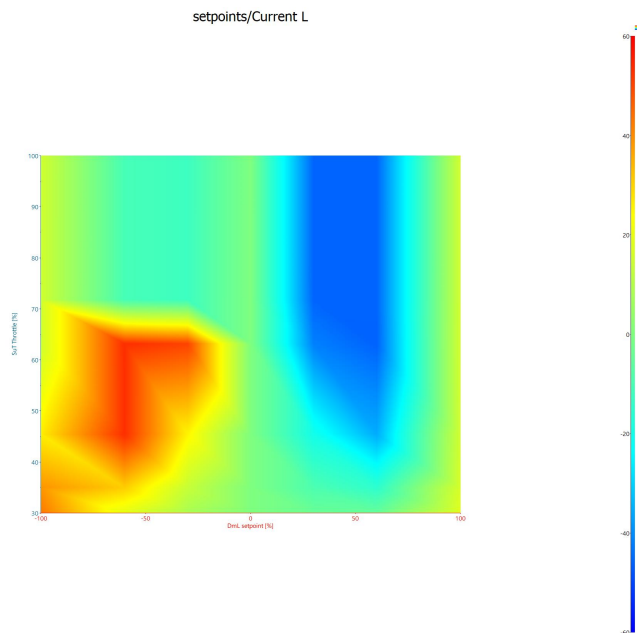


Figure 3.4: Load Motor L 2-D map input setpoints \rightarrow Current - top view

3.2 System outputs

The electrical and mechanical power flow response of the system is strictly connected to specific variables which are obtained directly by measured system signals or implicitly by applying some computations among these measured data.

In a mechatronic system variables from different domains are strictly related, and, surely, in a modeling approach, it is convenient to separate domains in order to make the identification/validation process clearer.

Moreover, the transient and the steady-state identified model features are divided.

3.2.1 Mechanical domain outputs

From a mechanical point of view, the power flow of the SimRod E-Powertrain SuT is simply represented by the concerning behavior of two main variables characterising the several rotating parts of the system: speed (w) and torque (T). Indeed,

$$Power_{mechanical} = T \cdot w \quad (3.2)$$

For this reason, torque and speed are the two system target variables that has been employed for several identification purposes:

- **Steady-state identifications** → Speed mapping for the SuT Motor, Torque mapping for the Load Motors, Friction curves at the axle level.
- **Transient identifications** → AC Speed controller operating behavior.

3.2.2 Electrical domain outputs

The electrical power flow, instead, is characterised by other two variables, also important system outputs: current i and voltage V . Indeed,

$$Power_{electrical} = V \cdot i \quad (3.3)$$

In this case, the research focuses just on steady-state system response and, in particular:

- **Steady-state identifications** → Current mapping for the Load Motors, Electrical Power mapping for SuT Motor and for Load Motors.

3.3 System Parameters

In EV powertrains several elements are characterised by specific parameters. These features have a direct physical and mathematical influence on the behavior of the variables involved in the analysed system. As a direct consequence, it is crucial in the modelling approach to individuate every needed parameter, studying the datasheet of the system components or identifying them from the analysis of acquired data.

In this research activity, the identification and analysis of the several system parameters is again differentiated in steady-state and transient analysis.

3.3.1 Mechanical domain parameters

As regards the system mechanical components, different parameters can be individuated.

The different motors (SuT and loads) reduction ratios are datasheet fixed values. The moment of inertia and the stiffness of the torque flange model employed onto the system are values taken from the datasheet. The moments of inertia of the other system rotating parts (SuT motor and load motors) are obtained with an identification campaign. The stiffness of the couplings between the drive semi-shafts and the load motors is identified.

The stiffness and the inertia values are identified by analysing the transient response.

3.3.2 Electrical domain parameters

In reality, for what concerns electrical field, the made identifications are not such relevant.

The main electrical system analysed part is the electrical power subsystem: how the power supply routes the electrical power flow to the SuT inverter and to the two loads. This subsystem is characterised by the input voltages parameters (fixed values chosen a priori in a specific range) and just a resistance value that needs to be identified.

The resistance identification is made by analysing steady-state power losses.

3.3.3 Signal domain - SuT Inverter parameters

The AC controller logic states the speed controller behavior practically defining the parameters which regulate the increasing/decreasing response of the SuT motor speed.

These parameters are device programmed parameters, but in real measurements there are some similarities and some discrepancies that need to be identified. The identification campaign concerning the inverter parameters is directly connected to the study of transient response.

Chapter 4

Test campaign definition and instrumentation

The modelling and identification research and development of a system is a direct consequence of a thorough and careful observation of data.

Indeed, for understanding the real system physical behavior, the measurement campaign is crucial in order to collect data, information, insights which reveal features and particularities that are extremely essential for the replication of the system on the software side. Moreover, this data acquisition phase is also important and useful for the improvement of the system.

This chapter presents, firstly, an overview of the employed test profiles (implemented for the system basic operating mode) and a more detailed description of the profiles designed expressly for identification purposes. Then, it will define in detail the instrumentation, the starting setup and the added changes.

4.1 Test profiles

The test profiles define, basically, as mentioned before, the inputs of the system operating in basic mode. Indeed, they specific a certain behavior of the SuT motor throttle and a certain behavior of both load motors phase current in a defined time interval.

Test profiles are designed on software tools such as *Matlab* in this specific case and then directly implemented on the test bench via PLC. Depending on the identification issue, different kinds of system response can be interesting for the research process.

For example, an important and central feature that helps to decide which kind of test profile is more appropriate is, surely, the research interest in transient responses rather than steady-state responses.

Moreover, certain profiles need to be designed in a purposeful way for identifying properties such as friction, acceleration rates, etc.

At last, the definition of such profiles is influenced by the testing actual resources and with a careful view to reduce time effort for measurements.

A test profile is made up of (currently) maximum 10 sets of values, in which each set contains:

- The duration over which the specified setpoints will be active.
- The SuT throttle setpoint [%] – corresponding to the target speed of the SuT motor.
- Two respective setpoint values [%] for the left and right load motor. These setpoints normally correspond to target phase current values – the current being roughly proportional to torque. In case of not activating the SuT, the load motors may be operating in speed mode. The load motor setpoints then correspond to their respective target speed values.
- Two Boolean values to choose between maintaining the specified setpoints, until stepping to the setpoint values of the following set, or linear interpolation between the current setpoints and the next ones. The first Boolean value applies to the SuT throttle setpoint, whereas the second Boolean value applies to the setpoints of both load motors.

The test campaign *20230831* is employed for the needed measurements for stiffness identification, instead the two test campaigns *20231023* and *20231024* are employed for all the other system features.

Every test profile is labeled as "TP «*num*»" and 14 test profiles are defined. TP01, TP02, TP03, TP04, TP05, TP06, TP07, TP08, TP09 are employed for the stiffness research. TP11 is employed for all the other identification researches. TP12, TP13, TP14 are integrated for the SuT inverter investigation. Moreover, TP07 is also employed for the final model validation. In the next lines, two main important designed test profiles are described: TP11, TP14.

4.1.1 Test Profile 11 - TP11

Test profile 11 is probably the most important designed test profile for the model test campaign. Indeed, the greatest amount of collected data in the identification

campaign comes mainly from post-processing the TP11 signal responses.

It is designed with the important aim to extrapolate steady-state regions of the system responses that are then mainly employed for every steady-state identification and, secondly, for some transient identifications concerning the SuT inverter parameters.

Before designing it, the interested steady-state operation range of the SuT is chosen. This operational range is showed in the following figures 4.1 and 4.2. The points in the figures are characterised by three coordinates (SuT throttle setpoints and load motor current setpoints L/R) and the requirement for the TP11 is to cover these points for its four steady-state steps (look at the figure 4.3). Besides, in addition to that, in these pictures it is possible to see that also other operational points are defined concerning the TP06: this test profile is just used as an integration of TP11 for friction identification purposes.

The two pictures describe the operational range of the SuT that needs to be covered by TP11 and, just for some runs by TP06. In particular, the involved setpoints regions for the SuT Throttle is, basically, the entire SuT motor forward region (the reverse region just with load motors deactivated) and for what concerns load motors setpoints the interested regions are basically both the motoring and the generating according to different SuT throttle setpoints.

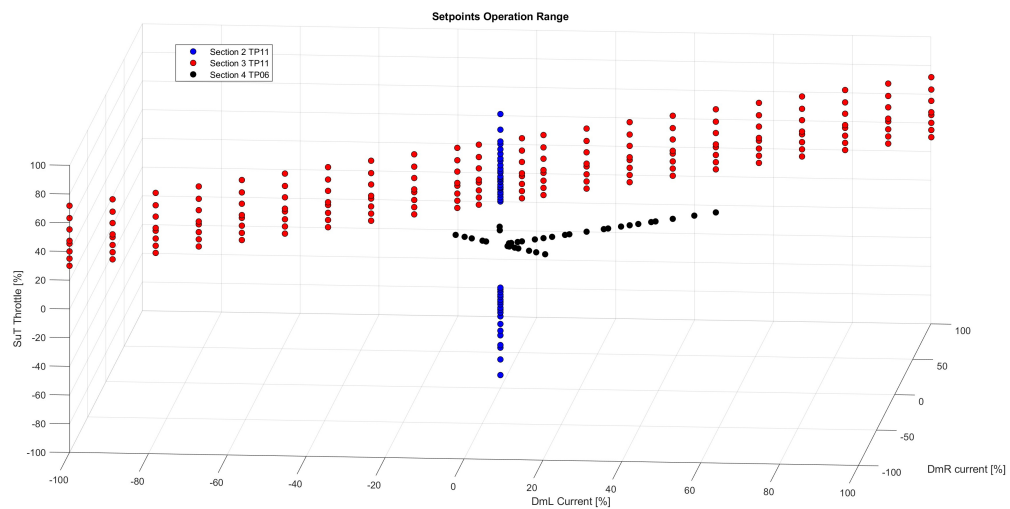


Figure 4.1: SuT operational range for identification

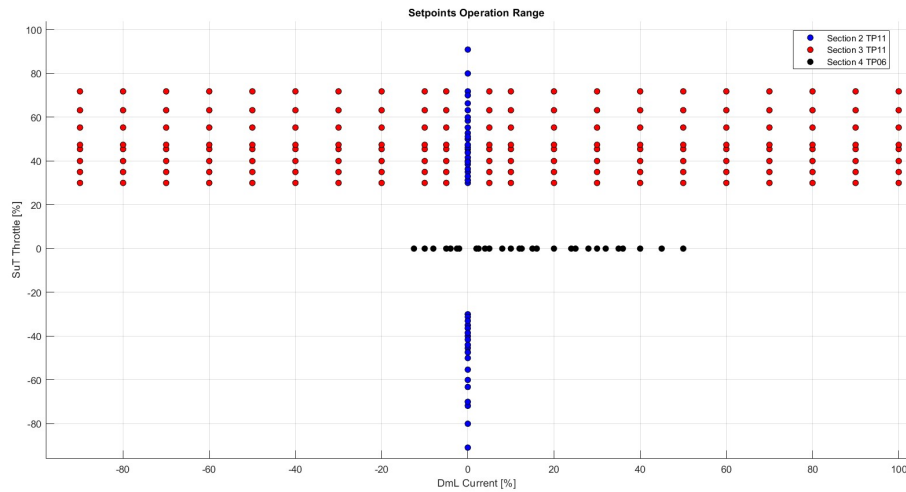


Figure 4.2: SuT operational range for identification - sideview

The test profile 11 (figure 4.3) is assumed to cover this operational range by following a certain approach:

- **SuT Throttle Setpoints** → profile which is characterised by four accelerations for getting four steady-state regions of interest and a slow final deceleration.
- **Load Motor Setpoints** → profile which reaches a steady-state region and remains constant, then it is followed by a final slow deceleration.
- **Scaling Factors** → the employment of scaling factors that can be implemented on the Human Machine Interface (HMI) of the test bench in order to change the steady-state plateaus regions of the test profile (practically the corresponding percentage amount) and cover the entire region without changing the input profile.

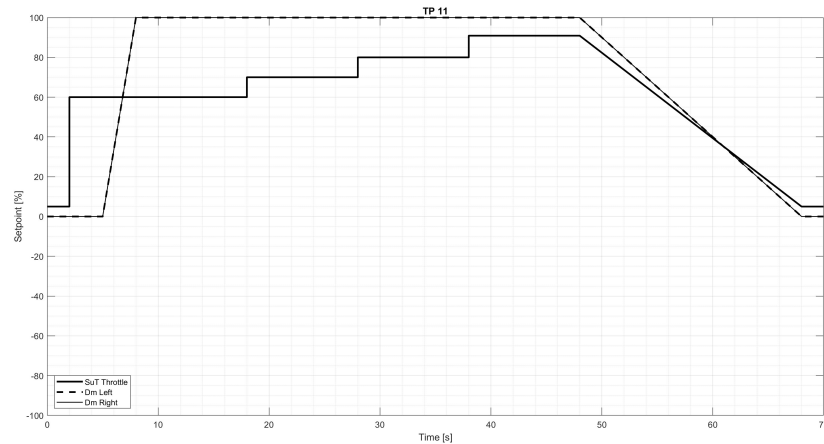


Figure 4.3: Test profile 11

4.1.2 Test Profile 14 - TP14

A group of test profiles is defined in order to complete the identification research for the rate parameters of the SuT inverter.

Indeed, TP12, TP13, TP14 are additions for the test campaign to cover some operating scenarios which are not covered by TP11. In particular, the interested operating scenarios are:

- **Full throttle** acceleration;
- **Partial** acceleration;
- **Partial** deceleration;
- **Neutral** deceleration;

In order to reproduce the previous listed situations, these test profiles are characterised by:

- **SuT Throttle Setpoints** → input profile for the SuT motor with several steps.
- **Load Motor Setpoints** → profile constantly at 0 (the integration of the identification process is focused on the SuT inverter logic).
- **Scaling Factors** → as before for TP11.

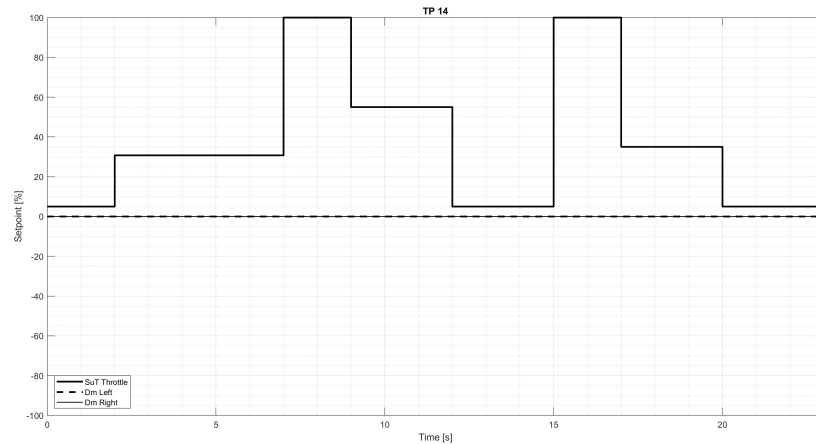


Figure 4.4: Test profile 14

The test profile is presented in figure 4.4.

TP14, basically, consists in two acceleration/deceleration stages of the SuT motor: the first is, firstly, partial, and then it turns into a full throttle operation followed by a deceleration which is again, firstly, characterised by a partial throttle (at a specific percentage) operation followed by a neutral throttle maneuver. The second acceleration does not present the partial phase, but just the full throttle one followed by a deceleration similar to the first one with just one difference in the percentage amount of the partial phase.

TP12 and TP13 shapes are very close to TP14, but they present just one acceleration/deceleration stage. The acceleration of TP12 is equal to the first TP14 acceleration, but the deceleration phase is just neutral (it does not present a partial step). The shape of TP13 is, practically, equal to the first acceleration/deceleration stage of TP14, but the partial amount of throttle in deceleration is different. At the end, these test profiles are designed experimentally just to cover more interesting transient cases and collect more specific information about the behaviour of the SuT inverter in acceleration/deceleration scenarios.

4.2 Instrumentation

This section provides a detailed view of the physical test setup instrumentation which is exploited for the test campaign. In particular, the word "instrumentation" in this case refers specifically to the SCADAS system setup.

At the beginning of the research activity, SimRod E-Powertrain setup presented a specific instrumentation that is summarized in table 4.1. The specific sensors are presented in table 4.2. A detailed picture of the sensors setup (mechanical and acoustic) is given in fig.4.5: The eight objects labeled as *Motor 1-8 Z* are uni-axial accelerometers mounted on the SuT motor, instead on the SuT inverter and on the differential there are two tri-axial accelerometers labeled respectively as *Inverter 1 X/Y/Z* and *Diff 1 X/Y/Z*. *Diff Mic* is the 1/2" microphone mounted on the differential for the measurement of the acoustic pressure. The encoders *SuT motor Enc*, *Siemens Enc* and the torque flanges *Kistler L/R* are characterised by the encoder *ppr* (pulses per revolution) feature and, moreover, for the *Siemens Enc* "A/B+ref" indicates that this device allows to quantify also the dynamic deformation of the flexible coupling (between the drive-shaft and the load motor R).

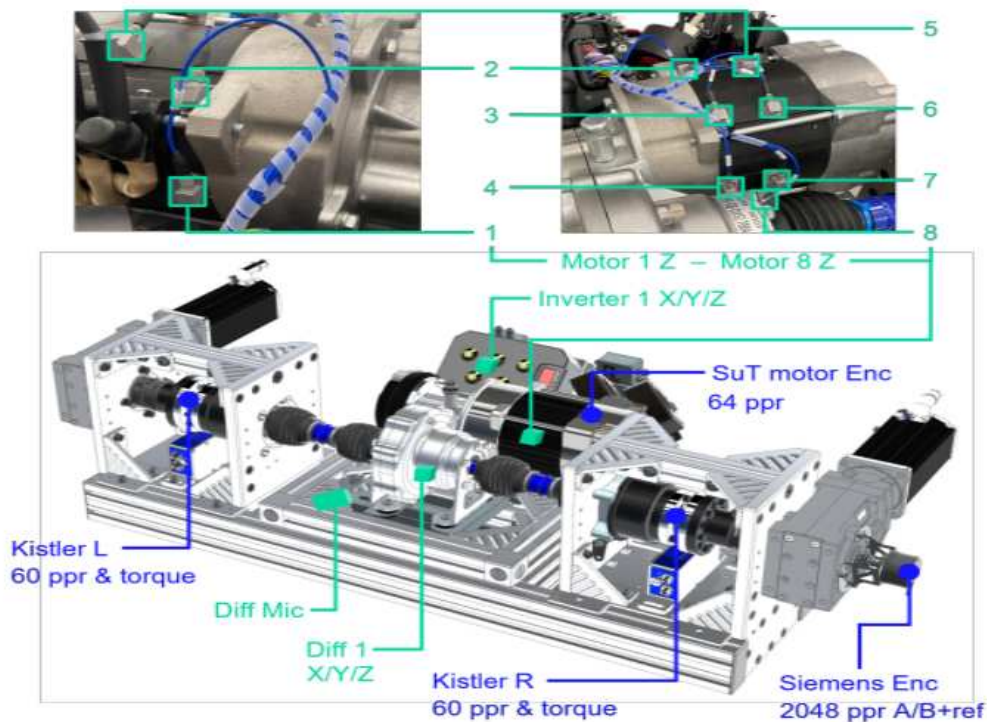


Figure 4.5: Mechanical and acoustic sensor placement [3]

Figure 4.5 does not show the voltage transducers and the current transducers mounted on the SuT motor/inverter side. By the way, the most relevant measured quantity among these sensors for this research is just the input voltage signal of

the throttle.

Domain	Component	Measurement
Mechanical & Acoustic	gearbox of load motor R	shaft speed (1)
	torque flanges	SuT axle(L,R) torques & speeds (2)
	SuT gearbox	accelerations (3) & acoustic pressure
	SuT motor	shaft speed stator accel. (4) stator temp.
Thermal	SuT inverter	heatsink temp.
Electrical		AC currents (5) & voltages (6) DC current(5) & volt. (6)
Driver input		throttle setpoint (6)

Table 4.1: Initial instrumentation [3].

Sensors	Type specification
Encoder gearbox R (1)	Siemens 6FX2001-2PC04
Torque flanges L,R (2)	Kistler KiTorq 4550A200 [option list: S2AN1WKS]
Accelerometers tri-axial (3) uni-axial (4)	PCB Piezotronics model 356A45 model 333B30
Voltage transducers (6)	LEM DVL 50
Current transducers (5)	Danisense DS200ID

Table 4.2: Initial sensors setup [3].

Table 4.1 shows the initial instrumentation capabilities in terms of measurable quantities for the different main parts of the system. Table 4.2 shows the employed sensors effectively connected to the SCADAS channels for the test campaigns of

this research activity. Numbers match the effectively measured quantities with their respective sensors. The only not matched quantity is the shaft speed of the SuT motor because it has its built-in encoder.

4.2.1 Setup changes

The needed setup changes, basically, concern just the electrical power system of the SuT. Indeed, voltage and current sensors are added to get more information and insights regarding the electrical power flow response of the system. Specifically, five more SCADAS channels are employed for four current sensors and one voltage sensor. They are summarized in table 4.3 and showed in figures 4.6 and in the scheme of figure 4.7.

Sensors	Type specification
Voltage probe busbars	Tektronix p5200
Current clamp power supply	Fluke i1010
Current probes x2 load motor L	Tektronix A622
Current probe load motor R	Tektronix A622

Table 4.3: Electrical power system added sensors

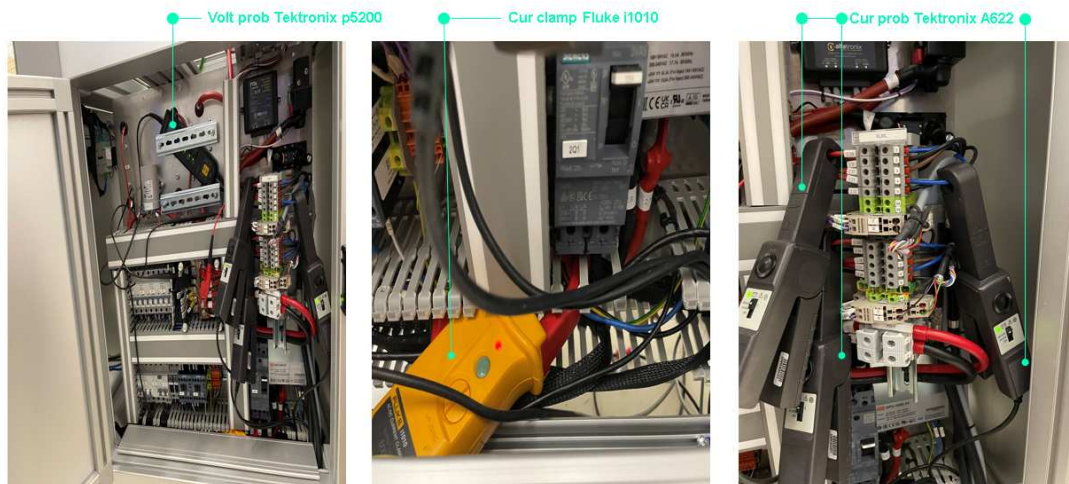


Figure 4.6: Electrical power system added sensors

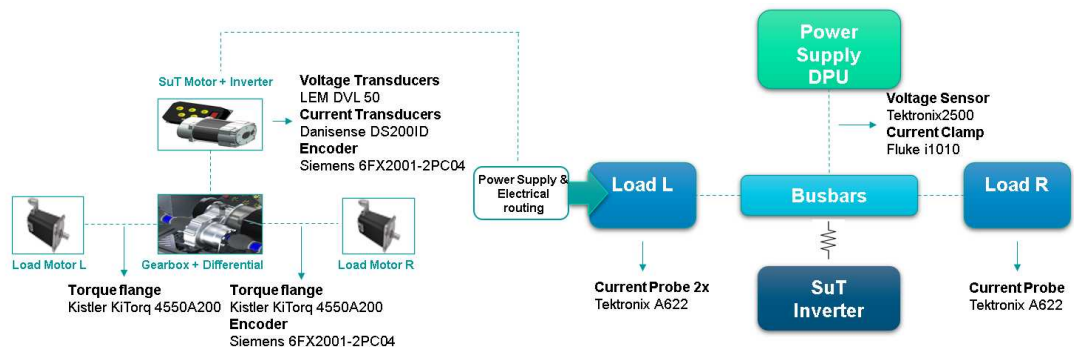


Figure 4.7: Instrumentation scheme with changes

Chapter 5

Test campaign implementation and Model identification

This chapter is the core of the research activity. The test campaign implementation is the actual on field work needed for collecting data. The model identification, on the other side, comprises every in-depth elaboration and analysis of acquired data during the test campaign. The identified insights are then exploited for building up the system model.

5.1 Test campaign

Test campaign is the primary manual and practical part of this thesis project. In these lines a general outlook of the measurements procedure is showed.

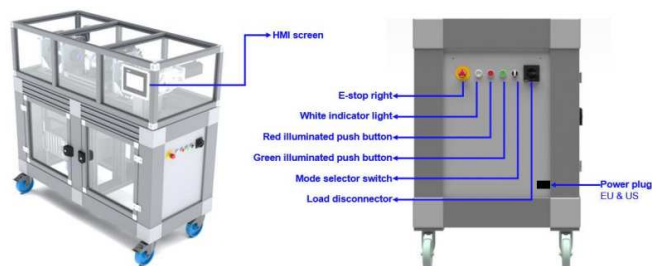


Figure 5.1: Overview of the test setup operating points.

In figure 5.1 the main important operative points of the setup are showed. Of course, there is a precise protocol to follow for making the test setup work in the correct way for measurements campaign.

Fig.5.2 describes clearly how to execute a test. After choosing an operating mode (by using the "mode selector" switch), basically, once the system is powered on ("load disconnecter"), it can be armed for starting a run of measurements. This run is stopped automatically if the CPU detects a fault or it can be forced to stop by pushing directly the "E-stop" button.

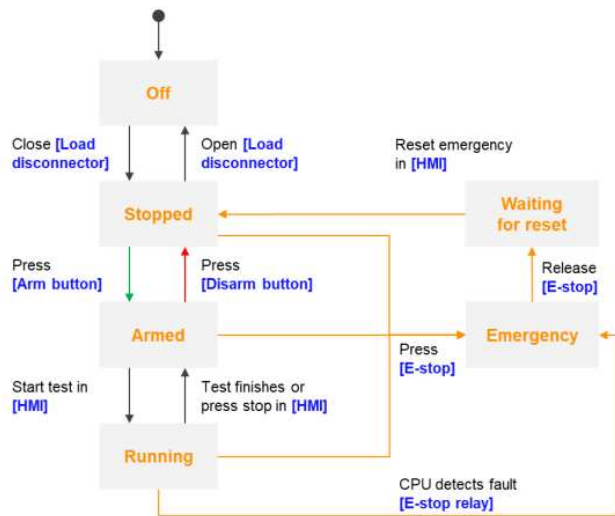


Figure 5.2: Test setup device states.

The test run is implemented via HMI:

- Test profile is chosen among the available.
- The "repeat" option can be selected in case it is needed to run the test more than once.
- For some test profiles (such as TP11 or TP14), there is the possibility to select a "scaling" option in which the interested scaling factor can be chosen and the sign of setpoints can be imposed: for the SuT throttle plus or minus sign means respectively forward or reverse motor mode, for the load motor setpoints plus or minus means regenerating or motoring mode.

During the execution of a test, it is possible to see a general outlook of the system response for some of its main important variables and the general state of the device (armed, disarmed, emergency, etc.). Moreover, the software tool *Simcenter Testlab Data Acquisition* shows the real-time response more in detail

and stores data via SCADAS (obviously for the active sensors channels).

After executing a test, the stored runs can be displayed via *Simcenter Testlab* as showed in figure 5.3. They can be then exported in other software environment in order to elaborate data.

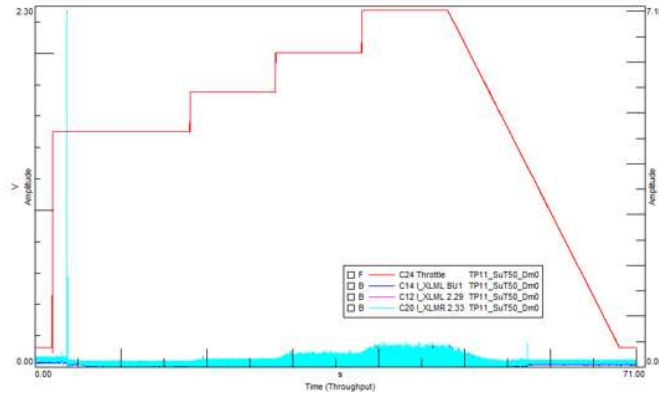


Figure 5.3: Run measurements displayed on *Simcenter Testlab*.

5.2 System Mapping

In the modeling process of the SimRod E-Powertrain test setup, the first problem to be faced is, for sure, how to implement the effective input variables in the model starting from the setpoints.

This section presents and describes, indeed, the model "input" maps, 1-D and 2-D *Ametables* (showed in figures 5.4 and 5.5), and, of course, the way of creating them starting from real acquired data. Moreover, the system mapping research also shows responses of the variables which characterize the real system for different operating points.



Figure 5.4: 1-D *Ametable*.



Figure 5.5: 2-D *Ametable*.

The general approach is to use TP11 to have enough operating test setup points in order to match input setpoints to the relative signal responses. This identification problem is classified as a steady-state problem and, indeed, exploits the steady-state

plateaus of the previously mentioned test profile.

In every case, the acquired data are exported in *Matlab* environment in which the signals are post-processed and elaborated.

For this identification problem the interested measured and computed signals are presented in table 5.1 and 5.2.

Name	Variable
Throttle	Throttle Voltage
SuTMotorEnc	SuT Motor Speed
C_Kistler_L	Torque SuT axle L
C_Kistler_R	Torque SuT axle R
T_Kistler_L	Speed SuT axle L
T_Kistler_R	Speed SuT axle R
I_XLML 2.2	Current Load Motor L
I_XLML BU1	Current Load Motor L
I_XLMR 2.3	Current Load Motor R

Table 5.1: System mapping measured variables.

Name	Variable
Torque_tot	$(\text{Torque_L} + \text{Torque_R})/2$
Torque_diff	$ \text{Torque_L} - \text{Torque_R} $
Speed_diff	$ \text{Speed_L} - \text{Speed_R} $
XLMLtot	$\text{XLML} + \text{XLML_BU1}$
XLMRtot	$2 * \text{XLMR}$

Table 5.2: System mapping computed variables.

The data exporting in *Matlab* is followed by a crucial phase in which signals are processed in order to build up the output models. In particular, in this specific case, the post-processing procedure is the following:

1. **Storage** → Variable signal is stored in a specific vector and a related time vector is defined.
2. **Extraction** → The four steady state region of the signal are extracted (TP11).
3. **Filtering** → The average value of the steady state regions is extrapolated (filtering case).

4. **Matching** → These collected filtered values are matched into tables and then plotted.

5.2.1 SuT Motor Map

The SuT motor behavior is driven by the throttle setpoint profile which is translated in an input voltage signal for the SuT inverter. The amount of mapped input throttle defines exactly the reference speed for the AC controller action. This speed, of course, will be exactly the speed of the SuT motor.

At the end, the identified map is a 1-D map between the mapped amount of throttle and the relative reference steady-state speed. The intermediate maps, for turning setpoints firstly into voltage and then in the amount of applied throttle, are just explained before in **chapter 3**: they are given directly from the *Kyburz* programmed parameters onto the SuT inverter.

The employed measurements are collected into two different sections:

- **Section 2 - 20232310 - SuT_mapping_Dm0** → 12 runs with 12 different scaling factors for SuT motor and 0 for load motors.
- **Section 3 - 20232310 - SuT_mapping_Dmvar** → 44 runs: 2 scaling factors for SuT motor (employed in forward and in reverse mode) and 11 different scaling factors for load motors.

The post-processing results are showed in the next figures and commented in the next lines.

Figure 5.6 shows the most relevant results for the 1-D map of the SuT motor. Run numbers refers to TP11 runs with different scaling factors.

The upper plot displays the SuT motor speed response with respect to the throttle setpoint percentage. It is clearly visible that results are reliable because of the lower plot which shows the correspondent *rms* error values that are very low with respect to the measured results. In forward and in reverse mode the speed starts to increase (in absolute value) at certain amounts of setpoint because of the deadband region of the inverter. Moreover, the most visible identified features of the SuT motor are directly related to its limits summarized in table 5.3.

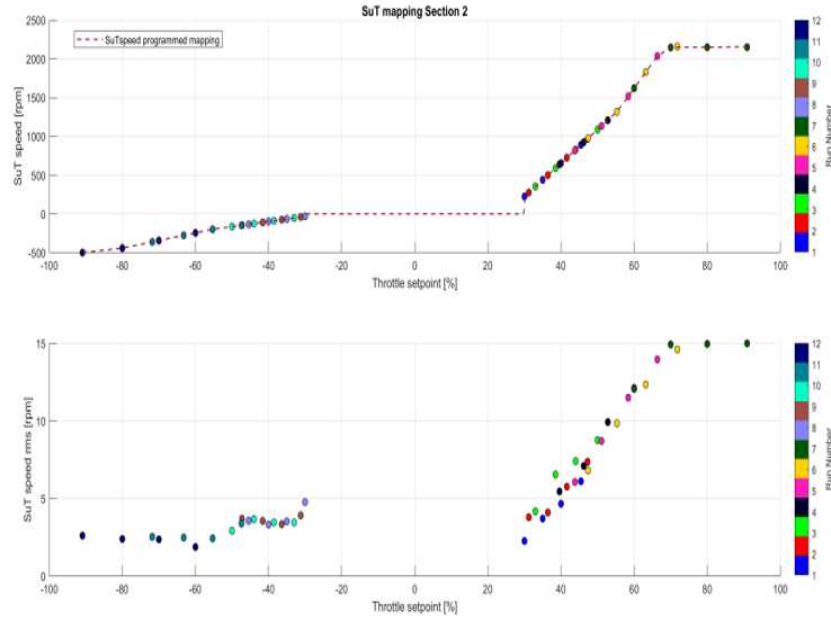


Figure 5.6: SuT Motor speed results for *Section 2*.

Motor Mode	Speed Limit
Forward	2100 rpm
Reverse	500 rpm

Table 5.3: SuT Motor Speed limits.

At the end of the post-processing phase, the results are exported on *Simcenter Amesim* into 1-D *Ametables* which are the needed software blocks to implement the resulting 1-D map (the important difference is that the throttle setpoints are turned into the inverter mapped throttle amount for the *Ametable*). The SuT motor speed *Ametable* is showed in figure 5.7 (around 0% mapped throttle there is a visible step because of the lack of matching collected measured speed values between -30% and 30% throttle setpoints visible in fig.5.6).

As showed in fig.5.7, the *Ametable* relates the mapped throttle to the SuT motor speed. For this reason, in the model, the input of this block is just the output signal coming from the previously mentioned maps that turns the throttle voltage signal in the final effective amount of throttle.

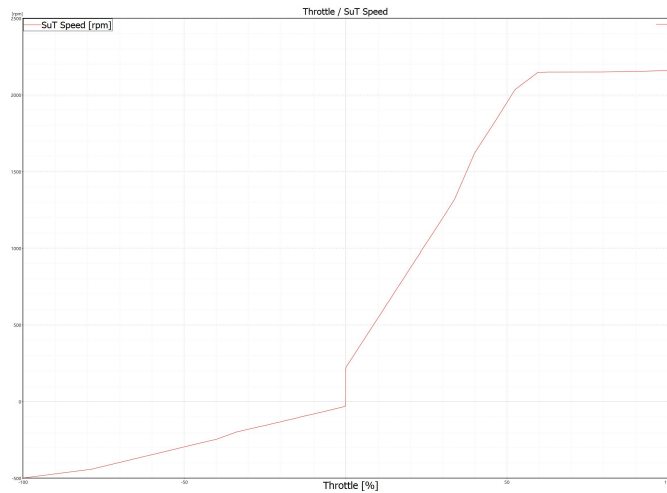


Figure 5.7: 1-D *Ametable* Throttle/SuT Motor Speed.

5.2.2 Load Motors Maps

As regards load motors, the model identification methodology is the same as before, but the emulation methodology is different.

In this case, indeed, the input for a load motor is the phase current setpoint. The setpoint is turned into the related current and, at the end the current turned in the torque. For replicating this, after observing acquired data, the chosen approach has been to use two 2-D maps (*Ametables*): the two inputs of these maps are the load setpoints and the SuT motor throttle setpoints and the output is the current for one of the two maps and the torque for the other.

The employed measurements are collected into two different sections:

- **Section 2 - 20232310 - SuT_mapping_Dm0** → 12 TP11 runs with 12 different scaling factors for SuT motor and 0 for load motors.
- **Section 3 - 20232310 - SuT_mapping_Dmvar** → 44 TP11 runs: 2 scaling factors for SuT motor (employed in forward and in reverse mode) and 11 different scaling factors for load motors.

Post-processing employed results for what concerns the current map are showed in fig. 5.8 and 5.9. In the first one, it is clearly noticeable, that for *Section 2*, the SuT motor is working and the two load motors are not active so that the measured current at the loads is always 0% except for the region over around 70% where the SuT limits are reached.

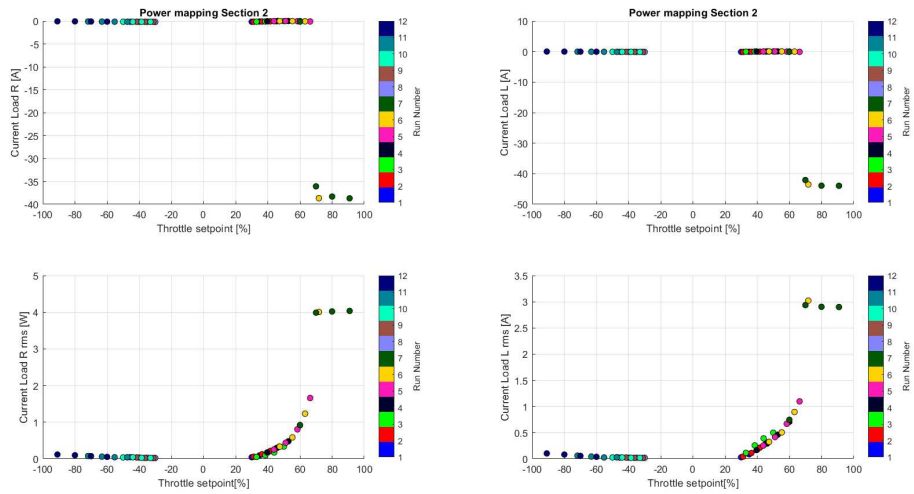


Figure 5.8: Load Current results for *Section 2*.

In this case both *Section 2* and *Section 3* information are mixed in order to build up the final *Ametable*: except for figure 5.8, the results are showed just for load L because, obviously, for both motors the responses are almost equal.

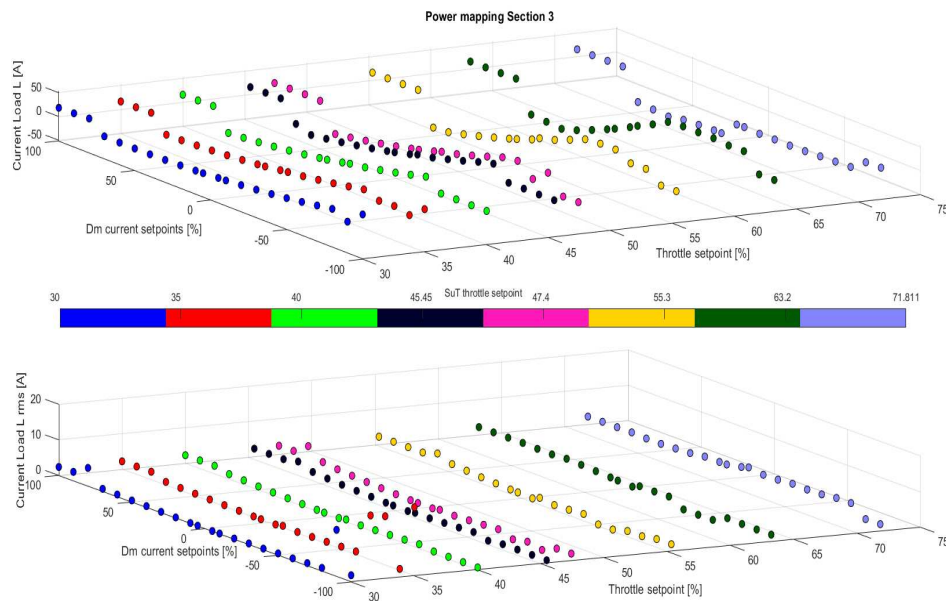


Figure 5.9: Load Motor L Current results for *Section 3*.

In both cases, looking at the *rms* values, results are reliable.

The resulting *Ametable* is presented in figures 5.10 and 5.11.

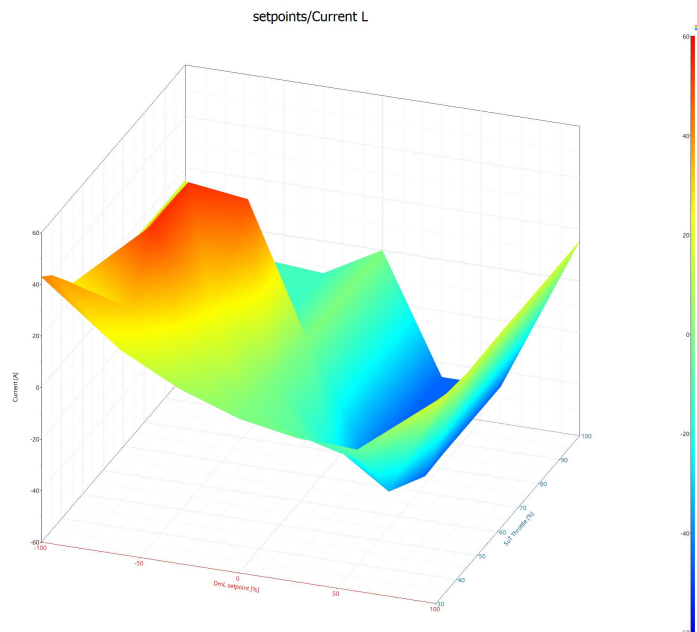


Figure 5.10: 2-D *Ametable* Load and SuT setpoints \rightarrow Current L.

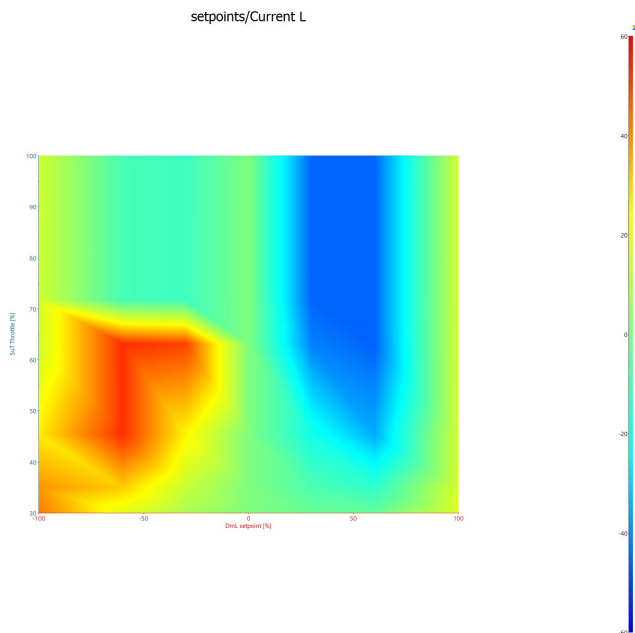


Figure 5.11: 2-D *Ametable* Load and SuT setpoints \rightarrow Current L. - top view.

5.2. System Mapping Test campaign implementation and Model identification

As showed in the previous pictures, from these plotted results it is clearly visible that the current response reaches a sort of limitations (around 60 A) in positive direction with load motors motoring (negative setpoints sign) and the same happens in regenerative direction, but with the opposite sign (around -60 A).

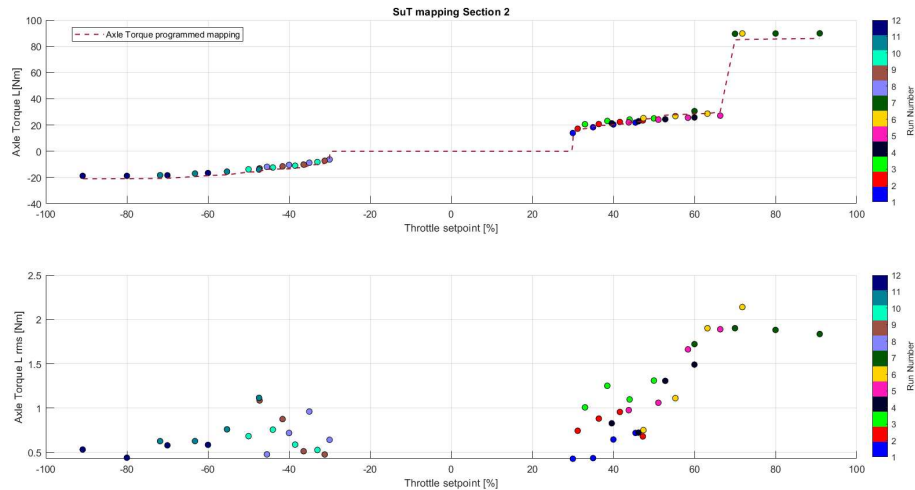


Figure 5.12: Axle Torque L results for *Section 2*.

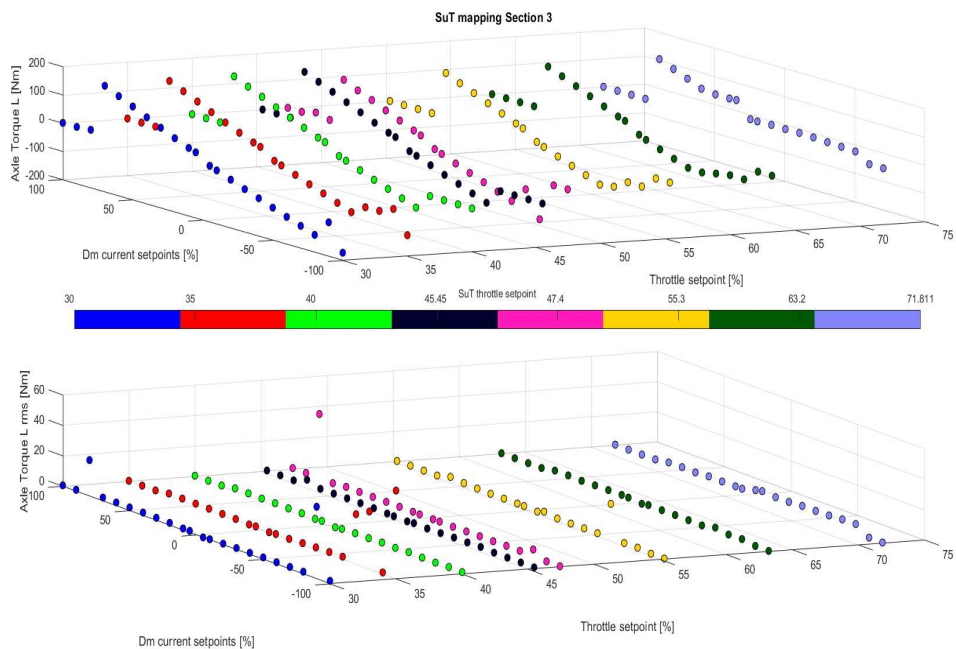


Figure 5.13: Axle Torque L results for *Section 3*

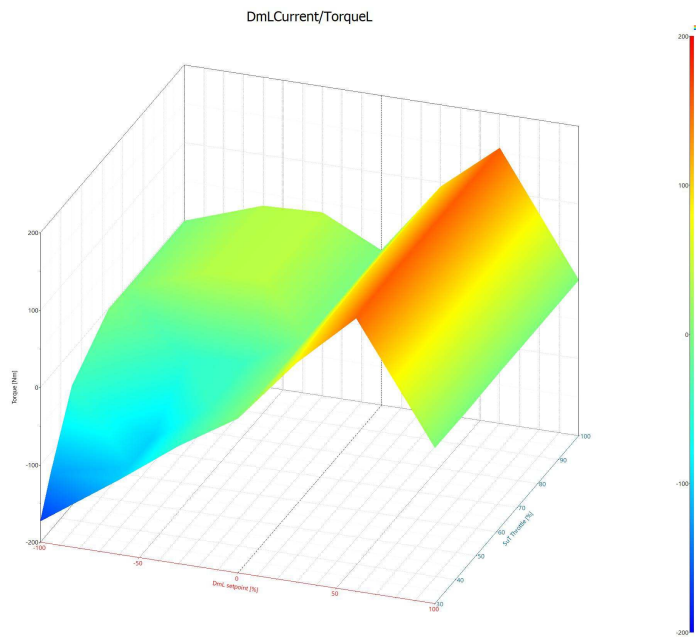


Figure 5.14: 2-D *Ametable* Load and SuT setpoints → Axle Torque L

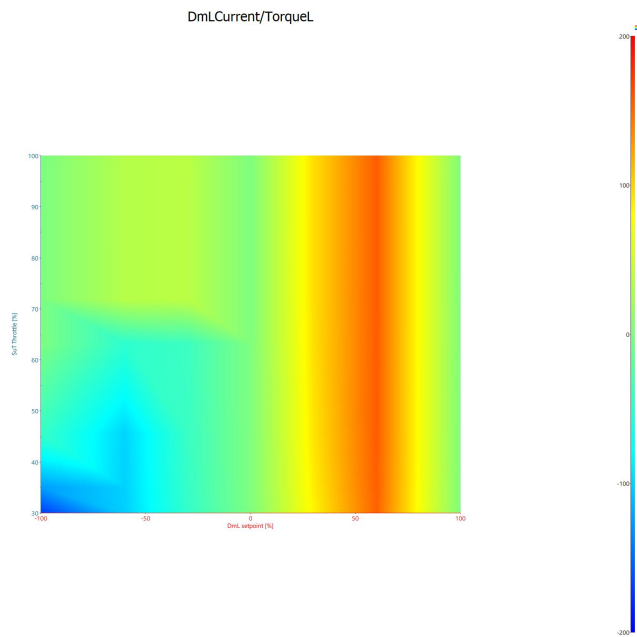


Figure 5.15: 2-D *Ametable* Load and SuT setpoints → Axle Torque L - top view

As regards axle torque response, results are showed in the fig. 5.12 and 5.13. Also in this case the information collected are mixed in order to build up the final

resulting 2-D *Ametable* showed in figure 5.14 and figure 5.15.

In this maps it is relevant to highlight again the limits regions: around 60% of the current setpoint in regenerating (red region) operations and around 100% in motoring (blue region).

5.2.3 Secondary results from System Mapping

In this section we show other post processing results from the system mapping investigations on other variable in mechanical field. By the way, these information are not directly employed to build up model maps or features of the component. These results are mainly related to the axle speed response.

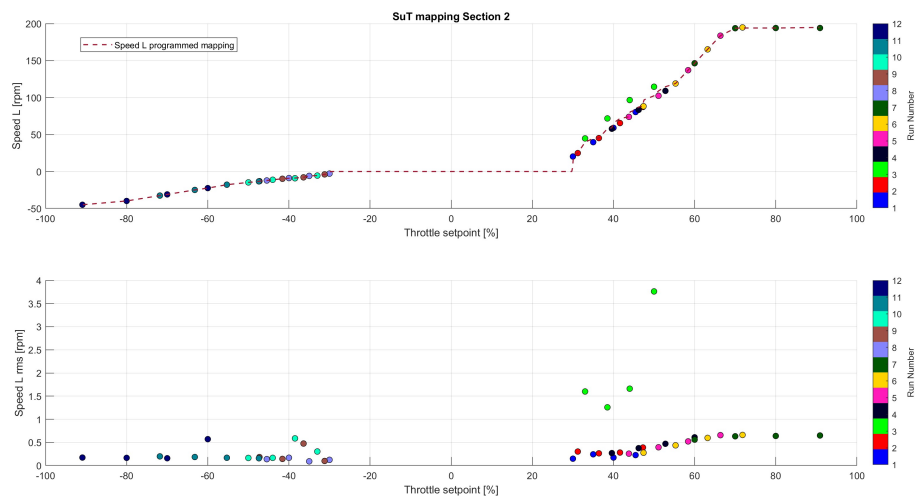


Figure 5.16: Axle Speed L results for *Section 2*

5.2. System Mapping Test campaign implementation and Model identification

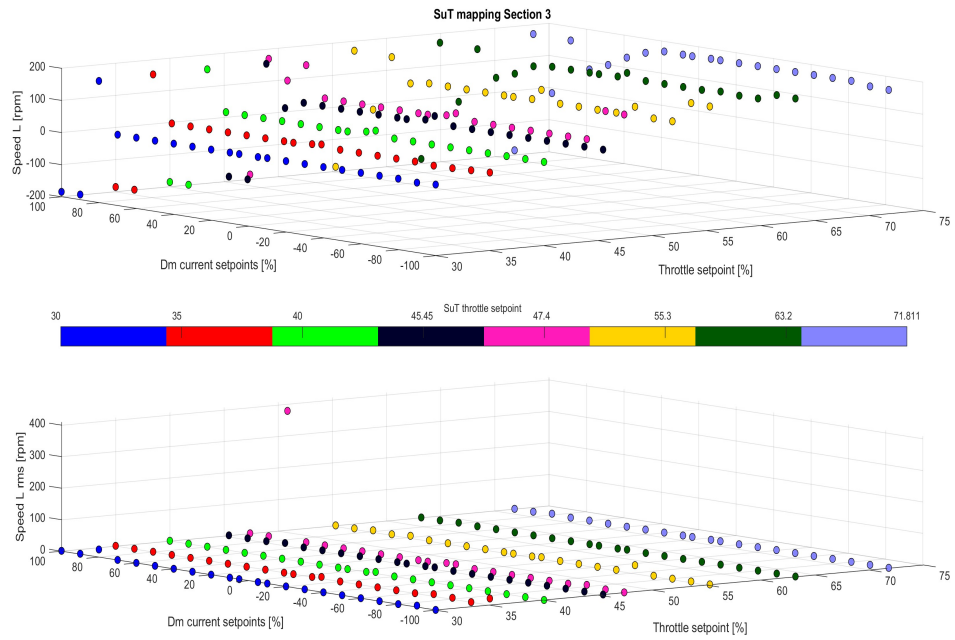


Figure 5.17: Axle Speed L results for *Section 3*

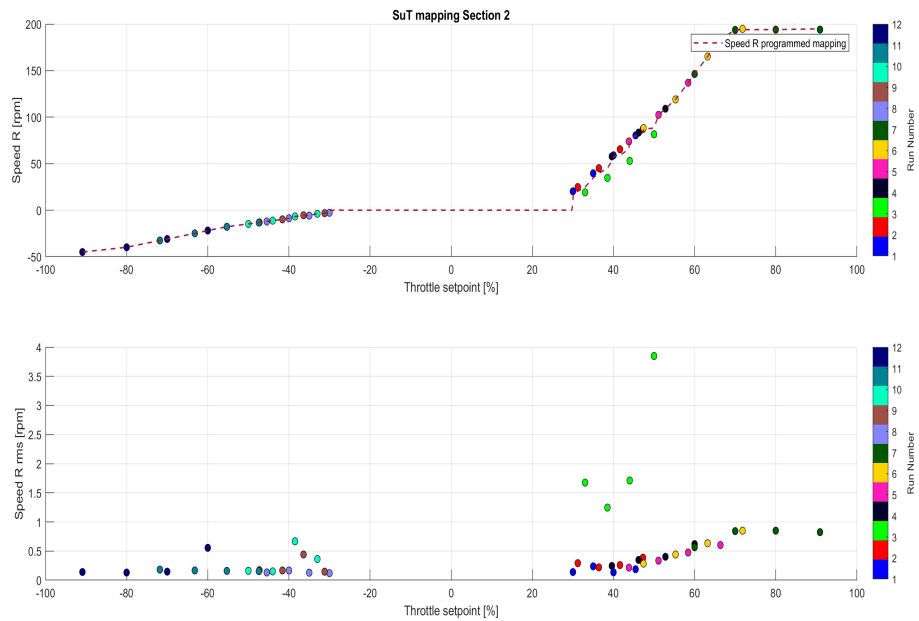


Figure 5.18: Axle Speed R results for *Section 2*

5.3. Friction and Inertia Identification Test campaign implementation and Model identification

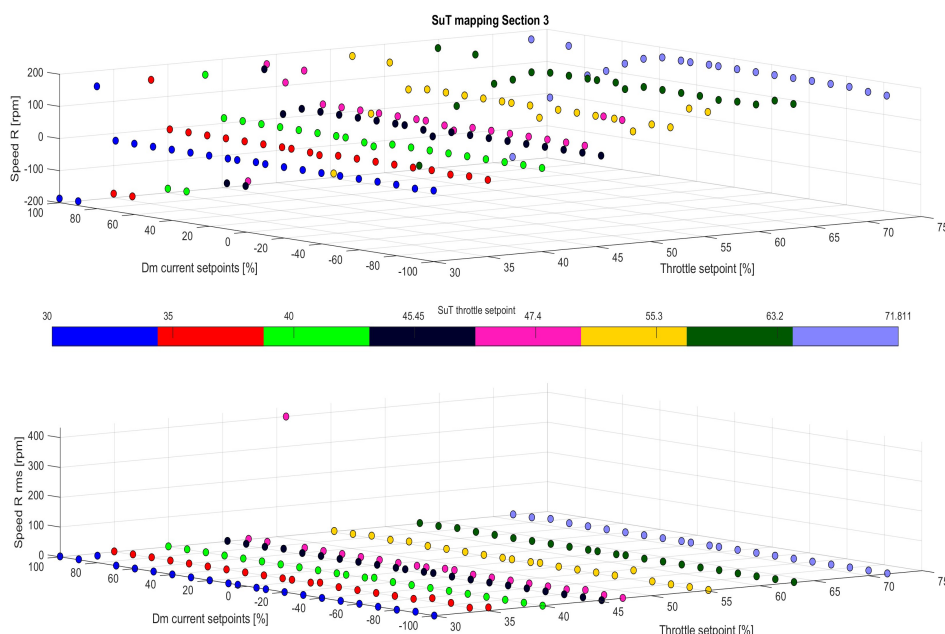


Figure 5.19: Axle Speed R results for *Section 3*

Figures 5.16 and 5.17 show the axle speed measured at the torque flange L, while figures 5.18 and 5.19 show the axle speed measured at the torque flange R.

Also in this case it is possible to summarize (table 5.4) the axle speed limits in forward and in reverse operation of the SuT motor.

SuT Motor Mode	Speed Limit
Forward	190 <i>rpm</i>
Reverse	50 <i>rpm</i>

Table 5.4: SuT Axle Speed limits

Moreover, of course, there are some discrepancies for what concerns the axle speeds measured at the left side of the drive shaft or at the right side: this is mainly due to friction effect that is obviously different in the two opposite sides of the shaft.

5.3 Friction and Inertia Identification

Friction models and inertia parameters in powertrain systems are relevant identification subjects in order to design a real-time and accurate simulation model of it.

5.3. Friction and Inertia Identification Test campaign implementation and Model identification

Indeed, an important amount of the nonlinear behavior of the powertrain response is mainly affected by these features.

In particular, this section will focus on the identification of friction effects and on the building-up of the friction maps at the SuT axle level. It will focus also on the analysis of the inertia effects arriving at the definition of identified parameters characterizing the system motors.

The approach here is to employ again TP11, but in two different ways for friction and inertia:

- **Friction** → to exploit a relevant number of steady-state operating points for create the friction curves.
- **Inertia** → to exploit transient regions in order to have a significant number of points for the parameter computation.

Also in this case the acquired data are exported and post-processed in *Matlab*. The measured and computed variables of this research problem are showed in the tables 5.5 and 5.6.

Name	Variable
C_Kistler_L	Torque SuT axle L Voltage
C_Kistler_R	Torque SuT axle R Speed
SuTMotorEnc	SuT Motor Speed
T_Kistler_L	Speed SuT axle L
T_Kistler_R	Speed SuT axle R

Table 5.5: Friction and Inertia identification measured variables

Name	Variable
Torque_tot	$(\text{Torque_L} + \text{Torque_R})/2$
Torque_diff	$ \text{Torque_L} - \text{Torque_R} $
Speed_diff	$ \text{Speed_L} - \text{Speed_R} $
Speed_tot	$(\text{Speed_L} + \text{Speed_R})/2$

Table 5.6: Friction and Inertia identification computed variables

In this case the post-processing procedure is different for the two different identifications so that it will be described specifically in the related sections.

5.3.1 SuT Axle Friction Model

Mechanical friction is extremely important in this research because it allows to reproduce some important nonlinear effects that are evident on the real test setup. Moreover, there are different theoretical approaches after the modelling methods employed for this issue.

Typical friction models include Coulomb friction, viscous friction, and Stribeck friction; mixed friction models such as Coulomb friction and viscous friction mixing model, Coulomb friction and hyperbolic tangent mixing model, Stribeck and viscous friction model, Stribeck and Dahl model and the Canudas de Wit model, which are applied to the control engineering [13].

Friction models can be divided into two categories: discontinuous friction models and continuous friction models. The approach of dealing with zero velocity discontinuity will affect the numerical stability of the real-time simulation in the discontinuous friction models. The smaller simulation step usually required by continuous friction models will reduce the efficiency of the simulation [13].

For what concerns this research activity, the real-time performance is not such relevant as the predictive capability of the model. Indeed, the continuous model is an important choice in order to try to emulate what happens at the axle level.

The mechanical friction contribution of this EV powertrain mainly affects the driveshaft and the differential. The investigated friction effect, in this thesis project, is just the one at the axle level. The friction effect on the differential side will be a topic of the future improvements and developments of the test setup.

At the end, the friction model definition is the direct consequence of a combination of theoretical approaches. Furthermore, the approach starts from the idea that the axle torque is made up by two different contribution, the inertial and the friction torque.

The article by Sungmin [14] is surely the main important theoretical reference for this purpose: it proposes a specific methodology for identifying the moment of inertia and the friction coefficients for a servo drive system. It gives an interesting starting idea for the identification problem. By the way, it is surely mainly employed for the computation of the moment of inertia.

Instead, for what concerns friction, the modelling approach starts from the paper method to collect torque measurements at different speeds of the servo drive system as showed in figure 5.20.

5.3. Friction and Inertia Identification Test campaign implementation and Model identification

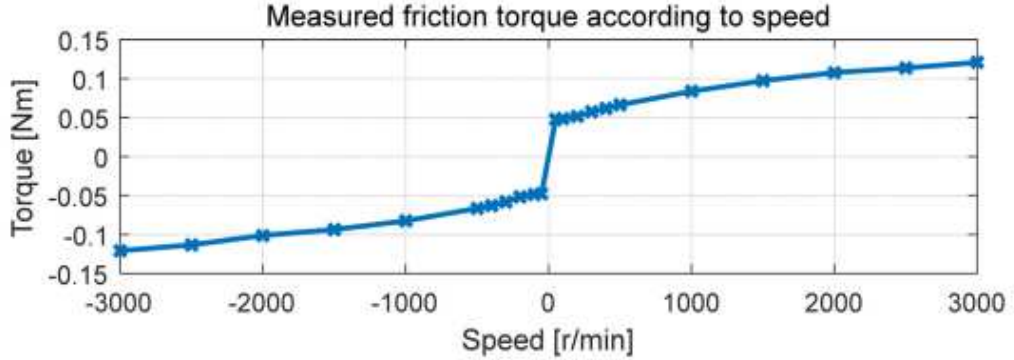


Figure 5.20: Measurement of the friction torque on the 600-W servo drive system [14].

In the paper by Sungmin [14] these measured curves are employed for identifying the Coulomb and the viscous friction coefficient for the final model:

$$T_{\text{friction}} = B_m \omega_{rm} + \text{sign}(\omega_{rm}) C_m \quad (5.1)$$

where ω_{rm} is the servo system mechanical speed, B_m and C_m are respectively the viscous and the Coulomb friction torque coefficients [14]. Instead, in this research case the followed route is just to collect and match correspondent steady-state values of axle torque and axle speed and replicate friction with a post-processed symmetric interpolation to build up 1-D maps onto the software model.

For this particular reason, the general approach is to test the system in two different "directions" to have an idea of the friction losses and to build up two different conceived models, even if at the end just one of the two routes is directly applied in the SimRod E-Powertrain test setup model.

In Sungmin [14] paper, to test the servo drive system in various conditions, the servo motor is connected to another permanent magnet synchronous machine, which serves as the load machine (figure 5.21).

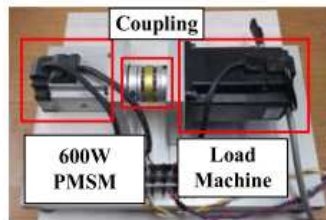


Figure 5.21: Servo drive experimental setup [14].

5.3. Friction and Inertia Identification Test campaign implementation and Model identification

To check only the friction torque, the load machine was not controlled. Therefore, the load machine was the only source of system inertia, as well as the source of some friction torque. In the no-load condition, the servo drive system controls the servo motor, running in the constant speed mode [14]. Because there was no load torque, the torque reference of the servo drive system can be assigned to the friction torque at a constant speed [14].

Starting from this no-load condition approach and moving to the SimRod E-Powertrain test setup, the developed idea is to measure the axle torque with two different kind of runs:

- **SuT Motor not active** → SuT motor as load (throttle setpoints constantly at 0), load motors active.
- **Load Motors not active** → load motors working with setpoints constantly at 0, SuT motor active.

The employed measurements are collected into two different sections:

- **Section 2 - 20232310 - SuT_mapping_Dm0** → 12 TP11 runs with 12 different scaling factors for SuT motor and 0 for load motors.
- **Section 4 - 20232410 - Dm** → 19 TP06 runs: different scaling factors for load motors and 0 for SuT.

The post-processing procedure is the following:

1. **Storage** → Torque and speed signals are stored in a specific vector and related time vector are defined.
2. **Extraction** → The steady state regions of the signals are extracted.
3. **Filtering** → The average values of the steady state regions are extrapolated.
4. **Matching** → These collected filtered values (speed/torque) are matched into tables and then plotted.
5. **Editing** → in order to visualize the typical friction curve symmetric behavior, some "empty" regions (not enough measurements for some technical reasons) are filled with virtual points.
6. **Interpolating** → the friction curve is generated according to a chosen interpolating approach.

5.3. Friction and Inertia Identification Test campaign implementation and Model identification

The next figures 5.22 and 5.23 show the post-processing results.

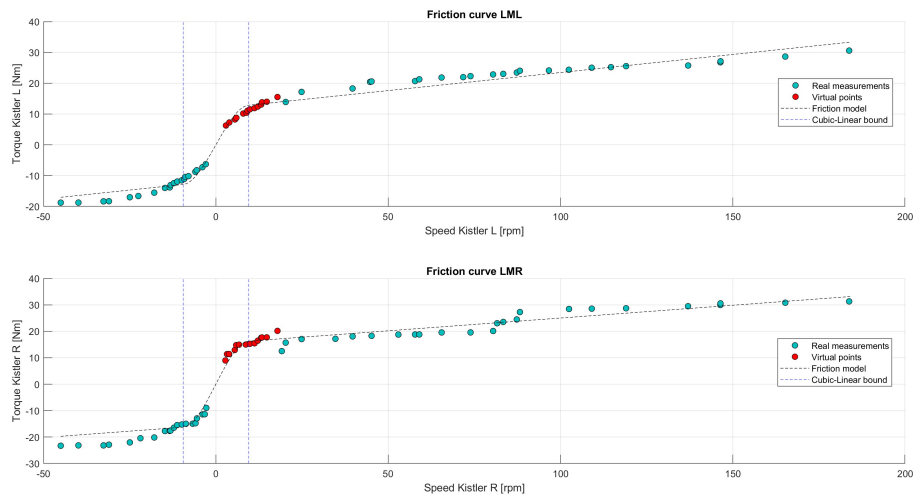


Figure 5.22: Axle Friction results from *Section 2*.

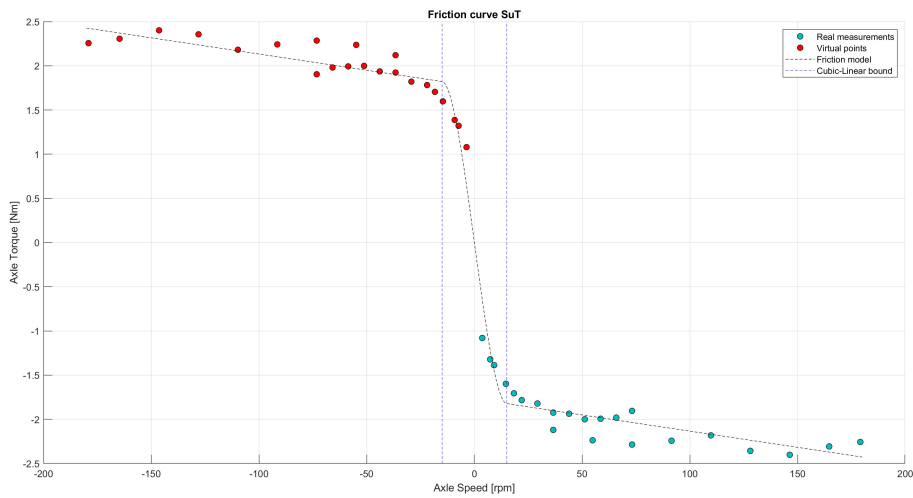


Figure 5.23: Axle Friction results from *Section 4*.

Fig. 5.22 shows the results coming from the *Section 2*. These two curves, surely, are the most relevant because they will be effectively employed in the *Amesim* model. Indeed, the speed and the torque values are sufficiently high and reliable if the SuT motor is active and, moreover, this approach allows to highlight the discrepancies between the two semi-shafts: the two curves (L and

5.3. Friction and Inertia Identification Test campaign implementation and Model identification

R) are slightly different because there are, of course, non-idealities in the real system.

Red points are virtual points added afterwards because there are not enough measured points in the region close to 0 speed for forward SuT motor operations: these virtual points are obtained just by mirroring the measured points for reverse SuT motor operations.

The most significant showed result is the dotted line (the friction model) that is obtained by employing the run points (both measured torque and virtual torque points) and by applying on them a specific experimental interpolation method. In this case, the curve is achieved by using a least square method that mixes a cubic interpolation in the region around 0 and a linear one in the other regions. The threshold between the cubic and the linear regions is just chosen by applying a very basic optimization algorithm which clearly shows the best fit. Some interesting statistics are reported in table 5.7, they state, basically, that the interpolation methods fit the data points in the correct way.

Fig. 5.23 is obtained from *Section 4*. Obviously, torque values are widely lower because for these measurements SuT motor is not acting. By the way, this friction model, built up in the same way described before for the other friction curves, is significantly important because it shows clearly that friction contribution is evident also at low torque values and that the interpolation approach used can be validated also in different cases from the previous one.

The only difference is that, for this specific case, the axle speed and the axle torque are not measured quantities at the torque flanges. They are obtained averaging the two measured values at the two semi-shafts.

The built up models in fig. 5.22 are then used for the two semi-shafts 1-D maps (*Ametables*) of the software model. They are presented in figures 5.24 and 5.25.

The curves are identical to the resultant models of the post-processing campaign with two important differences: the model is mirrored completely for reverse operations (minus sign region) and the extremities are characterized by a sort of step which represents, basically, the achievement of the motor limitations at certain speed values, so that, of course, friction model is not valid anymore.

The *Amesim* model interested part is presented in fig.5.26.

5.3. Friction and Inertia Identification Test campaign implementation and Model identification

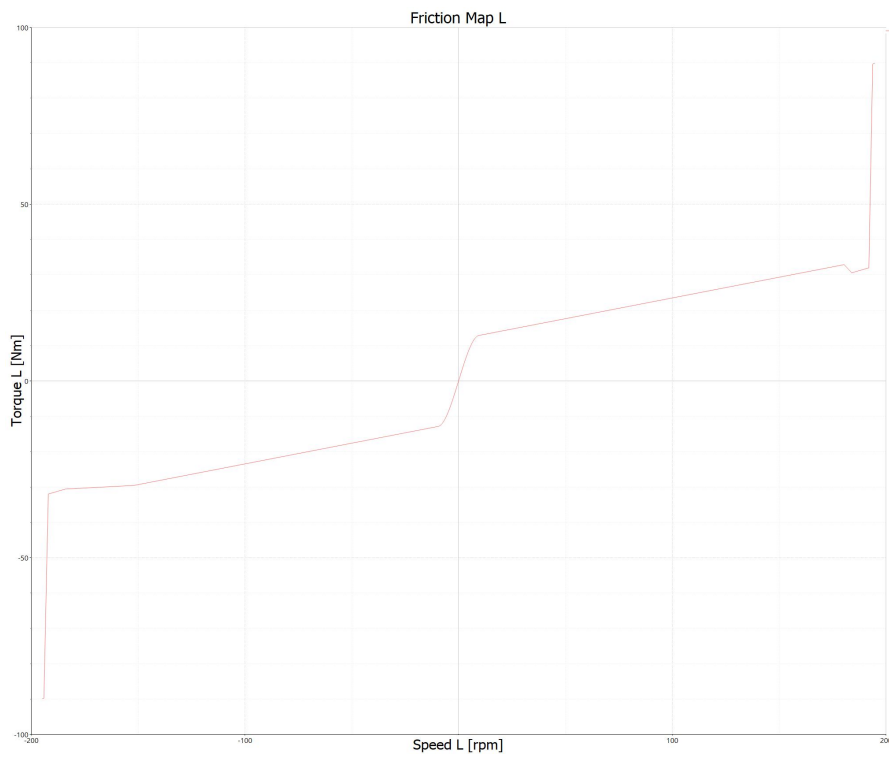


Figure 5.24: Axle Friction *Ametable* for semi-shaft L.

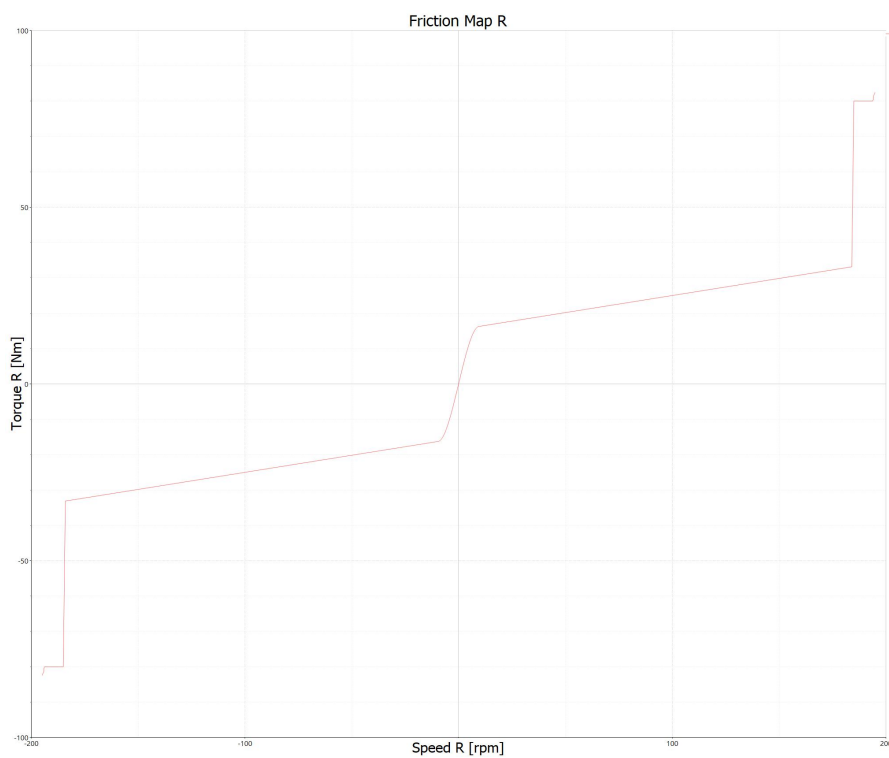


Figure 5.25: Axle Friction *Ametable* for semi-shaft R.

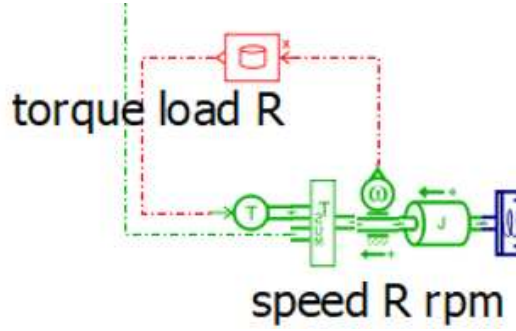


Figure 5.26: Friction *Ametable* implementation on *Amesim* model

Model	<i>RMSE</i>	r^2
Axle L <i>Section 2</i>	1.7583 Nm	0.9882
Axle R <i>Section 2</i>	2.2156 Nm	0.9857
Axle <i>Section 4</i>	0.1372 Nm	0.995

Table 5.7: Friction Models Statistics

5.3.2 System Moments of Inertia

The moment of inertia J is another relevant parameter that needs to be identified in order to allow the system software model to emulate in the correct mathematical way the real SuT. In particular, in this research case, the interested parameters are the moments of inertia of the three main motors (the two load and the SuT motor). Besides, there is one less relevant moment of inertia into the system: the one which characterizes the two torque flanges. Anyways, this last parameter is just taken from the datasheet of the torque sensor: it is reported in table 5.8. Fig. 5.27 shows the crucial investigated points.

For what concerns the actual investigated parameters, the approach is again inspired by the Sungmin [14] paper. In that particular case, The overall torque in the drive system T_e consists of the inertia torque, the friction torque, and the load torque, given in (5.2)

$$T_e = T_{\text{inertia}} + T_{\text{friction}} + T_L \quad (5.2)$$

and the inertia contribution is given in (5.3)

$$T_{\text{inertia}} = J_m \frac{d\omega_{rm}}{dt} \quad (5.3)$$

where J_m is the moment of inertia and ω_{rm} is the angular speed of the system [14]. Therefore, the total torque is made up by three different contributions: the load

5.3. Friction and Inertia Identification Test campaign implementation and Model identification

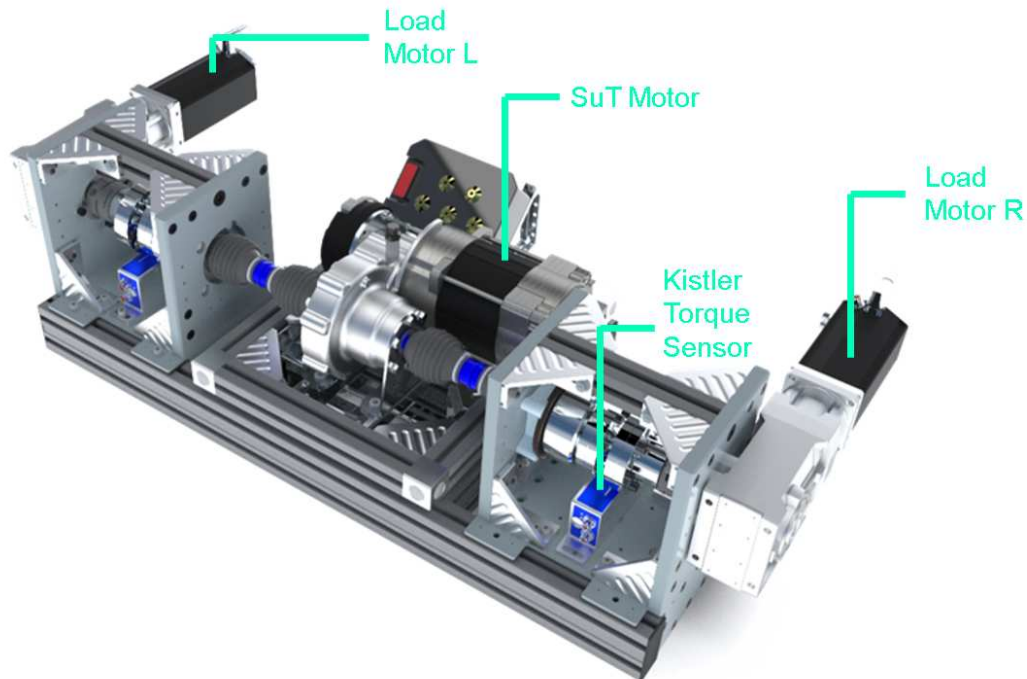


Figure 5.27: SimRod E-Powertrain test setup inertia investigated components.

contribution, the friction contribution and the inertial contribution. The no-load condition is fundamental because, it simplifies the equation: the load contribution is obviously zero. So, at the end, the inertial torque is obtained just by subtracting the friction torque (properly measured) to the overall torque.

This theoretical basis is directly applied into the identification process of the moments of inertia in the SimRod E-Powertrain test setup. The inertial contribution of the torque is computed subsequently to the friction contribution measurements and the moment of inertia is then computed by employing equation (5.3) taking in account just transient phases (it will be explained in the next lines more in detail).

The employed measurements are the same as before for friction identification and they are collected into two different sections:

- **Section 2 - 20232310 - $SuT_mapping_Dm0$** → 12 TP11 runs with 12 different scaling factors for SuT motor and 0 for load motors.
- **Section 4 - 20232410 - Dm** → 19 TP06 runs: different scaling factors for load motors and 0 for SuT.

The post-processing procedure is the following:

5.3. Friction and Inertia Identification Test campaign implementation and Model identification

1. **Storage** → torque/speed signal are stored in a specific vector and related time vector are defined.
2. **Extraction** → Transient regions (acceleration/deceleration phases) torque peaks of the signal are extracted. Initial and final speed of these transient regions are extracted in order to compute the acceleration values needed for the equation (5.3).
3. **Subtracting** → The previous measured friction torque values are subtracted from the collected torque values in order to get the inertial torque contributions.
4. **Matching & Computing** → Every inertial contribution is matched to the relative acceleration (they belong to the same transient phase) and the moment of inertia is computed.
5. **Filtering & Averaging** → These several computed moments of inertia are filtered (outliers are excluded) and averaged in order to get a final value.

The moment of inertia of the SuT motor is obtained from *Section 4*, instead the moments of inertia of the two loads are obtained from *Section 2*.

Figure 5.28 shows the post-processing results for the moments of inertia of the load motors. Results are divided for forward and reverse operation of the SuT motor.

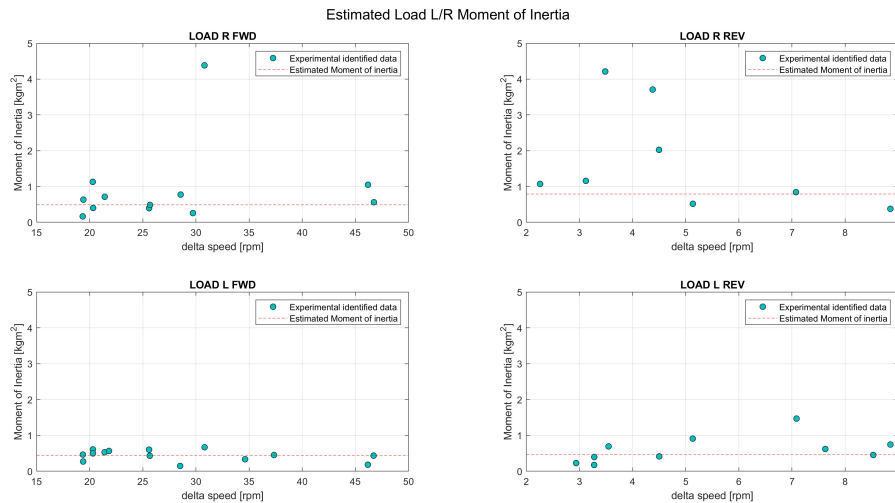


Figure 5.28: Load Motors Moment of Inertia results from *Section 2*.

Figure 5.29 shows the post-processing results for the moment of inertia of the SuT motor.

5.3. Friction and Inertia Identification Test campaign implementation and Model identification

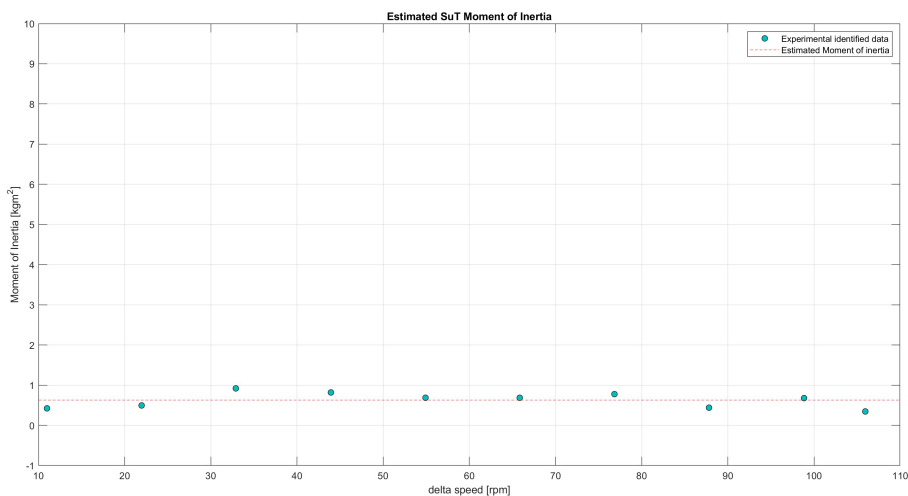


Figure 5.29: SuT Motor Moment of Inertia results from *Section 4*.

In this last case, of course, there is no specification for forward/reverse SuT motor operation because the motor is not active in *Section 4* respecting the no-load condition.

However, results from this identification campaign present some issues. From figures 5.28 and 5.29, it is possible to see that generally it has not been such easy to collect from measurements an important amount of points (moment of inertia values). Plus, among these collected points, some of them are discarded because they are barely outliers (specially for what concerns the identification made on the load motors).

This problem is strictly connected to the nature of the measurements: generally, indeed, it is not such easy to find significant torque peaks among the transient region of the runs and, therefore, in lots of cases, following the approach previously mentioned, the total torque coincides exactly with just the friction contribution so that the inertial torque is zero (it is then impossible to compute the moment of inertia).

This is clearly showed in figure 5.30 in which it is possible to notice a visible torque peak just in the first acceleration phase, in the other phases, practically, inertial contribution is negligible.

Moreover, the collected identified points, most of the time, are obtained from low inertial torque values: sometimes the difference between the friction and the inertia contribution is very low, other times the overall torque is just low (looking at the SuT motor results).

At the end, it is possible to conclude that this identification campaign gives just

5.3. Friction and Inertia Identification Test campaign implementation and Model identification

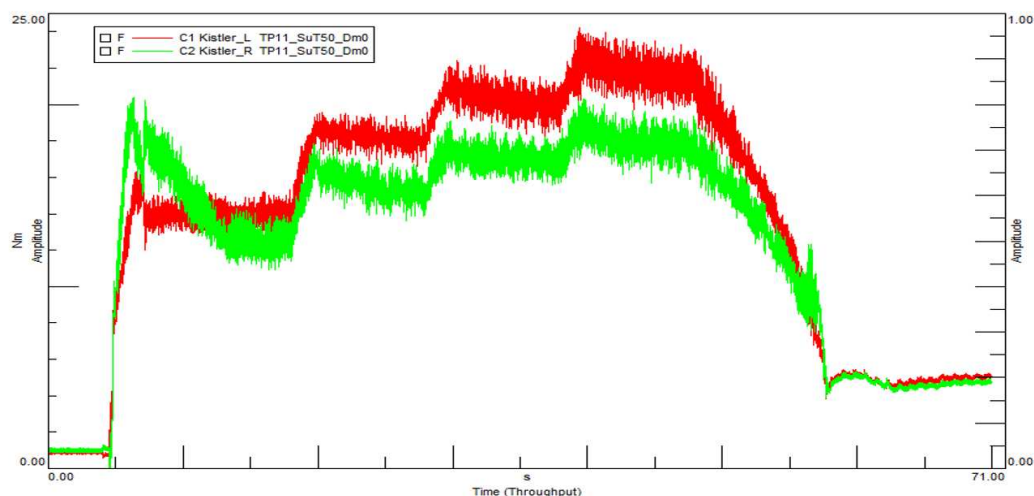


Figure 5.30: Measured Axle Torque L/R for a TP11 run from *Section 2*.

an idea of the real amount of these moment of inertia parameters (the red dotted lines in figures 5.28 and 5.29), but, of course, it is difficult to state the effective reliability of these values because of the general low inertial contribution.

However, identified parameters are summarized in table 5.8.

Component	Identified Moment of Inertia J_m
SuT Motor	0.6271 kgm^2
Load Motor L	0.4543 kgm^2
Load Motor R	0.6401 kgm^2
Kistler Torque Sensor	0.0023 kgm^2

Table 5.8: Identified Moments of Inertia Parameters

Finally, these parameters are directly applied on the model. Basically, specific mechanical blocks (figure 5.31) of *Amesim* are employed for replicating this inertial effect of these components. These blocks are characterised by a moment of inertia that needs to be inserted by the model programmer. The blocks will be better discussed in **Appendix A**.

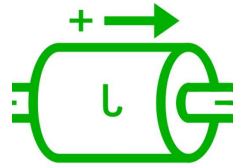


Figure 5.31: Load *Amesim* component.

5.4 Mechanical Stiffness of the Couplings Identification

Another feature of the SimRod E-Powertrain test setup is the mechanical stiffness of the couplings along the drive-shaft. In particular, the two main investigated stiffness parameters concerns two component of the system: the couplings between the semi-shafts and the load motors (figure 5.32) and the stiffness of the Kistler torque flange (figure 5.33).

However, the stiffness of the torque sensors is just taken from the datasheet (table 5.11).

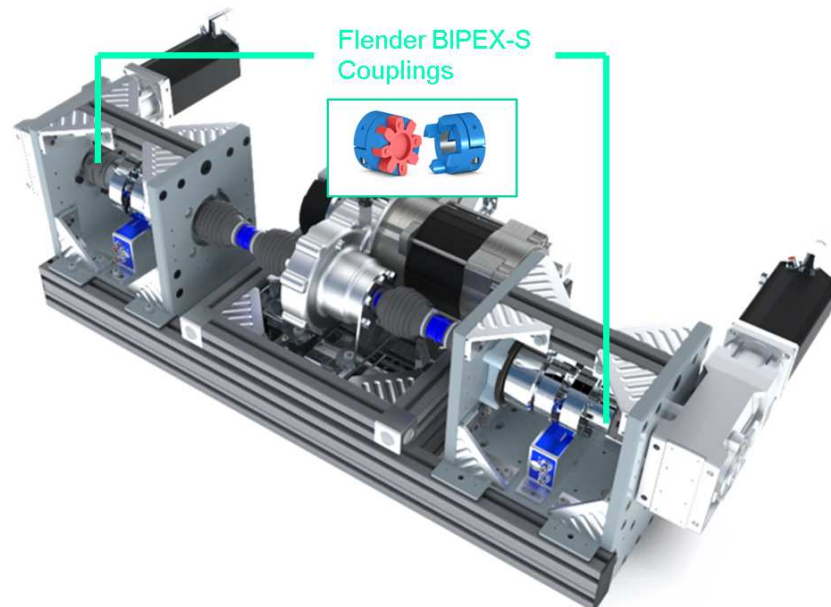


Figure 5.32: Investigated couplings for stiffness.

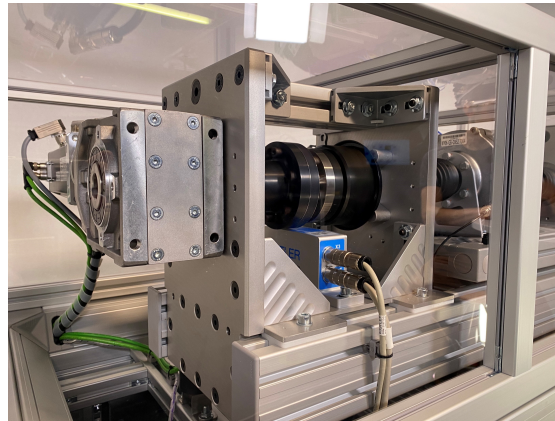


Figure 5.33: Kistler Torque sensor.

The flexible coupling bridges two rotating components, not only compensating the relative displacement, but also behaving the function of cushioning and absorbing vibration. It is widely used in vehicle power train to change the torsional dynamics behaviors. So, it is important to identify coupling dynamics parameters for system dynamic optimization [15].

The analysed and identified couplings of this research activity are employed in between both the semi-drive shafts (L,R) and the load motors. The model used for the couplings is the *Flender BIPEX-S*.

Flender BIPEX-S couplings are torsional flexible couplings and they are free of backlash in the pretensioned state. The damping properties of the couplings can be varied by the use of cam rings made of elastomer of various degrees of hardness.

The torsional stiffness of this couplings is identified in this research starting from a datasheet reference value. In the next lines, the identified results will be compared with the previously mentioned reference. At the end, a specific *Amesim* component is updated with the identified stiffness parameter. The component is showed in figure 5.34.

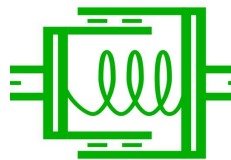


Figure 5.34: Torsional Spring *Amesim* component.

Anyhow, as discussed in chapter 3, the stiffness identification part of this thesis

5.4. Mechanical Stiffness of the Couplings

Identification

Test campaign implementation and Model identification

research is, basically, one of the transient identification problems. Indeed, the approach which is employed for this modelling phase is just to start from the basic mechanical equation (5.4) of the torsional stiffness τ :

$$\tau = \frac{T}{\theta} \quad (5.4)$$

where T is the measured torque and θ is the relative displacement variation of the coupled parts.

Interested variables are the torque and speed signals measured by the *Kistler* sensor (drive-shaft side) and the speed measured by the *Siemens* encoder mounted on the right side of the test setup (load motor side). Indeed, for this identification process, every measurement is related on the right side of the powertrain.

The first idea was just to take the measured torque values as the numerator for the (5.4) and to compute the relative displacement by integrating the relative measured speed, but the presence of a wiring problem has moved us to choose another different route.

The wiring problem regards the detected pulses by the *Siemens* encoder: practically, it detects less pulses than the effective amount of pulses indicated by its resolution feature, the Pulses Per Revolution (PPR). This issue is very relevant because it creates errors in the detected speed signal (figure 5.35).

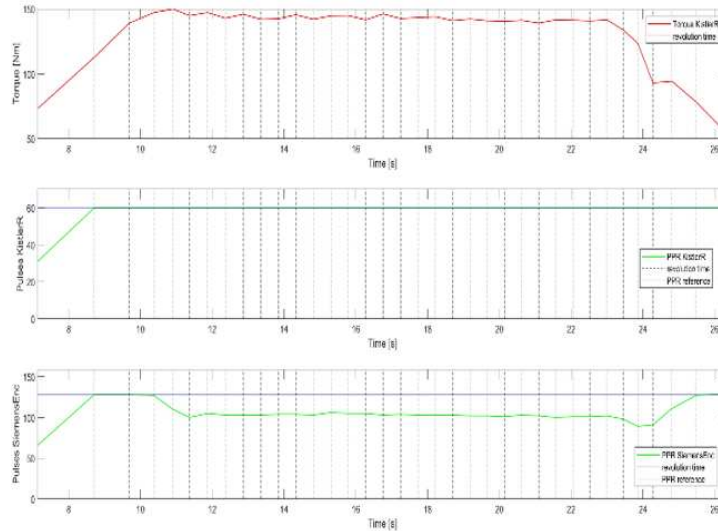


Figure 5.35: PPR error on Siemens Encoder - TP01

Fig. 5.35 shows clearly the previously described issue: in the first subplot there is just the torque response to the relative test profile, the second subplot shows the pulses per revolution detected on the *Kistler* encoder side and they exactly match the encoder resolution (*Kistler* encoder is characterised by 60 PPR), instead in the last subplot there are the pulses per revolution detected by the *Siemens* encoder which are visibly less than its proper resolution (128 PPR indicated by the blue line). For this example (fig. 5.35) TP01 is employed, but, generally all the test profiles from 01 to 09 (08 excluded because it is just a "zero" run for checking CAN setup), are characterised more or less by this problem, especially when the speed is relatively high (figure 5.36).

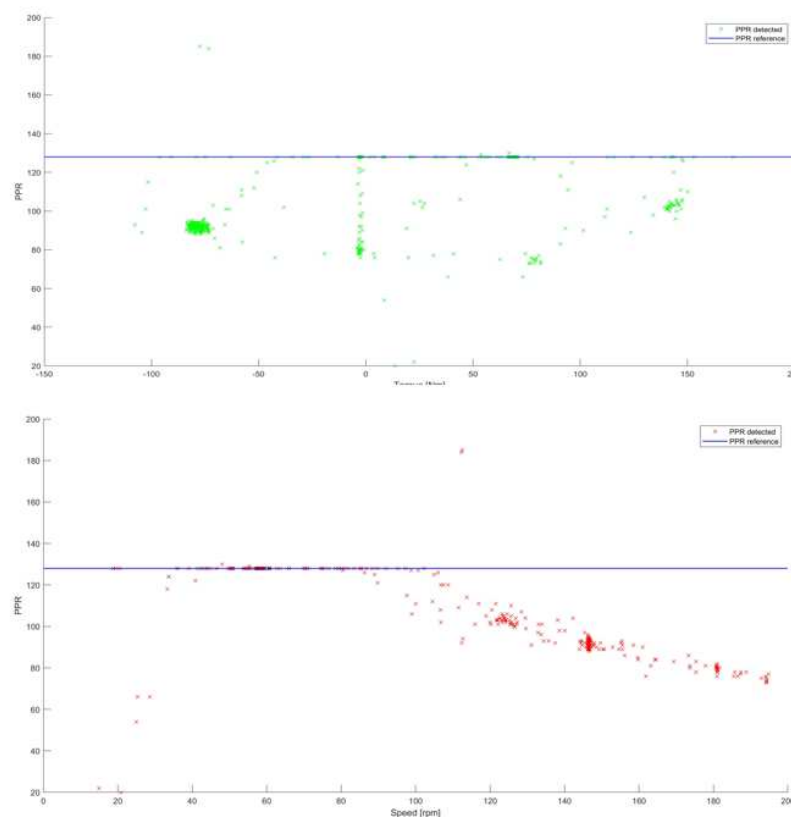


Figure 5.36: PPR error on Siemens Encoder according to different torque/speed values

For this reason, the second path followed concerns the detection of pulses on both sides and some modifications in order to fix the problem and try to get some more reliable data. Indeed, by counting and comparing the *Siemens* encoder pulses and the *Kistler* encoder pulses, it is possible to understand exactly the relative displacement in degree.

By the way, this identification problem is properly classified as a transient problem because, of course, pulses are detected instantaneously and the interested signals regions are not consequentially the steady-state regions of the variable responses. Moreover, a previous test campaign is used in which there were not test profiles from 11 to 14, but except for TP08, the other test profiles from 01 to 09 has been exploited in order to filter reliable data and build a stiffness model.

The interested measured variables are showed in table 5.9:

Name	Variable
C_Kistler_R	Torque SuT axle R Speed
T_Kistler_R	Speed SuT axle R
SiemensEnc	Speed SuT axle R
inc:SiemensEnc	Pulses Siemens Encoder
inc:Kistler	Pulses Kistler R

Table 5.9: Stiffness identification measured variables

These measured variables are, as for the other times, exported to *Matlab* and they are then post-processed.

The post-processing procedure is the following:

1. **Storage** → torque, speed and pulses signal are stored in a specific vector and related time vector are defined.
2. **Extraction** → From all the measured runs, just the runs and the regions in which the correct number of pulses is detected for the Siemens Encoder are effectively extracted.
3. **Selection** → PPR are different on the two encoders (Kistler/Siemens): Kistler has 60 PPR, Siemens 128. For computing sensible instantaneous relative displacements just 60 reference pulses of the Siemens Encoder are selected among the 128.
4. **Matching & Interpolating** → 60 time intervals (between two consecutive pulses) $\Delta(t)$ are extracted and matched with the corresponding interpolated virtual speed (the speed is computed assuming that the encoder starts from a reference "zero" position).
5. **Computing** → Stiffness is computed for every $\Delta(t)$ by employing the related measured torque.

6. Filtering & Averaging → These instantaneous values are filtered by averaging them and a final value of stiffness is extracted for every run. The final identified stiffness parameter is again the average among all the run extracted values.

At the end of the analysis and elaboration phase, after filtering all the "good" run regions for the torsional stiffness computation, ten significant values are obtained and the model is, of course, build up on these points (dotted line in figure 5.37).

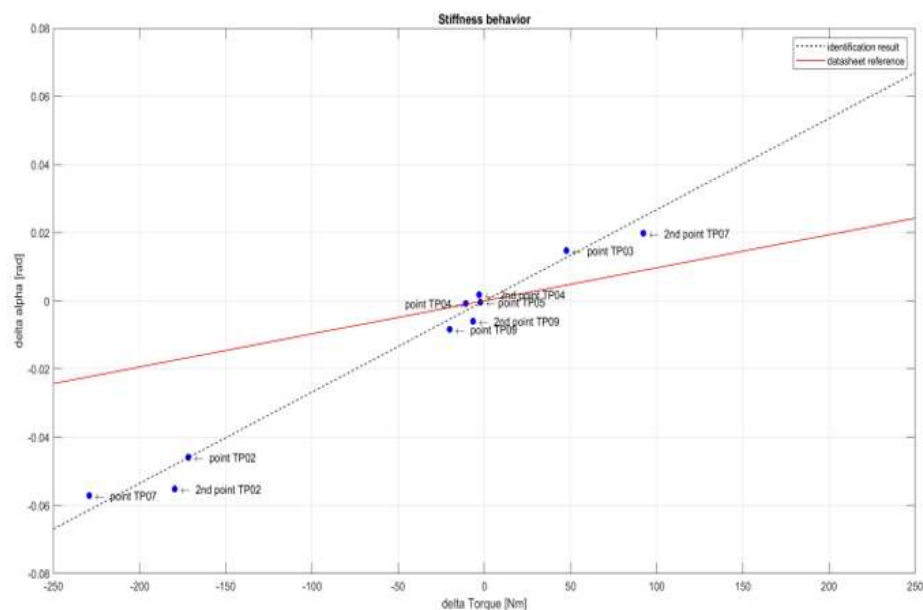


Figure 5.37: Torsional Stiffness Identified Model.

It is possible to conclude from figure 5.37 that the identified model gives at least a rough idea of the effective torsional stiffness parameter which characterizes the couplings. Indeed, red line (the datasheet reference), is not really matched. So, for sure, it can be possible to state that the model is not actually very reliable due to the faced issues previously described: the number of significant data points is very low, they are not enough to build a precise and definite model of the torsional stiffness and, moreover, the computed variance among those is high. On the other side, it is not really possible to trust completely the datasheet value because it is not known how the specific parameter has been previously computed. The results are summarized in table 5.10.

5.5. Electrical Power Flow Mapping and Resistance Identification Test campaign implementation and Model identification

Dataheet Stiffness	Identified Stiffness	Identified Variance
10310 <i>Nm/rad</i>	4369.434 <i>Nm/rad</i>	3632.395 <i>Nm/rad</i>

Table 5.10: Flender BIPEX-S Stiffness Results.

Dataheet Stiffness
349 <i>KNm/rad</i>

Table 5.11: Kistler sensor Stiffness.

5.5 Electrical Power Flow Mapping and Resistance Identification

EV powertrains, nowadays, are cutting-edge systems from an electrical point of view. Research attention is increasingly moving to improve the energy efficiency and the performances of these mechatronic systems for following much more sustainable paths.

For these purposes, it is crucial to experiment different methods and/or ways to identify the electrical power flow when systems like SimRod E-Powertrain are tested.

In this research activity, besides, a deep and accurate analysis of the electrical power flow allows to replicate it in a correct manner in order to generate a final simulation model capable to predict the electrical response of the system according to different input setpoints. This is relevant surely for de-risking purposes.

Indeed, the main objective of this part of the thesis project is to understand how the electrical power system works in the test setup, to analyse the response both in motoring/regenerating mode. For doing that, it is important to exploit the test campaign measurements in order to collect a great amount of data points which are needed for building up maps or for other specific identification purposes. Therefore, the investigation is a clear steady-state investigation.

Before delving into the identification and modeling process in detail, however, it is important to introduce the electrical power system architecture. Basically, the electrical power system of the SimRod E-Powertrain test setup is composed by the central plug-in power supply which electrically feeds the entire

5.5. Electrical Power Flow Mapping and Resistance Identification Test campaign implementation and Model identification

system by routing the power flow into the different motors. The scheme is showed in figure 5.38.

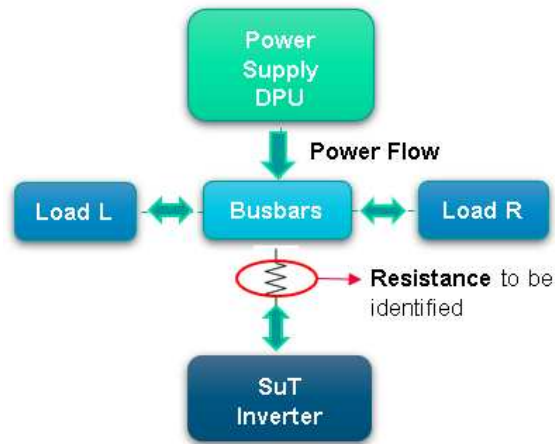


Figure 5.38: SimRod E-Powertrain test setup Electrical Power System scheme

As it is possible to see from the scheme depicted in fig. 5.38, the power supply feeds the system through a system of busbars in which the flow is divided between the two DC brushless load motors and the SuT motor inverter according to the different input setpoints of the employed test profiles. Indeed, the double-headed arrows indicate just that the power flow can be directed in two opposite ways depending on which operating mode the powertrain is behaving (motoring/regenerating).

Moreover, it is possible to notice that in correspondance of the connector between the busbars system and the SuT Inverter there is a resistance which is identified in this campaign in order to replicate its effect onto the model.

For replicating the previous described scheme, the *Amesim* simulation model needs, ultimately, 1-D and/or 2-D *Ametables* (the same approach used for system mapping case) and a resistance *Amesim* component (figure 5.39) characterised by the identified parameter.

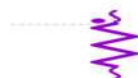


Figure 5.39: Resistance *Amesim* component.

Plus, as it has been mentioned, this identification problem is a steady-state problem and lots of data points are needed to build up the maps and to identify

5.5. Electrical Power Flow Mapping and Resistance Identification Test campaign implementation and Model identification

the electrical resistance. For this reason, TP11 is exactly the needed test profile to collect enough data points in steady-state regions.

In the next lines the measured and computed signals of this identification campaign are discussed and, in addition, the post-processing procedure is described as for the other identification campaigns.

The computed and measured variables are presented in tables 5.12 and 5.13.

Name	Variable
I DPU 2.7	Power Supply Current
I XLML 2.2	Load Motor L Current 1st
I XLML BU1	Load Motor L Current 2nd
V DC busbars	Voltage SuT busbars side
I XLMR 2.3	Load Motor R Current
I DC	SuT inverter Current
V DC	Voltage SuT inverter side

Table 5.12: Power Flow measured variables

Name	Variable
P DPU	V DC busbars*I DPU 2.7
XLMLtot	XLML 2.2+XLML BU1
XLMRtot	2*XLMR
P SuT busbars	V DC busbars*I DC
P SuT inv	V DC*I DC
P LML	XLMLtot*V DC busbars
P LMR	XLMRtot*V DC busbars

Table 5.13: Power Flow computed variables

The post-processing procedure is very similar to the one employed for system mapping. The only difference regards the electrical resistance identification which is computed at the end following a simple theoretical approach summarized by the equation:

$$R = \frac{(V_{DCbusbars} - V_{DC})}{I_{DC}} \quad (5.5)$$

The post-processing procedure is the following;

5.5. Electrical Power Flow Mapping and Resistance Identification Test campaign implementation and Model identification

1. **Storage** → Variable signal is stored in a specific vector and a related time vector is defined.
2. **Extraction** → The four steady state region of the signal are extracted (TP11).
3. **Filtering** → The average value of the steady state regions is extrapolated (filtering case).
4. **Matching** → These collected filtered values are matched into tables and then plotted.
5. **Computing** → Resistance is computed by employing equation (5.5).
6. **Filtering & Averaging** → Computed values are filtered by averaging them in order to get a final identified value.

The employed measurements are collected into two different sections:

- **Section 2 - 20232310 - SuT_mapping_Dm0** → 12 runs with 12 different scaling factors for SuT motor and 0 for load motors.
- **Section 3 - 20232310 - SuT_mapping_Dmvar** → 44 runs: 2 scaling factors for SuT motor (employed in forward and in reverse mode) and 11 different scaling factors for load motors.

The three main identification results are focused on the power flow at the motors level (SuT inverter and both load motors). In particular, they are directly employed for the three 2-D *Ametables* which reproduce their power flow onto the model.

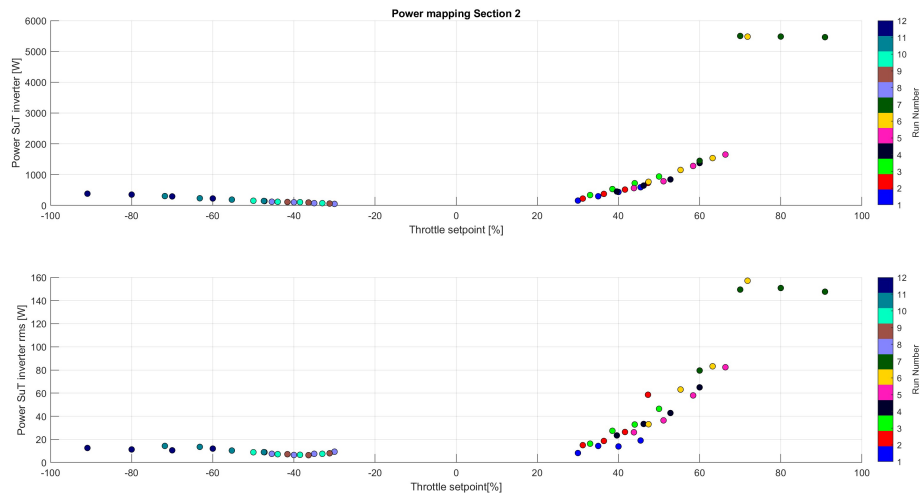


Figure 5.40: Power SuT Inverter from *Section 2*.

5.5. Electrical Power Flow Mapping and Resistance Identification Test campaign implementation and Model identification

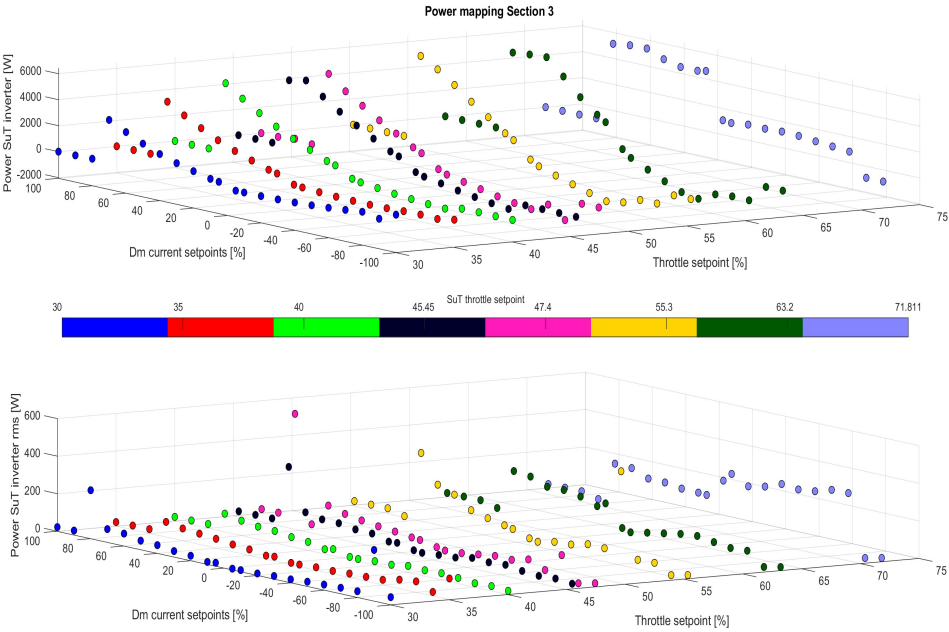


Figure 5.41: Power SuT Inverter from Section 3.

The figures 5.40 and 5.41 are the employed results for building the 2-D map for the power flow at the SuT inverter showed in figures 5.42 and 5.43.

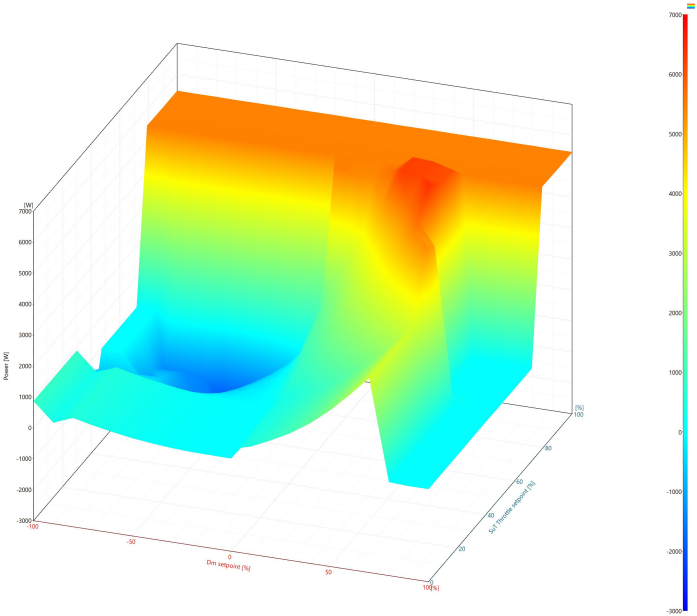


Figure 5.42: Power SuT Inverter Ametable.

5.5. Electrical Power Flow Mapping and Resistance Identification Test campaign implementation and Model identification

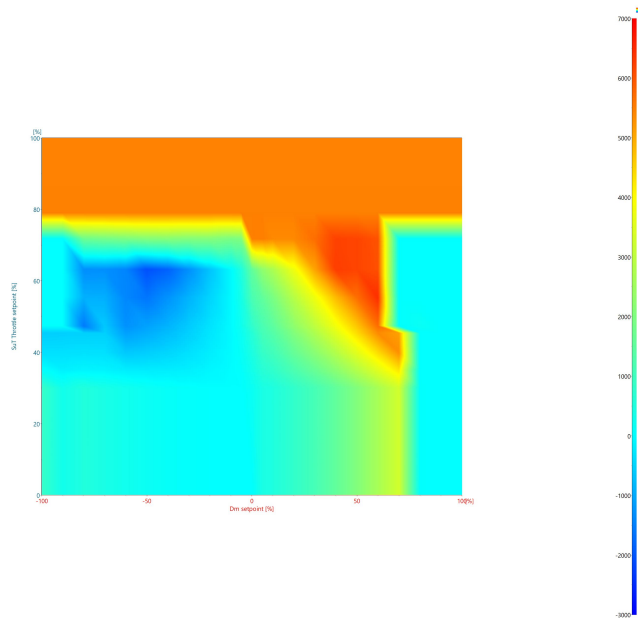


Figure 5.43: Power SuT Inverter *Ametable* - top view.

From figures 5.42 and 5.43, it is possible to highlight some interesting features of the electrical system: the power flow at the SuT inverter level reaches upper limit (red region over 80% throttle setpoint for every load motors setpoint) at 6000 W, instead the lower limit is about -1600 W and it is reached when load motors are regenerating (blue region).

For what concerns load motors the two power flow responses (L/R) are practically equal and for this reason just the results and consequentially the map of the power flow which characterizes the load motor L are reported.

Results are reported in figures 5.44 and 5.45.

5.5. Electrical Power Flow Mapping and Resistance Identification Test campaign implementation and Model identification

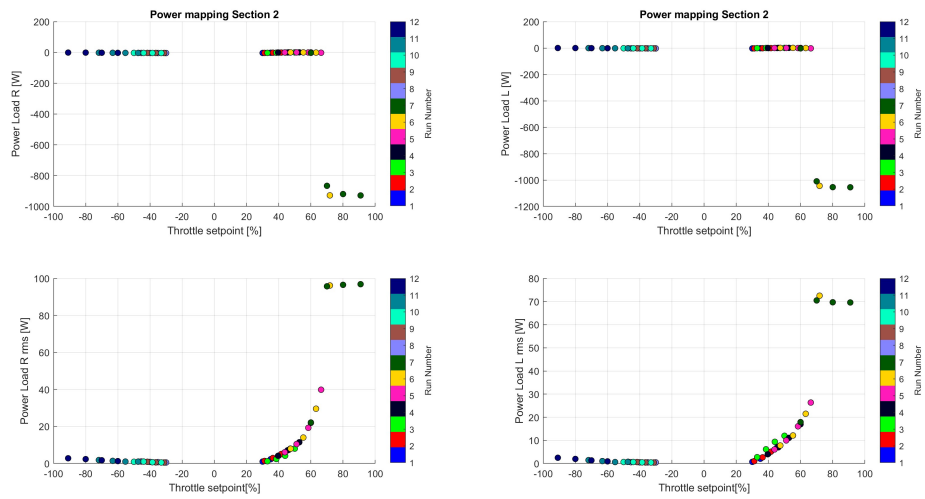


Figure 5.44: Power Load Motor L/R from *Section 2*.

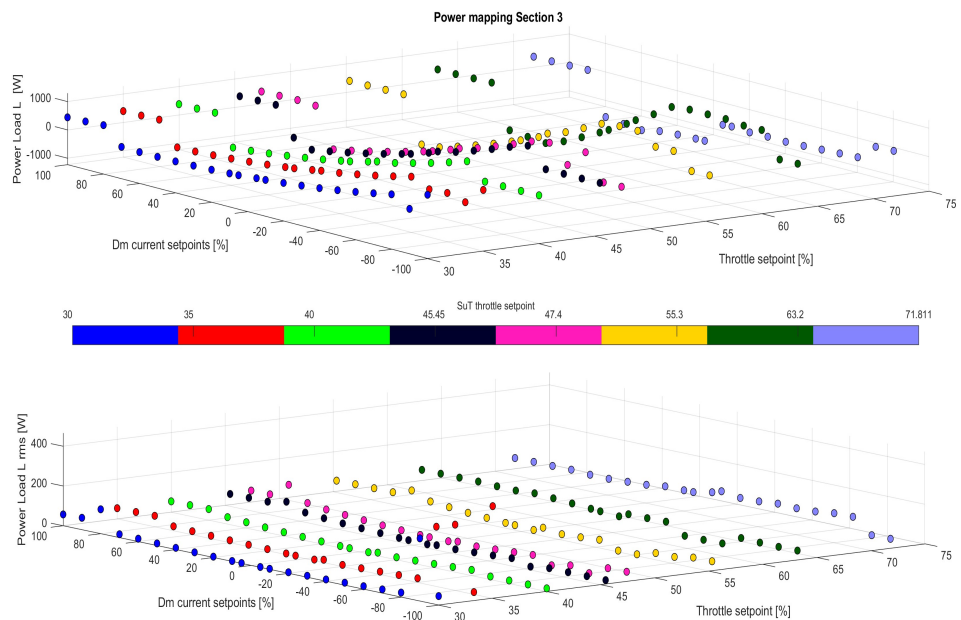


Figure 5.45: Power Load Motor L from *Section 3*.

5.5. Electrical Power Flow Mapping and Resistance Identification Test campaign implementation and Model identification

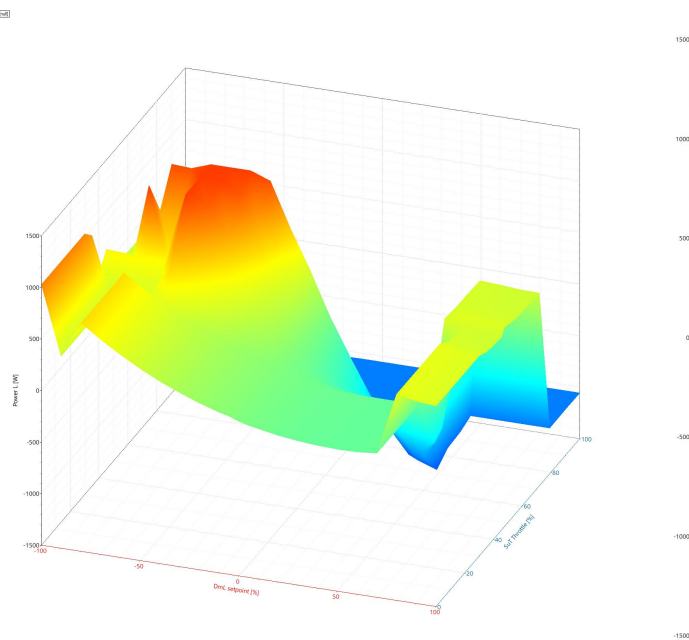


Figure 5.46: Power Load Motor L *Ametable*.

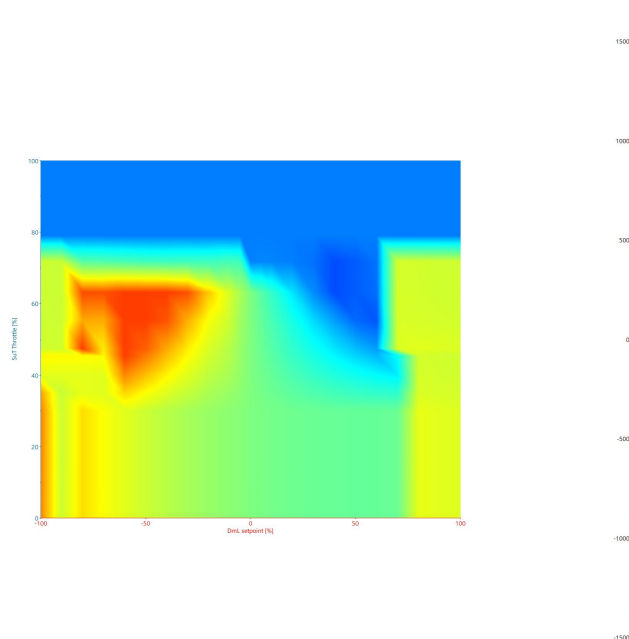


Figure 5.47: Power Load Motor L from *Ametable* - top view.

From these results, again, the 2-D maps are built up for each load motor. In this case just the 2-D map from load motor L is reported in the two figures 5.46

and 5.47.

Also in this case some important highlights about power flow at load motor level can be described: the lower limit is reached at high SuT throttle setpoints around -1100 W , instead, the higher limit is reached between 40% and 60% of throttle setpoint while load motor is regenerating and it is around 1250 W .

Moving to the resistance identification, at the end, from *Section 2* and from *Section 3* two different values are identified and then averaged in order to implement on the simulation model just a final definite value. They are reported in table 5.14. However, resistance values prove that clearly the losses in the path between the busbars system and the SuT inverter are not such relevant

Identified Resistance <i>Section 2</i>	Identified Resistance <i>Section 3</i>	Identified Resistance final
0.0166 Ω	0.0255 Ω	0.0196 Ω

Table 5.14: Resistance Identification results.

5.6 SuT Inverter Transient Analysis

The last identification problem is focused on the *Curtis 1232E/SE* AC controller which acts in speed controller mode (figure 5.48). The objective of this investigation is to understand the real effect on the speed of the controller and replicate it on the software model.

As explained in *chapter 3*, the SuT inverter receives the throttle voltage signal as input and turns it into a percentage amount according to its programmed parameters/maps (figure 3.2). The percentage amount of mapped throttle tells the AC controller the target speed according to the map presented in fig.5.7. The actual speed increasing/decreasing behavior (for reaching the target) is not random, but, of course, it follows specific rules imposed by parameters appropriately programmed by *Kyburz* on the device according to the requested performances.

Therefore, this investigation, practically, concerns:

1. Reading and analysing the datasheet of the SuT inverter to comprehend the actual effect of the parameters on the controller action.
2. Reading the programmed parameters on the *Curtis 1232E/SE* programmer.

5.6. SuT Inverter Transient Analysis Test campaign implementation and Model identification

3. Looking at the acquired data and compare the effective behavior of the SuT motor speed to the expected one according to the parameters.

Because the research interest is strictly on the SuT inverter controller according to different throttle inputs, the needed test runs, basically, are characterised by a specific test profile for the throttle setpoints and, instead, load motors setpoints are constantly set to zero. TP11 is employed, but it does not really cover all the speed/throttle cases (it will be explained better in the next pages) and for this reason other three test profiles are designed and integrated to the test campaign: TP12, TP13, TP14. TP14 is presented in fig.4.4, TP12 and TP13 are very similar to it, there are just some differences due to the specific investigated aspect.

Practically, indeed, the interested measured signals of this identification campaign are just the throttle and the SuT speed response as showed in table 5.15.

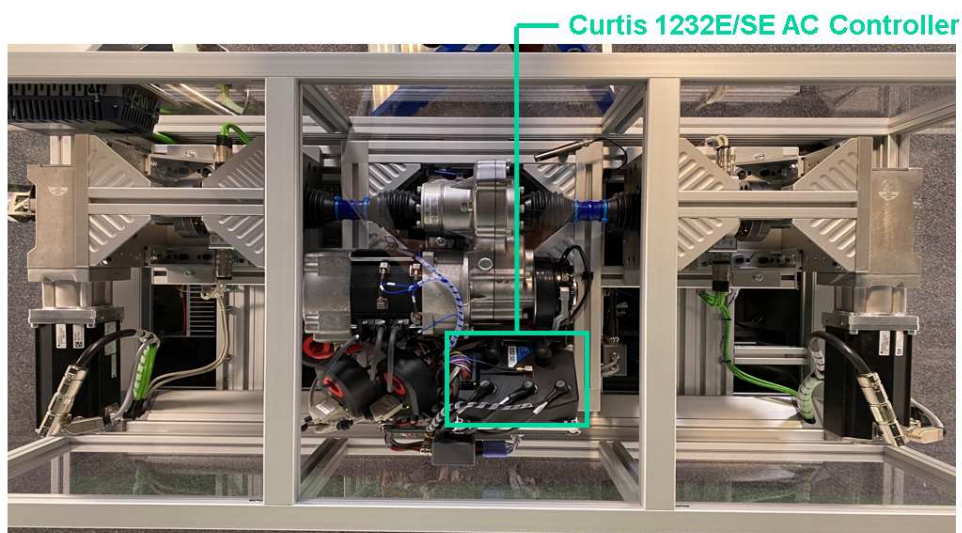


Figure 5.48: Curtis 1232E/SE AC controller.

Name	Variable
Throttle	Throttle Voltage
SuTMotorEnc	SuT Motor Speed

Table 5.15: SuT Inverter transient analysis measured variables.

The employed measurements are collected into two different sections:

5.6. SuT Inverter Transient Analysis Test campaign implementation and Model identification

- **Section 2 - 20232310 - SuT_mapping_Dm0** → 12 runs with 12 different scaling factors for SuT motor and 0 for load motors.
- **Section 7 - 20232410 - Transient_runs** → 31 runs: different scaling factors for SuT motor (employed in forward and in reverse mode) for three test profiles: TP12,TP13,TP14.

Before going into details for what concerns the post-processing and elaboration procedure, it is important to introduce the main important and investigated parameters (table 5.16) of the SuT inverter and describe their effects on the controller.

Parameter Name	Programmed Value
Max Speed Fwd	5000 <i>rpm</i>
Max Speed Rev	1000 <i>rpm</i>
Typical Max Speed	3300 <i>rpm</i>
HS/LS Fwd	70%/30%
HS/LS Rev	70%/30%
Accel Rate HS/LS Fwd	3.8 <i>s</i>
Accel Rate HS/LS Rev	3.8 <i>s</i>
Low Accel Rate Fwd	30 <i>s</i>
Low Accel Rate Rev	30 <i>s</i>
Neutral Decel Rate HS/LS Fwd	2.5/3 <i>s</i>
Neutral Decel Rate HS/LS Rev	2.5/3 <i>s</i>
Partial Decel Rate Fwd	10 <i>s</i>
Partial Decel Rate Rev	10 <i>s</i>

Table 5.16: SuT Inverter programmed parameters.

Approximately, the throttle operations are classified as full throttle acceleration when mapped throttle is over 90%, partial throttle acceleration when it is in between 10% and 90%, low throttle acceleration below 10%. The parameter functions are described below:

- *Max Speed Fwd/Rev* → defines the maximum requested SuT motor rpm at full throttle. Partially applied throttle is scaled proportionately; e.g., 40% applied throttle corresponds to a request for 40% of the set Max Speed Value. "Fwd" is for forward mode and "Rev" for reverse mode.
- *Typical Max Speed* → the typical maximum SuT motor speed of the test setup. This value does not need to be set precisely; an estimate will do. All of the vehicle response rates are normalized to *Typical Max Speed*.

5.6. SuT Inverter Transient Analysis Test campaign implementation and Model identification

- *HS/LS Fwd/Rev* → "High speed" sets the percentage of the *Typical Max Speed* above which the "HS" parameters will be used. "Low speed" sets the percentage of the *Typical Max Speed* below which the "LS" parameters will be used.
- *Accel Rate HS/LS Fwd/Rev* → "HS" sets the rate (in seconds) at which the speed command increases when full throttle is applied at high vehicle speeds. Larger values represent slower response. "LS" sets the rate (in seconds) at which the speed command increases when full throttle is applied at low vehicle speeds.
- *Low Accel Rate Fwd/Rev* → sets the rate (in seconds) at which the speed command increases when a small amount of throttle is applied. This rate is typically adjusted to affect low speed maneuverability.
- *Neutral Decel Rate HS/LS Fwd/Rev* → "HS" sets the rate (in seconds) that is used to slow down the vehicle when the throttle is released to neutral at high vehicle speeds. "LS" sets the rate (in seconds) that is used to slow down the vehicle when the throttle is released to neutral at slow vehicle speeds.
- *Partial Decel Rate Fwd/Rev* → sets the rate (in seconds) that is used to slow down the vehicle when the throttle is reduced without being released to neutral. Larger values represent slower response.

Moreover, TP12, TP13 and TP14 are added to collect data points for some specific cases which are not faced with TP11. They are reported in fig.5.49: full throttle acceleration, neutral throttle deceleration, partial throttle deceleration.

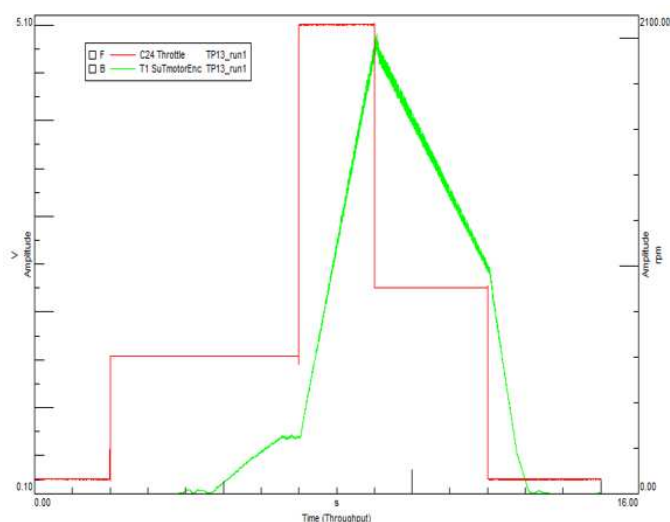


Figure 5.49: Example - TP13 *Testlab* results.

Approximately, the throttle operations are classified as:

- **Full throttle acceleration** → mapped throttle is over 90%.
- **Partial throttle acceleration** → mapped throttle is between 10% and 90%.
- **Low throttle acceleration** → mapped throttle is below 10%.
- **Neutral throttle deceleration** → throttle is at 0%.
- **Partial throttle deceleration** → throttle is in between 99% and 1%.

After understanding the effective way of reasoning of the SuT inverter controller, the identification problem moves to actual investigation on the real acquired SuT motor speed responses. Indeed, by exploiting these information, then it is possible to compute the actual rates on the test setup and compare them with the rates expected looking at the programmed parameters.

The post-processing procedure is the following:

1. **Storage** → Variable signals are stored in a specific vector and a related time vector is defined.
2. **Extraction** → Transient regions (throttle steps) are identified and starting/-final speed steady-state values are extracted.
3. **Computing** → The speed Δ are divided by the respective time intervals in order to compute, firstly, the acceleration and turning it into the rate value in seconds.
4. **Matching** → These collected rates are matched with the respective imposed throttle signal and plotted in order to identify the different controller cases.

So, by analysing the practical situation: the logic of the SuT inverter controller reads two inputs values: the amount of mapped throttle in percentage and the related target speed value. These two inputs are references for it in order to impose a specific rate parameter. Of course, in the model logic, this is replied with a switching logic that reads the values and understands in which switch case the system is for imposing the correct rate parameter. The *Amesim* logic is presented in figure 5.50.

5.6. SuT Inverter Transient Analysis Test campaign implementation and Model identification

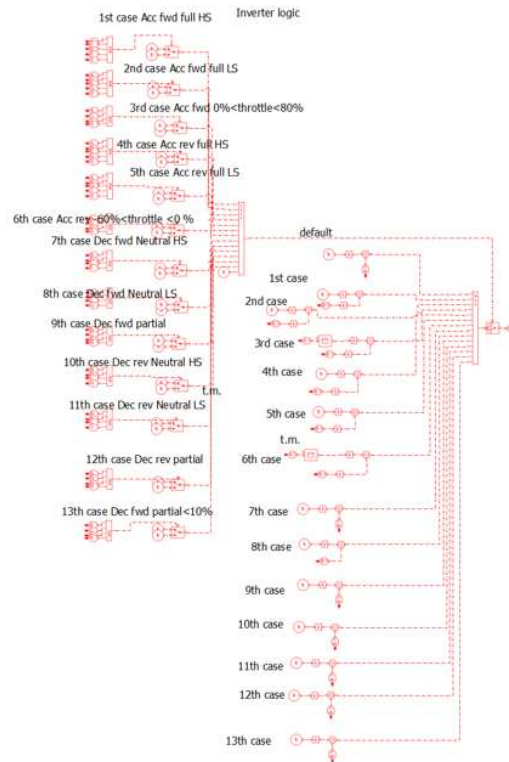


Figure 5.50: Switching Logic *Amesim* representation.

Post processing results are in figures 5.51 and 5.52. Table 5.17 summarizes the identified parameters.

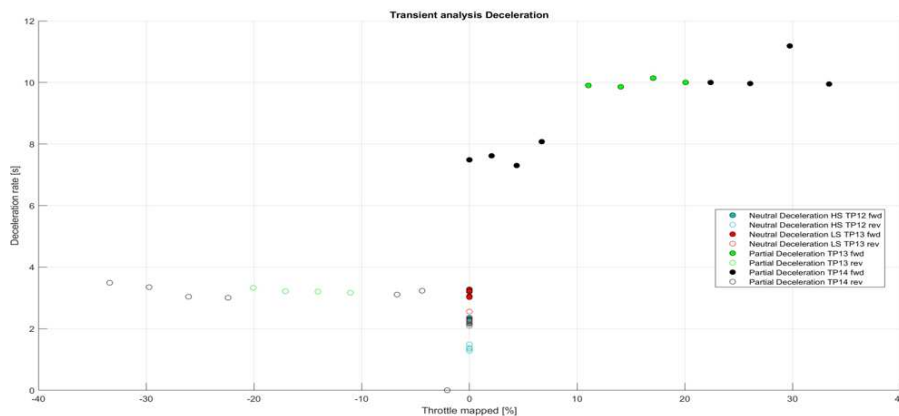


Figure 5.52: Deceleration rate results.

The identified parameters presented in table 5.17 are then employed into the

5.6. SuT Inverter Transient Analysis Test campaign implementation and Model identification

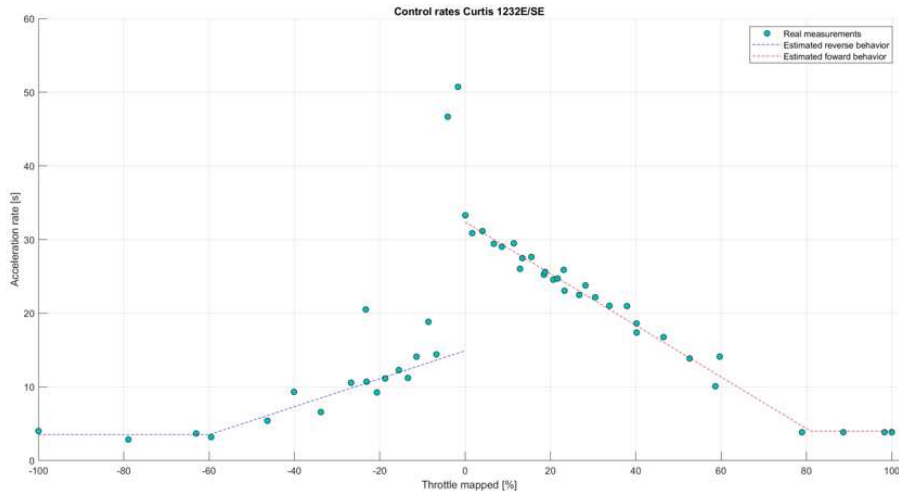


Figure 5.51: Acceleration rate results.

Parameter Name	Identified Value
Max Speed Fwd	5000 <i>rpm</i>
Max Speed Rev	1000 <i>rpm</i>
Typical Max Speed	3300 <i>rpm</i>
LS Fwd	40%
LS Rev	20%
Accel Rate HS/LS Fwd	3.9845 <i>s</i>
Accel Rate HS/LS Rev	3.5125 <i>s</i>
Low Accel Rate Fwd	32 <i>s</i>
Low Accel Rate Rev	12 <i>s</i>
Neutral Decel Rate HS/LS Fwd	2.2693/3.1399 <i>s</i>
Neutral Decel Rate HS/LS Rev	1.3724/2.2993 <i>s</i>
Partial Decel Rate Fwd	9.9752 <i>s</i>
Partial Decel Rate Rev	3.2641 <i>s</i>

Table 5.17: SuT Inverter identified parameters.

switching logic: the logic imposes to the actual speed a specific rate for increasing/decreasing according to these identified results.

It is relevant to compare the identified results with the initial programmed setup: this clearly states that in reality the behaviour of the controller differs from the expected one.

Indeed, the most important differences are:

- *HS Fwd/Rev* are not identified because speed never overcomes the "High Speed" threshold.
- *LS Fwd/Rev* identified parameters are clearly different from the programmed parameters: "LS Fwd" threshold is higher than the expected one. "LS Rev" threshold is lower than the expected one.
- Generally, for all the rates parameters, the identified result in forward operations is very close to the programmed one, instead, in reverse operation the results are clearly different.

The reasons which cause these discrepancies are not always really clear and are not really investigated in this thesis research. For further improving the model, probably, it will be necessary to investigate more in details the programmed parameters by *Kyburz* by looking for more information from the vehicle manufacturer.

Chapter 6

Model validation

This chapter introduces, describes and comments the validation results of the SimRod E-Powertrain test-setup simulation model (showed in fig.6.1).

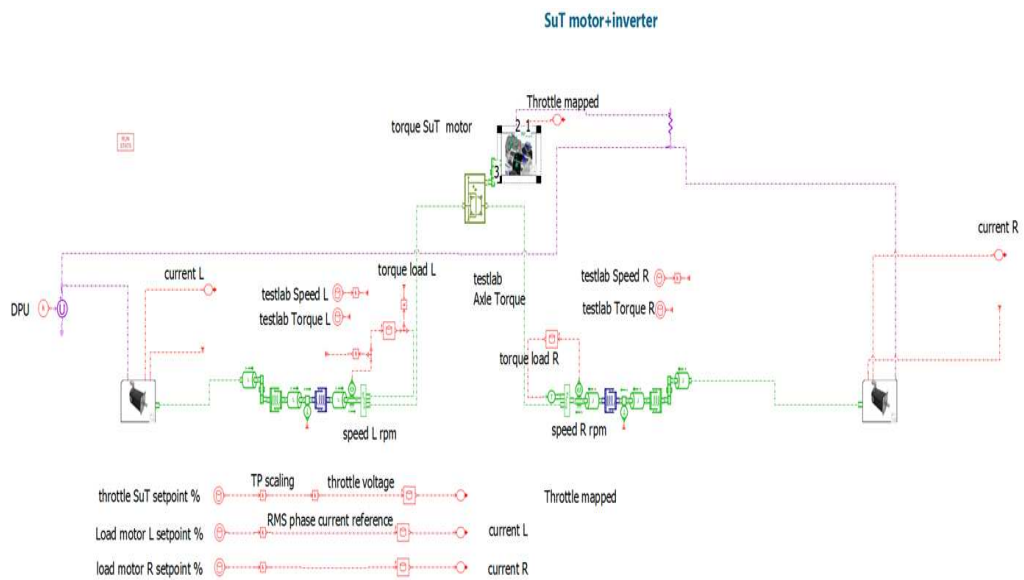


Figure 6.1: SimRod E-Powertrain test setup *Amesim* draft model.

Indeed, validation phase is one of the most relevant part of the modelling methodologies and, specifically, of this research activity. Validation can reveal explicitly every significant feature of the model: this procedure states where the model works in the correct way, where the model needs to be improved, it gives a general outlook of the model performances and capabilities.

It is very important to mention the fact that, during this thesis project, the

SimRod E-Powertrain test setup *Amesim* model is just the starting draft version of the definitive one (also because just the longitudinal dynamics are investigated in this work). The model will be further improved and developed in order to predict in the most accurate way the test setup response.

Generally, the most significant feature in this thesis project is the accuracy: for preventing risks, it is very important that the model is reliable, the simulation data response has to be as similar as possible to the real response of the system. For this reason, the results that will be showed in this chapter will be evaluated mostly for the accuracy of the software response with respect to the acquired real data.

In lots of cases, in MBT, the real-time capability of the designed simulation model is another important requirement. Real-time capability means that the simulation runs at the same rate and time interval of the physical system operation that wants to simulate. This property can be very useful especially for HIL test solutions by allowing to make modifications and changes on the system earlier in the development process: this is a general benefit for reducing cost and time efforts. However, in this thesis project, this requirement is not crucial because the shape of the transient/steady-state regions of the reproduced signals is the most important achievement more than the specific run-time of the simulation.

As regards this research, the validation phase can be, basically, divided into two subphases:

- **TP11 simulation** → the model is simulated with the most employed test profile, TP11, to verify and compare results with respect to the data collected from the identification runs.
- **TP07 validation** → the actual validation of the model: SimRod E-Powertrain test setup *Amesim* model is simulated by employing another completely different test profile to evaluate its versatility (if it is valid in every case) and to look at its critical aspects.

Overall, the model output results which will be showed in this chapter are basically the simulated power (mechanical and electrical) responses of the system (appropriately compared to the *Testlab* real acquired responses). In particular, the specific interested responses are:

- **SuT Motor Speed**
- **SuT Axle Speed**
- **SuT Axle Torque**

- **SuT Inverter Electrical Power**
- **Load Motor Electrical Power**

These quantities are the most relevant for demonstrating the actual properties of the simulation model.

6.1 TP11 Simulation

The first validation stage is discussed in this section. Practically, the *Amesim* model is simulated by implementing on it the TP11 as input.

Specifically, in this document, the results from *Section 2 - run 6* will be presented: this TP11 run is characterised by SuT throttle setpoints with a scaling factors equal to 0.79 and load motors setpoints at 0 (it is one of the most complete run in terms of SuT operating range). Moreover, the results will be presented with *Amesim* plots in which:

- **Red curve** → Real acquired response signal exported from *Simcenter Testlab*.
- **Blue curve** → Simulated response signal.

First results concern the SuT motor speed response (figures 6.2 and 6.3). The map presented in 5.7 is implemented on the final model. As we will see from the results (fig. 6.2), this map gives few issues for what concerns the region around 0% throttle: basically, from the identification process, the SuT motor speed follows a very steep jump from 0 to 200 *rpm* and this jump, then, is really visible on the results. In reality, this jump does not exist because the physical inverter behavior, for turning the mapped throttle input percentage into the speed target for its controller, consists in just taking a reference speed value indicated by a parameter (*Max Speed Fwd/Rev*) which corresponds to the full throttle operation and match the other amounts of throttle by scaling proportionally the speed. The big problem in replying this second real approach into the model is that actually the programmed expected behavior, as stated in **chapter 5**, differs from the real system behavior and, for this reason, the first path is chosen.

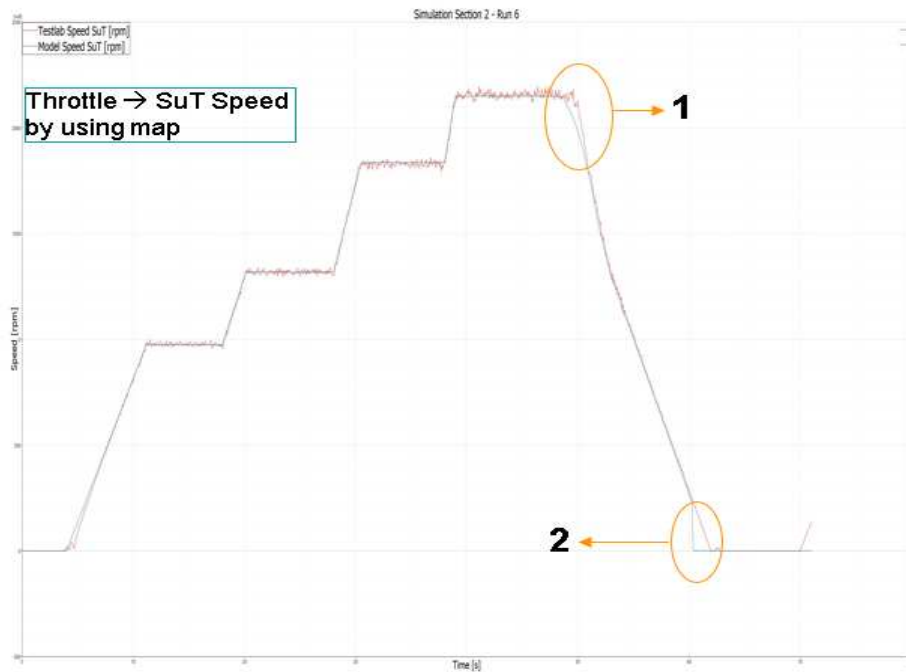


Figure 6.2: SuT Speed *Amesim* model results - TP11/run6 - employing map in fig.5.7.

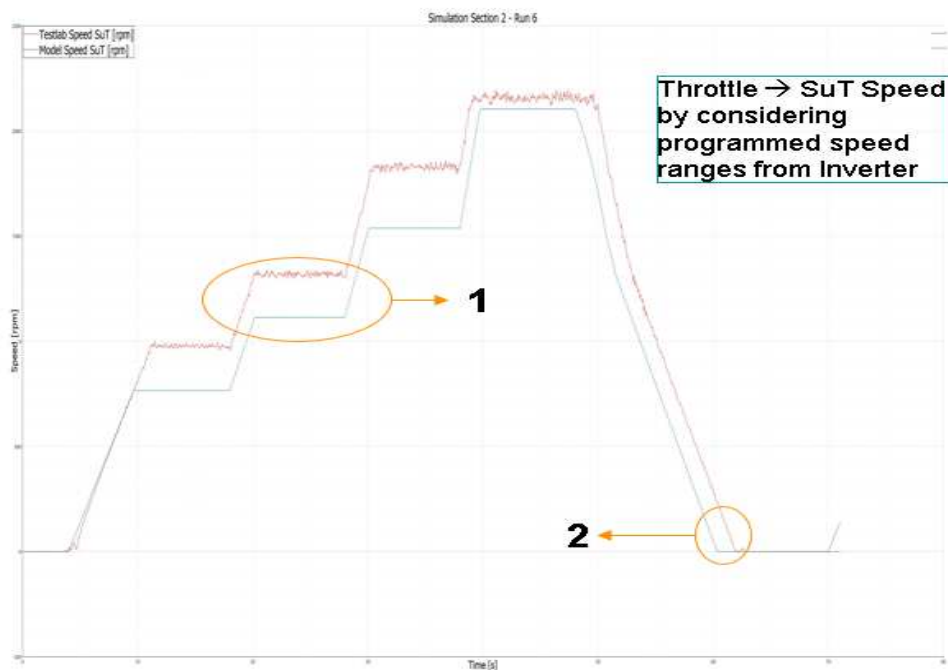


Figure 6.3: SuT Speed *Amesim* model results - TP11/run6 - employing "parameter" approach.

In fig.6.2, it is possible to look at the SuT motor speed response when the previously discussed map is employed. Overall, looking at the real and at the simulated signals, it can be said that the speed of the real system is tracked in the correct way for what concerns both transient and steady-state. "1" and "2" are the two most critical points. The first mismatch (at the beginning of the deceleration phase) probably depends on different factors: the speed is at the limits of the SuT motor capabilities, the filtering action has a relevant influence (the real signal is obviously noisy, especially in transient phases), a delay in the SuT speed response with respect to the throttle signal has been seen (probably due to the controller performances) and for this reason, the real curve starts to decrease after the simulated signal (the model controller is theoretically ideal). The second mismatch, instead, depends just on the previously mentioned reasons: the employed map steps which is directly reproduced into the model response.

Fig.6.3 is practically reported to highlight, generally, the fact that the second approach presented before is not such accurate. Indeed, in point "1" and more or less in every steady-state region, the discrepancy between the real and the simulated signal is evident and not negligible. Point "2", instead, shows that, of course, the second approach deletes the error connected to the employed map.

Every other response of the model is obtained by employing the map approach. Besides, reported speed and torque results at the SuT axle are referred to the L semi-shaft (the response considerations are practically the same on the right side). Figures 6.4 and 6.5 are the SuT axle model results.

The considerations on the axle torque and on the axle speed are practically the same. Results show a global nice accuracy for both transient and steady-state regions: this practically means that also the friction identified model at the axle level works in the correct way.

In figure 6.4 point "1" underlines the greatest mismatch between the simulated and the real torque response. Reasons are listed here: as stated previously, in the fourth step SuT limits are reached and the noise, especially for torque measurements, is very high so that the accuracy is difficult to evaluate and, moreover, friction identification is not really completed in this campaign because the friction analysis at the differential side is missing. In figure 6.5 point "1" highlights again, basically, the mismatch due to friction analysis. Surely, with further identifications at the differential side, the accuracy will be increased. For both responses critical point "2" depends on the SuT motor speed map mentioned before.

For what concerns, specifically, transient response, the accuracy is quite high,

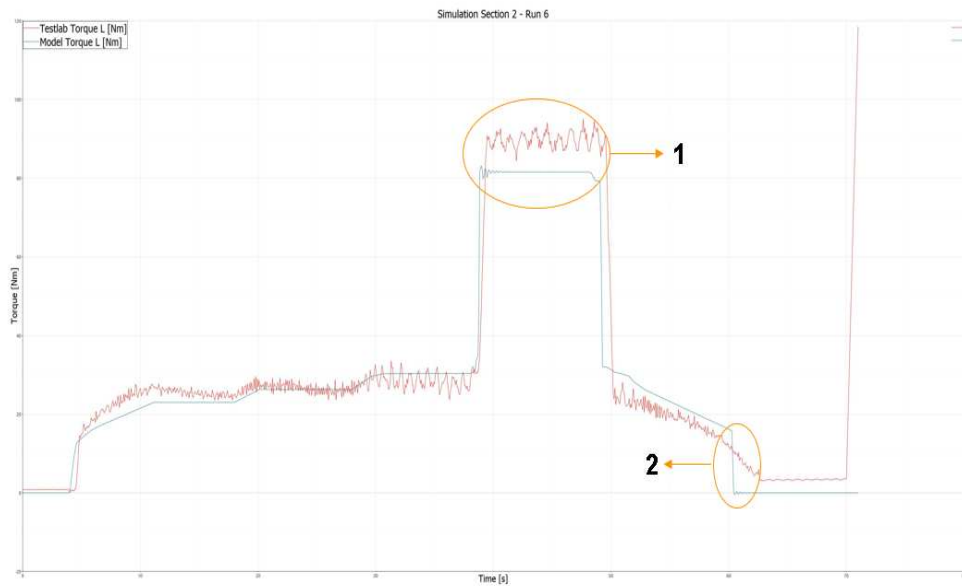


Figure 6.4: Axle Torque L *Amesim* model results - TP11/run6.

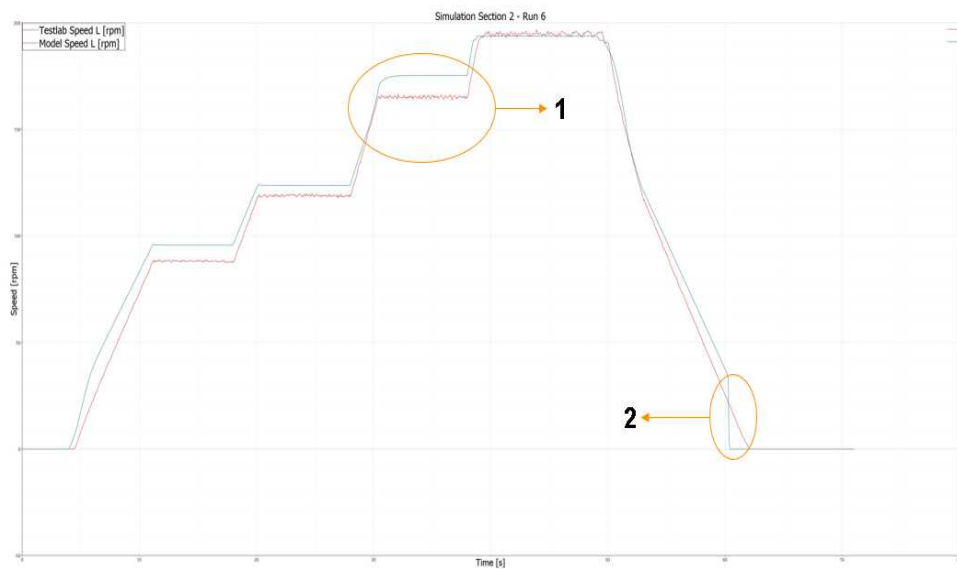


Figure 6.5: Axle Speed L *Amesim* model results - TP11/run6.

the mismatch is again very influenced by the lacks in the friction identification, but the most interesting result regards the general increasing/decreasing slope of the simulated response which is very close to the real one.

In fig.6.6 and fig.6.7, the electrical power response at the SuT inverter and at

the load motor L of the simulation model is presented (the response at the load motor R is practically almost equal to the one at the left side).

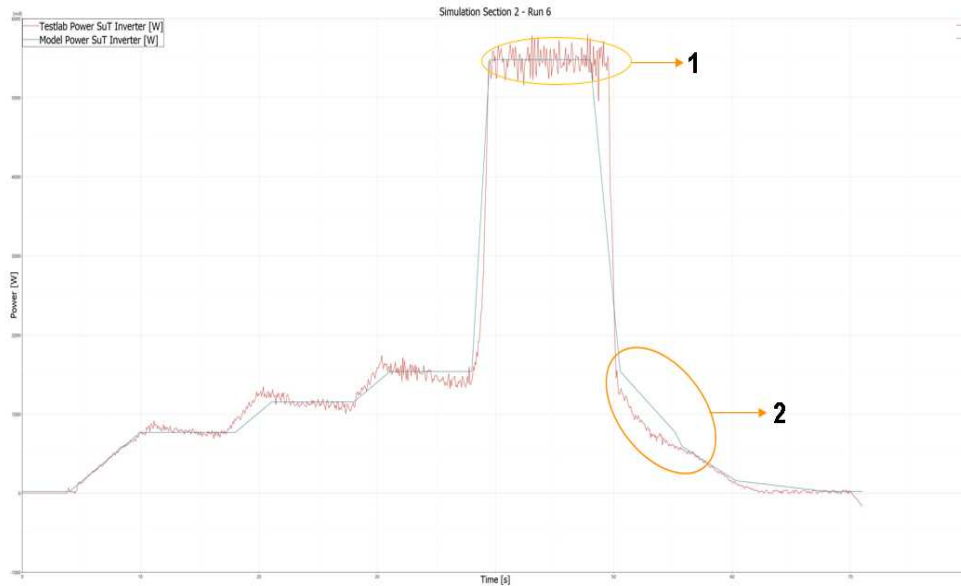


Figure 6.6: SuT Inverter Electrical Power *Amesim* model results - TP11/run6.

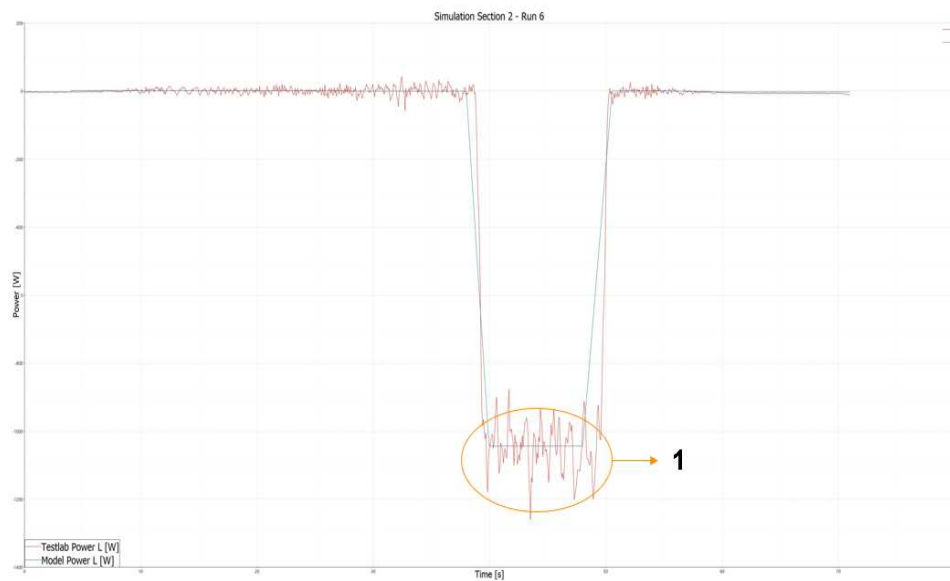


Figure 6.7: Load Motor L Electrical Power *Amesim* model results - TP11/run6.

Before commenting more in detail the results concerning the electrical power, it is important to underline a crucial fact: in reality, the current measurements are

quite noisy and the filtering action, especially from a post processing point of view, simplifies a lot the real physical situation.

Going more specifically to figure 6.6, it is possible to notice the two critical points: in point "1" the SuT operating limits are reached so that the noise is much larger and the track of the simulated signal can not be such accurate. Moreover, in point "2" the same reasons create a visible mismatch between the real and the simulated response, plus further investigations on the current decreasing/increasing rates are needed in order to improve the accuracy level of the simulation.

In figure 6.7, point "1" is critical again for the noise of the measured current at SuT limits.

Overall, the level of accuracy in the simulation of the electrical power of the system is quite high, even if it needs further improvements and finishings. This means that the identified and built up maps work in the correct way.

At the end, it is possible to state that the accuracy result is very good especially for the steady-state behavior of the system, except for the axle variables because of the future needed friction investigations. Transient response is reproduced quite nicely too, but the model surely needs more improvements and/or developments.

6.1.1 TP07 Validation

This part of the project thesis is the final validation stage of the model. For this reason, a test profile different from the one used for the identification process, is used in order to have more insights on the simulated response of the model.

In this case, for this specific validation, TP07 is employed. It is called "Demo run" because this test profile is characterised by a large and varied number of setpoints for both the SuT throttle and the load motors current. Indeed, there is a significant presence of acceleration/deceleration phases and the system behaves in motoring/regenerating mode. Indeed, for these features, probably, it is the most suitable for the validation phase. It is reported in fig.6.8.

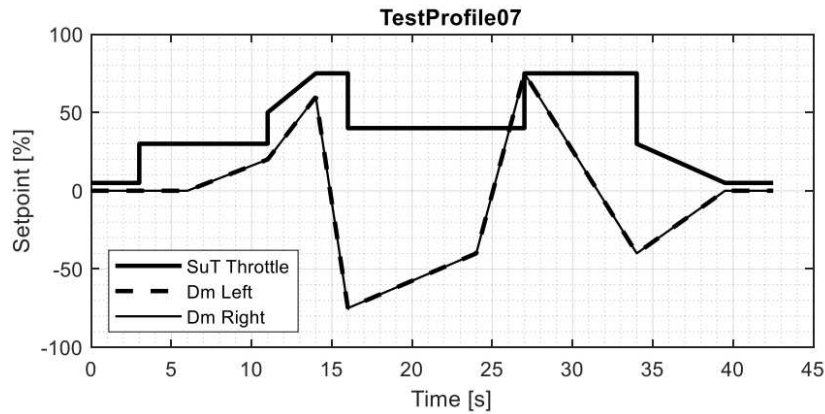


Figure 6.8: Test Profile 07 - Demo Run.

Results are showed in the same previous way:

- **Red curve** → Real acquired response signal.
- **Blue curve** → Simulated response signal.

Figure 6.9 shows the results concerning the SuT motor speed. Immediately, it is noticeable that the accuracy is not such good as for the previous section (TP11 simulation): some transient/steady-state regions of the real acquired signal are tracked in a proper way, but other regions are not exactly followed. In particular, the deceleration phases are the most critical regions, it seems that the simulated response anticipates the real one. Moreover, some nonlinear transient phases are other points which need more attention.

The described problems, probably, suggest that more investigations on the system transient responses are needed, especially, for what concerns inertia and inverter rates. Indeed, TP07 is characterised by strong accelerations/decelerations in which the transient effects coming from inertia and from the inverter operations are not negligible and, besides, these features are very sensible to the specific operation of the system so that these effects become very relevant. Plus, another important further improvement will be given by more identifications on the SuT response when it works in regenerating mode: indeed, an important region in which the mismatch between the simulated and the real respons is largely visible is the middle part of the plot in fig.6.9 in which, accordingly to TP07, load motors are in regenerating operation.

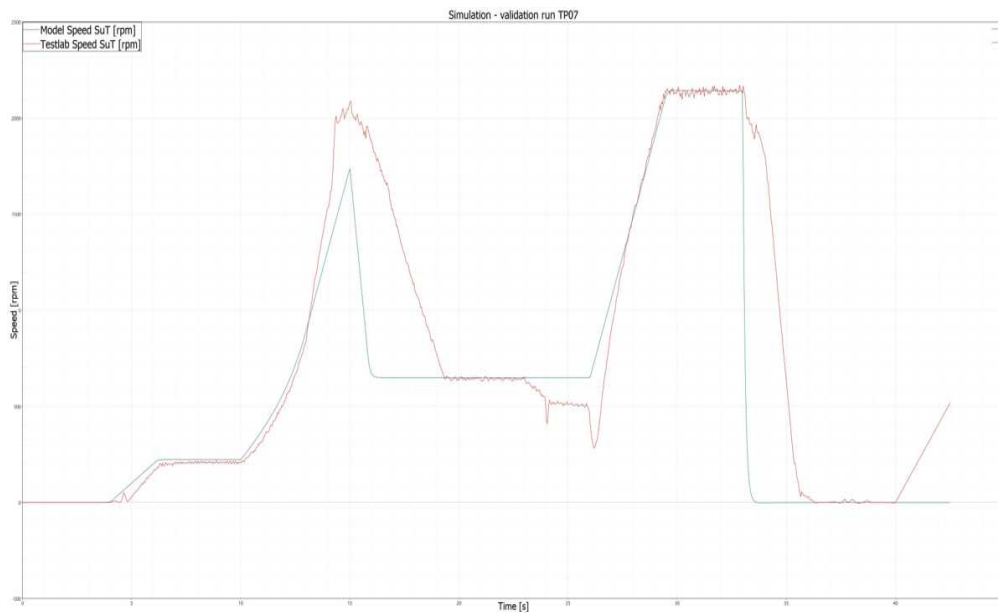


Figure 6.9: SuT Speed *Amesim* model results - TP07.

Figures 6.10 and 6.11 present the axle torque/speed response of the system.

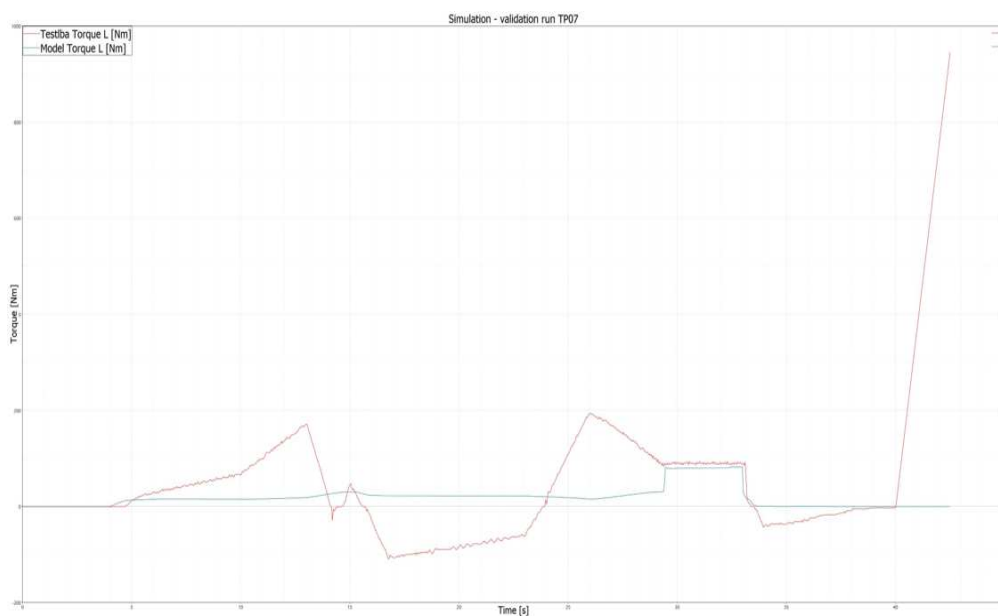


Figure 6.10: Axle Torque L *Amesim* model results - TP07.

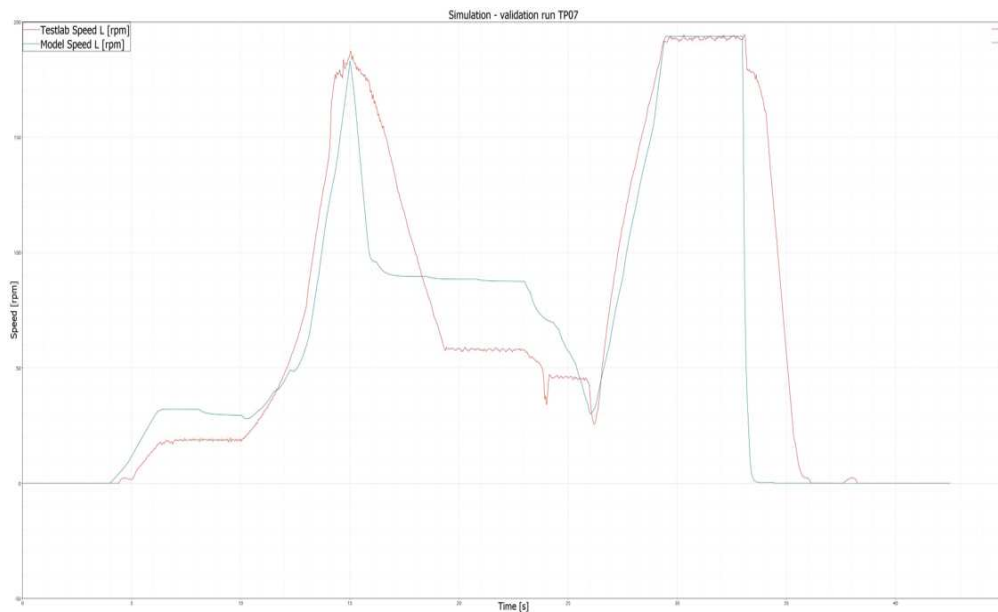


Figure 6.11: Axle Speed L *Amesim* model results - TP07.

Generally, the problems discussed before for the SuT motor speed are again present into the responses of these variables and, in some cases, their effects are accentuated.

Overall, some steady-state and transient regions, specially for the axle speed, are tracked in the correct way (acceleration regions are tracked better than deceleration as before).

The mismatches, here, are wider. It is very likely that the inertial problems are more relevant in this case and this is mostly noticeable by looking at the axle torque: the inertial contribution is probably more significant because of the strong accelerations/decelerations which characterise the test profile and this can cause visible issues in the software computation of the simulated signal. Another important contributions that can create these problems could be, surely, the couplings stiffness model which is not such reliable and precise, as stated in the previous chapter.

To conclude the discussion about the results concerning the SuT axle, obviously, the lack of identifications for regenerating operations does not help for the accuracy point of view.

Figures 6.12 and 6.13 show the electrical power results.

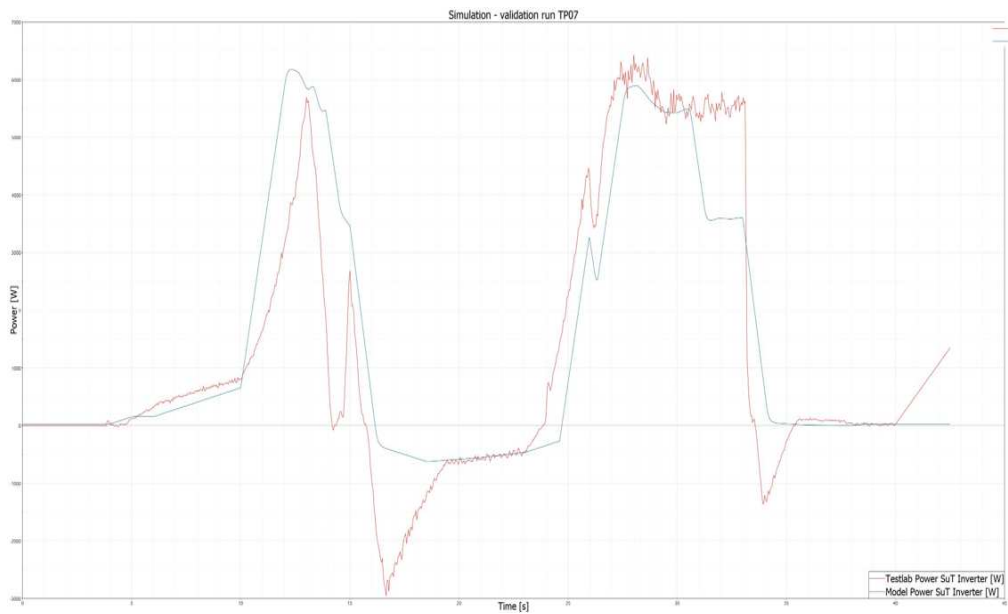


Figure 6.12: SuT Inverter Electrical Power *Amesim* model results - TP07.

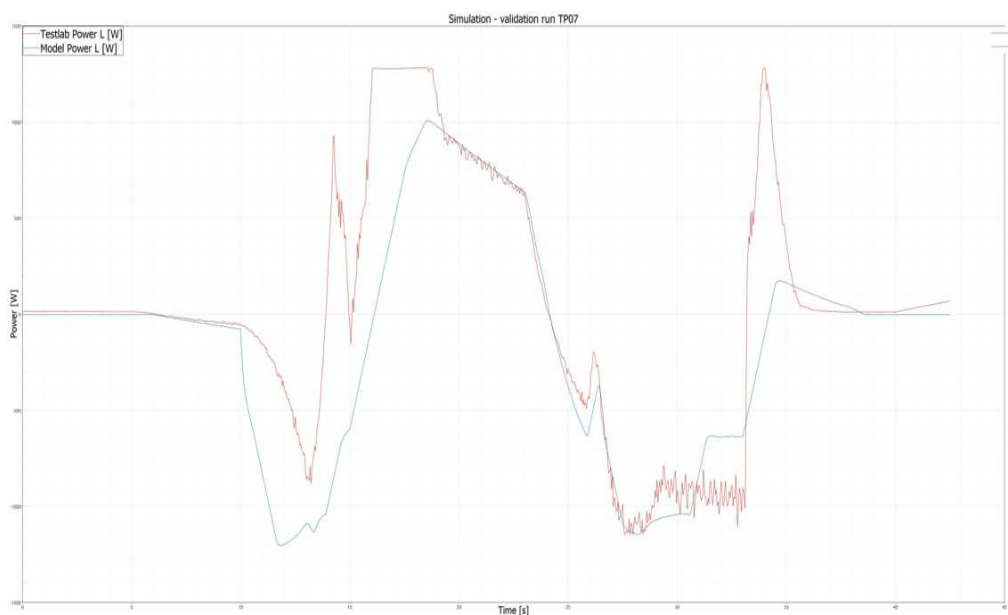


Figure 6.13: Load Motor L Electrical Power *Amesim* model results - TP07.

For what concerns the electrical power response of the system, the simulated response (for both SuT inverter and load motors) tracks the real one in a more or less accurate way according to the identification research made during this thesis project.

Indeed, surely, the output signal of the model can be improved and its accuracy can have an higher level. The improvements, probably, will concern the 2-D maps employed onto the model described in the previous chapter and will be strictly connected to the more unknown operating scenarios of the SuT: the regenerative operating mode, some specific transient operations and some operations at the limits of the system capabilities in which the general noise of the system increases significantly and a stronger filtering action will be needed.

TP07 is a very complete test profile which covers all the SuT operating points previously mentioned and, for this reason, perhaps, the mismatch of the results is such evident.

At the end, considering the initial perspective of the research project, the overall accuracy of the validating simulation is coherent with the expectations. The model is capable to predict in a first partial way the response of the SimRod E-Powertrain test setup to some specific input setpoints, but, of course, to be more definite and to improve its accuracy, further researches and analysis are needed to perfect the model for getting more reliable and safe results. However, a first rough de-risking estimation on the system longitudinal dynamics operations can be done and this is an important preliminary goal which has been reached.

6.1.2 Simulation Time Performances

The main important requirement for the model simulations is the accuracy and the reliability of the reproduced system responses. The real-time capability, at this stage and, specifically, for this thesis project, is not really a priority.

Indeed, the offline predictive model of the SimRod E-Powertrain test setup wants to give in output the system response before running real test scenarios on the final XiL test setup. Of course, a real-time simulation with the best possible level of accuracy will be the perfect achievement, but a larger number of identification campaigns is needed for collecting more insights and build up a more finite model.

For this reason, as regards simulation performances, the most interesting achievement of the entire research consists in the fact that the *Amesim* model is fast enough in terms of computation time so that the simulation runs in a trouble-free way. This reveals some important model features: the fact that the model does not present annoying simulation discontinuities among the components, the fact that the model is built up with a practical and smooth approach.

Figure 6.14 shows the computation time of a specific simulation run (for every validation run CPU time results are practically very similar). As indicated in the figure 6.14, the computation time of the control process unit is very low with respect to the effective time of the run (about 70s). This result reveals the regularity of the simulation model and its effortless implementing way.

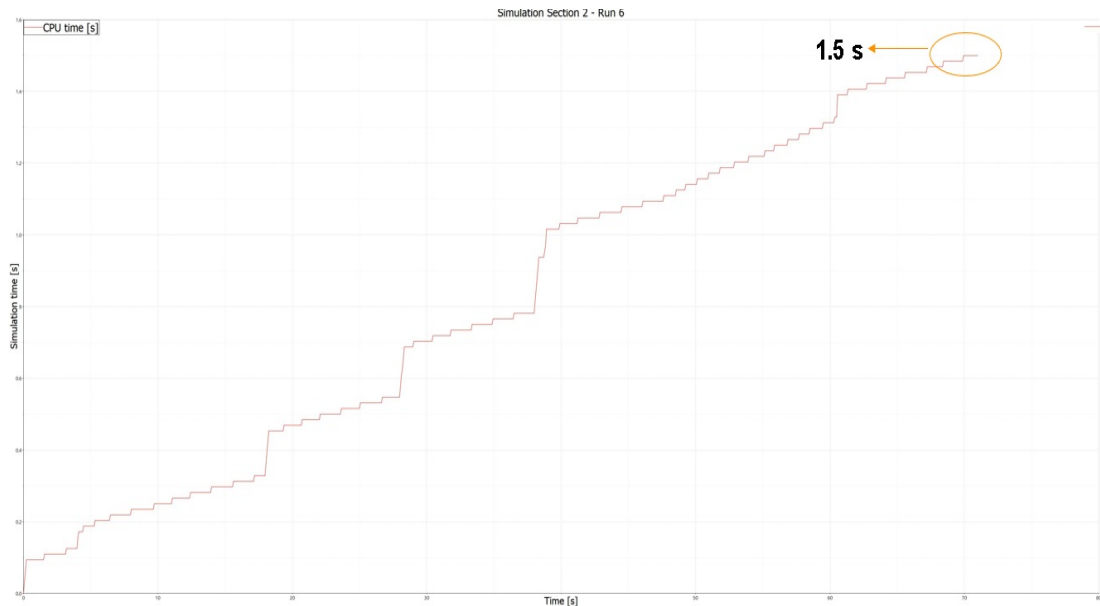


Figure 6.14: CPU time *Amesim* model - TP11/run6.

Chapter 7

Conclusions

The research project presented in this document has been conceived with the starting proposal to integrate the development of a mechatronic system test setup with a model-based approach. To be precise, these kind of systems (in this specific case the protagonist is the EV powertrain) are facing new testing methods which have the important purpose to reduce the production efforts in terms of time and money. These novelties act on the earlier design stages of these mechatronic systems by exploiting XiL testing functionalities and simulation models are crucial protagonists in order to develop them.

The important goal of the work has been to generate the software simulation model of the SimRod E-Powertrain test setup for the off-line prediction of the power flow (mechanical/electrical) of the system in longitudinal dynamics in order to avoid damages and risks on the physical test bench. This off-line predictive model is an important necessary integrative part for the evolution of the XiL test setup. The model needs to be the starting sketch of the test setup in a software environment which at least gives a coherent simulation result characterised by a fair accuracy and by a reduced simulation time.

The development of the SimRod E-Powertrain test setup has passed through several important steps which are presented and described in detail in this thesis document: the analysis and observation of the test setup, the definition and implementation of the measurements campaign, the collection and elaboration of real acquired data, the actual identification and modelling phase and the final validation of the simulation system.

The analysis and the observation of the physical test setup has showed immediately important features and characteristics and the observation and studying of the physical instrumentation has allowed to understand how to define the

test campaign and the critical and crucial points to identify in order to reach the final goal. The identification part, instead, has revealed relevant information and has suggested other needed researches for improving and elaborating the model.

Specifically, for what concerns the features of the model:

- **System Mapping** → The maps needed for turning the input setpoints into the effective input variables of the system are identified. The throttle maps at the SuT inverter side are correctly replied on the simulation model. The current/torque maps at the load motors are built up with a more "virtual" approach and needs to be improved.
- **Friction Identification** → The campaign has identified a correct friction model at the SuT axle level which is correctly reported on the model, but more investigations are needed in different crucial points of the system in order to reduce the mismatches.
- **Inertia Identification** → The moments of inertia of the three motors are identified from the test campaign, while the one which characterizes the torque flanges is taken from the datasheet. The inertial effects are minimal so that the parameters identification is not easy and, surely, not complete.
- **Torsional Stiffness Identification** → The torsional stiffness of the flexible couplings at the drive shaft side is identified and the stiffness parameter of the torque flanges is taken from datasheet. Because of the issues related to some sensors, the stiffness identification needs to be improved in order to individuate a more precise parameter. However, the influence on the simulation results is partially relevant.
- **Electrical Power Flow Mapping and Identification** → The electrical power system identification has important results which are used to reproduce with accurate performances what really happens into the physical test setup. The regenerative operating mode of the EV powertrain test setup is not really analysed and will be needed for further improving the simulation model.
- **SuT Inverter Transient Analysis** → The AC controller behavior has been studied and identified from datasheet and measured data and, consequentially, added to the model. The switch logic reproduces correctly the SuT inverter reasoning way into the model.

At the end, it is possible to state that the first *Amesim* sketch model of the SimRod E-Powertrain test setup shows an initial enough accurate predictive simulation of the system general longitudinal response, but, however, more validation

runs are needed in order to collect results for a large number of specific cases.

The accuracy of the prediction needs surely to be improved and some future investigations are crucial stages for getting this objective. In particular, as regards the mechanical power flow, the identification on some mechanical system parts (e.g. differential) for what concerns friction are necessary in order to reproduce the real effects of this important system features. For what regards the electrical power flow, instead, it is very relevant to reduce the noise of the measurements in order to further increase the accuracy which is, overall, already at a good level.

It is essential, also, to introduce the future developments that will be needed for improving the model, firstly, and to contribute to the evolution of the XiL operating mode of the powertrain test setup. They are listed here:

- **Longitudinal Dynamics Identifications** → Other identifications need to be developed in order to have a complete idea of the system response for what regards longitudinal dynamics.
- **Different Test Profiles Validations** → More validation runs are required to have a more detailed overview of the adaptability of the simulation model.
- **Lateral Dynamics Identifications** → Lateral dynamics will be investigated and identified to make even more total the final model.
- **Vehicle and Road Emulation** → The vehicle and road digital twins development will be completed in order to be integrated to the XiL test setup. This stage is crucial for emulating real test driving environment.

is replied into the software environment. It must be previously specified that the *Amesim Supercomponents* are, basically, special blocks which contain a subsystem of elementary components. Firstly, the main parts of this sketch can be highlighted:

- **Input Setpoints** → Setpoints maps.
- **Load Motors *Supercomponents*** → The *Supercomponents* whose content is the load motors sketch.
- **SuT Motor+Inverter *Supercomponent*** → The *Supercomponent* whose content is the SuT motor sketch and the logic of the inverter.
- **Electrical Power system** → The electrical sources, resistances and maps of the simulation model.
- **Differential+SuT axle** → All the employed components for sketching the connections and the main identified mechanical parts of the system.

Specifically, for what concerns input setpoints, it is needed to look at the bottom part of the sketch in figure A.1. The three setpoints (the SuT throttle and the load motors current setpoints) are defined through a signal source whose content is the specific test profile multiplied by a gain (the scaling factor). In particular, the throttle setpoints for the SuT motor are turned into the voltage signal and the final mapped one through an *Ametable*. Instead, moving to the load motors current setpoints, they are just turned into the current signal through an *Ametable*. The final signal is then used as an input for the related motor *Supercomponent*.

While, looking at the left, the starting point of the electrical power system is represented by the Power supply voltage source ("DPU") which is then connected to the three *Supercomponents*. The connection with the SuT motor+inverter subsystem pass through the resistance component.

The differential+SuT axle is represented by the differential component whose input is directly connected to the output of the SuT motor+inverter *Supercomponent* through a reducer component (that represents the gearbox). Instead, the two differential outputs are connected to the two semishafts subsystems through the two friction models of the SuT axle (*Ametables*) directly connected to two load components (which reply the physical/mathematical effect of the moment of inertia of the SuT motor splitted in two, half of the contribute per semi-shaft). Then, it is possible to notice the replication of the two torque flanges through a load component (its moment of inertia) and a torsional spring component (its torsional stiffness). These torque flanges are, at the end, connected to the two load components which represent the moments of inertia of the load motors through

another rotary damper (the torsional stiffness of the flexible couplings) and a reducer component (the gearbox at the load motors level).

Finally, the three *Supercomponents* are described in the next two sections.

A.1 SuT Motor+Inverter *Supercomponent*

This section describes the *Amesim Supercomponent* which contains the subsystem that represents the SuT motor and the inverter. In fig.A.2, in particular, the AC controller replication is reported, instead the inverter switching logic is reported in fig.A.3.

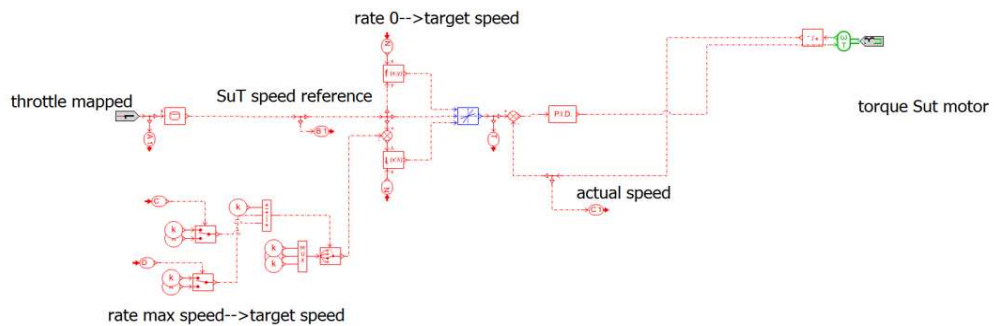


Figure A.2: SimRod E-Powertrain SuT Motor+Inverter controller.

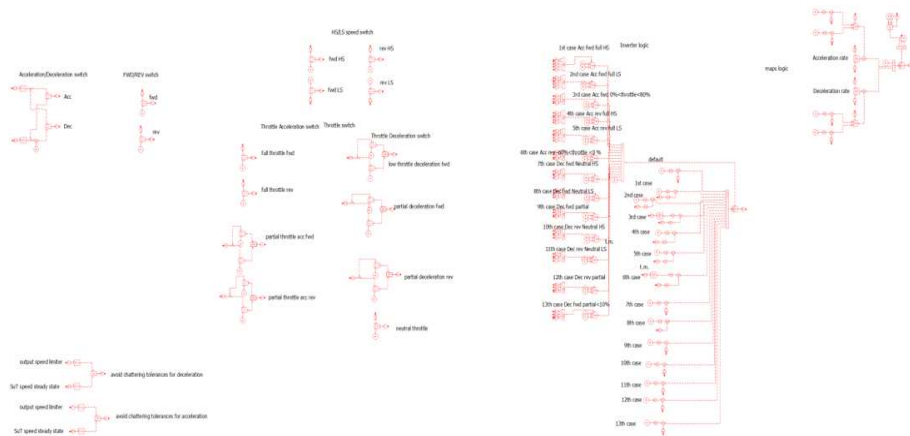


Figure A.3: SimRod E-Powertrain SuT Inverter logic.

In figure A.2, it is possible to see how the SuT motor speed is imposed to the system: basically, firstly, the throttle amount is mapped into the related speed

through an *Ametable*, this speed is the reference of the PID controller component which acts in order to follow this reference. On the speed, it is imposed a specific increasing/decreasing rate parameter which is the output of the switching logic of the inverter through the blue component (a rate limiter). The actual speed in output from the controller is then turned into the related torque.

Figure A.3 shows the switching logic which decides in output the specific rate parameter that needs to be imposed on the controller. The input are, basically, the actual speed of the subsystem and the current amount of throttle. This logic is composed by *Amesim* switch components, *Ametables*, multiplexer/demultiplexer components.

The figure A.4 shows how the power at the SuT inverter is reproduced in the *Supercomponent*. Basically, it is reproduced through the 2-D *Ametable*, then its increasing/decreasing rate is corrected through a specific rate limiter component and at the output this power result is divided through a gain by the voltage in order to compute the related current signal that is directly connected to the external electrical power system.

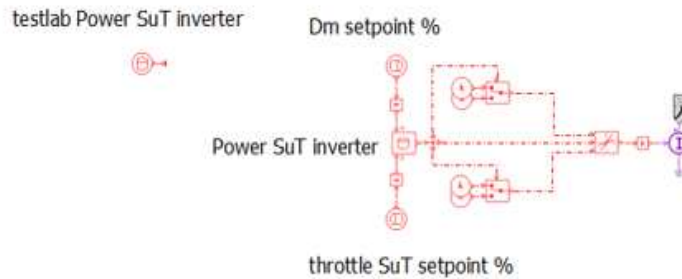


Figure A.4: SimRod E-Powertrain SuT Inverter Electrical Power.

A.2 Load Motor *Supercomponent*

This *Supercomponent* is, of course, equal for both the load motors so that just the load L model is presented here.

Figure A.5 shows the entire *Supercomponent* with the part regarding the input current and the part which reproduces the electrical power response.

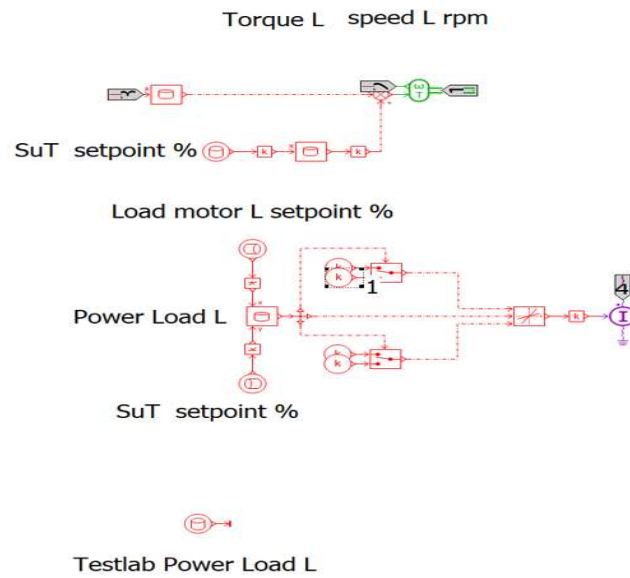


Figure A.5: Load Motor L *Supercomponent*.

Looking at the picture, in the part at the top of the sketch, it is possible to see the input current signal coming from setpoints which is turned into the related torque through an *Ametable*: in reality, this sketch is not updated because last changes have been done after the end of the internship so that actually in the final model there is a 2-D *Ametable* which take as inputs the throttle setpoints and the current setpoints. This load motor torque is then turned, at the end, into the related speed.

For what concerns the electrical power reproduction, the same approach of the SuT inverter is employed: the *Ametable*, the rate limiter and the final gain to compute the current flowing into the external electrical power system.

Acronyms

MBT Model Based Testing.

XiL X-in-the-Loop.

EV Electric Vehicle.

DISW Digital Industries Software.

CPU Control Process Unit.

SiL Software-in-the-Loop.

MiL Model-in-the-Loop.

HiL Hardware-in-the-Loop.

SuT System under Test.

L Left.

R Right.

DC Direct Current.

AC Alternating Current.

RT Real Time.

xDT executable Digital Twin.

SCADAS Signal Conditioning and Data Acquisition System.

NVH Noise Vibration Harshness.

BG Bond Graph.

C Channel.

TP Test Profile.

HMI Human Machine Interface.

RMSE Root Mean Square Error.

PPR Pulses Per Revolution.

CAN Controller Area Network.

PID Proportional Integrative Derivative.

List of Tables

3.1	Resume table for Model I/O & Parameters	15
4.1	Initial instrumentation [3].	30
4.2	Initial sensors setup [3].	30
4.3	Electrical power system added sensors	31
5.1	System mapping measured variables.	36
5.2	System mapping computed variables.	36
5.3	SuT Motor Speed limits.	38
5.4	SuT Axle Speed limits	46
5.5	Friction and Inertia identification measured variables	47
5.6	Friction and Inertia identification computed variables	47
5.7	Friction Models Statistics	54
5.8	Identified Moments of Inertia Parameters	58
5.9	Stiffness identification measured variables	63
5.10	Flender BIPEX-S Stiffness Results.	65
5.11	Kistler sensor Stiffness.	65
5.12	Power Flow measured variables	67
5.13	Power Flow computed variables	67
5.14	Resistance Identification results.	73
5.15	SuT Inverter transient analysis measured variables.	74
5.16	SuT Inverter programmed parameters.	75
5.17	SuT Inverter identified parameters.	79

List of Figures

1.1	XiL in embedded software and system development [5].	2
1.2	SimRod E-powertrain test setup: overview of the mechanical, electrical and communication layout [3].	4
1.3	SimRod E-powertrain test setup: complete assembly - including permanent equipment only [3].	5
2.1	Model Based System Testing application tree [9].	9
2.2	SimRod E-powertrain model starting design scheme.	12
2.3	Basic mode inputs scheme.	13
2.4	Setpoint profiles for SuT throttle and load motor currents, specifying the ‘TP14’ basic test scenario.	13
3.1	Test profile 01 → run-up and run-down/SuT motoring	17
3.2	Relation between Voltage inverter input and effective related Throttle	18
3.3	Load Motor L 2-D map input setpoints → Current	19
3.4	Load Motor L 2-D map input setpoints → Current - top view	19
4.1	SuT operational range for identification	25
4.2	SuT operational range for identification - sideview	26
4.3	Test profile 11	27
4.4	Test profile 14	28
4.5	Mechanical and acoustic sensor placement [3].	29
4.6	Electrical power system added sensors	31
4.7	Instrumentation scheme with changes	32
5.1	Overview of the test setup operating points.	33
5.2	Test setup device states.	34
5.3	Run measurements displayed on <i>Simcenter Testlab</i>	35
5.4	1-D <i>Ametable</i>	35
5.5	2-D <i>Ametable</i>	35
5.6	SuT Motor speed results for <i>Section 2</i>	38
5.7	1-D <i>Ametable</i> Throttle/SuT Motor Speed.	39

5.8	Load Current results for <i>Section 2</i> .	40
5.9	Load Motor L Current results for <i>Section 3</i> .	40
5.10	2-D <i>Ametable</i> Load and SuT setpoints → Current L.	41
5.11	2-D <i>Ametable</i> Load and SuT setpoints → Current L. - top view.	41
5.12	Axle Torque L results for <i>Section 2</i> .	42
5.13	Axle Torque L results for <i>Section 3</i> .	42
5.14	2-D <i>Ametable</i> Load and SuT setpoints → Axle Torque L	43
5.15	2-D <i>Ametable</i> Load and SuT setpoints → Axle Torque L - top view	43
5.16	Axle Speed L results for <i>Section 2</i> .	44
5.17	Axle Speed L results for <i>Section 3</i> .	45
5.18	Axle Speed R results for <i>Section 2</i> .	45
5.19	Axle Speed R results for <i>Section 3</i> .	46
5.20	Measurement of the friction torque on the 600-W servo drive system [14].	49
5.21	Servo drive experimental setup [14].	49
5.22	Axle Friction results from <i>Section 2</i> .	51
5.23	Axle Friction results from <i>Section 4</i> .	51
5.24	Axle Friction <i>Ametable</i> for semi-shaft L.	53
5.25	Axle Friction <i>Ametable</i> for semi-shaft R.	53
5.26	Friction <i>Ametable</i> implementation on <i>Amesim</i> model	54
5.27	SimRod E-Powertrain test setup inertia investigated components.	55
5.28	Load Motors Moment of Inertia results from <i>Section 2</i> .	56
5.29	SuT Motor Moment of Inertia results from <i>Section 4</i> .	57
5.30	Measured Axle Torque L/R for a TP11 run from <i>Section 2</i> .	58
5.31	Load <i>Amesim</i> component.	59
5.32	Investigated couplings for stiffness.	59
5.33	Kistler Torque sensor.	60
5.34	Torsional Spring <i>Amesim</i> component.	60
5.35	PPR error on Siemens Encoder - TP01	61
5.36	PPR error on Siemens Encoder according to different torque/speed values	62
5.37	Torsional Stiffness Identified Model.	64
5.38	SimRod E-Powertrain test setup Electrical Power System scheme	66
5.39	Resistance <i>Amesim</i> component.	66
5.40	Power SuT Inverter from <i>Section 2</i> .	68
5.41	Power SuT Inverter from <i>Section 3</i> .	69
5.42	Power SuT Inverter <i>Ametable</i> .	69
5.43	Power SuT Inverter <i>Ametable</i> - top view.	70
5.44	Power Load Motor L/R from <i>Section 2</i> .	71
5.45	Power Load Motor L from <i>Section 3</i> .	71
5.46	Power Load Motor L <i>Ametable</i> .	72

5.47	Power Load Motor L from <i>Ametable</i> - top view.	72
5.48	Curtis 1232E/SE AC controller.	74
5.49	Example - TP13 <i>Testlab</i> results.	76
5.50	Switching Logic <i>Amesim</i> representation.	78
5.52	Deceleration rate results.	78
5.51	Acceleration rate results.	79
6.1	SimRod E-Powertrain test setup <i>Amesim</i> draft model.	81
6.2	SuT Speed <i>Amesim</i> model results - TP11/run6 - employing map in fig.5.7.	84
6.3	SuT Speed <i>Amesim</i> model results - TP11/run6 - employing "param- eter" approach.	84
6.4	Axle Torque L <i>Amesim</i> model results - TP11/run6.	86
6.5	Axle Speed L <i>Amesim</i> model results - TP11/run6.	86
6.6	SuT Inverter Electrical Power <i>Amesim</i> model results - TP11/run6. .	87
6.7	Load Motor L Electrical Power <i>Amesim</i> model results - TP11/run6. .	87
6.8	Test Profile 07 - Demo Run.	89
6.9	SuT Speed <i>Amesim</i> model results - TP07.	90
6.10	Axle Torque L <i>Amesim</i> model results - TP07.	90
6.11	Axle Speed L <i>Amesim</i> model results - TP07.	91
6.12	SuT Inverter Electrical Power <i>Amesim</i> model results - TP07.	92
6.13	Load Motor L Electrical Power <i>Amesim</i> model results - TP07.	92
6.14	CPU time <i>Amesim</i> model - TP11/run6.	94
A.1	SimRod E-Powertrain test setup <i>Amesim</i> draft model.	98
A.2	SimRod E-Powertrain SuT Motor+Inverter controller.	100
A.3	SimRod E-Powertrain SuT Inverter logic.	100
A.4	SimRod E-Powertrain SuT Inverter Electrical Power.	101
A.5	Load Motor L <i>Supercomponent</i>	102

Bibliography

- [1] *plm.sw.siemens.com*. URL: <https://plm.sw.siemens.com/en-US/simcenter/simulation-test/model-based-system-testing/> (cit. on p. 1).
- [2] Viktor Schreiber, Ivanov Valentin, Augsburg Klaus, Noack Matti, Shyrokau Barys, Sandu Corina, and Schalk Els Pieter. «Shared and Distributed X-in-the-Loop Tests for Automotive Systems: Feasibility Study». In: *IEEE Access* 6 (2018) (cit. on p. 2).
- [3] Bart Forrier, Thomas D'Hondt, Karl Janssens, and Jan Debillé. «A novel E-powertrain test setup for validation and demonstration of multi-attribute and model based testing approaches». In: *Mechatronics 2023 - 17th Mechatronics Forum International, Leuven, Belgium*. 2023 (cit. on pp. 2–5, 13, 14, 29, 30).
- [4] Bart Forrier, Thomas D'Hondt, Leonardo Cecconi, and Mathieu Sarrazin. «Validation of a novel XiL setup for frontloaded testing of an electric vehicle powertrain». In: *Resource Efficient Vehicles Conference 2021, Stockholm, Sweden*. 2021 (cit. on pp. 2, 3).
- [5] Ghizlane Tibba, Christoph Malz, Christoph Stoermer, Natarajan Nagarajan, Licong Zhang, and Samarjit Chakraborty. «Testing automotive embedded systems under X-in-the-loop setups». In: *2016 IEEE/ACM International Conference on Computer-Aided Design (ICCAD), Austin, TX, USA*. IEEE, 2016 (cit. on p. 2).
- [6] Roland Pastorino. *sw.siemens.com*. 2023. URL: <https://blogs.sw.siemens.com/simcenter/digital-twin-xil-testing-testlab-rt/> (cit. on p. 3).
- [7] Dirk Hartmann and Herman Van der Auweraer. «The Executable Digital Twin: merging the digital and the physics worlds». In: (2022) (cit. on p. 3).
- [8] *www.plm.automation.siemens.com*. URL: <https://www.plm.automation.siemens.com/global/en/industries/automotive-transportation/nvh-acoustics.html> (cit. on p. 5).

- [9] Fabio Marques dos Santos, Roland Pastorino, Bart Peeters, Cassio Faria, Wim Desmet, Luiz Goes, and Herman Van der Auweraer. «Model Based System Testing: Bringing Testing and Simulation Close Together». In: Jan. 2016 (cit. on p. 9).
- [10] Bart Forrier. «Virtual torque sensing - A model-based approach for indirect measurement of dynamic operational loads on mechatronic powertrains». PhD thesis. KU LEUVEN, Arenberg Doctoral School, Faculty of Engineering Science, 2018 (cit. on pp. 10, 11).
- [11] Peter C. Breedveld. «Port-based modeling of mechatronic systems». In: *Mathematics and Computers in Simulation* 66.2 (2004), pp. 99–128 (cit. on p. 10).
- [12] D. Karnopp, D. Margolis, and R. Rosenberg. *System Dynamics: Modeling, Simulation, and Control of Mechatronic Systems*. 2nd ed. John Wiley & Sons, 2006 (cit. on p. 11).
- [13] Hsin Guan, Song Haiyanand, Xu Liang, and Lu Pingping. «Friction Model for Real-Time Simulation of Powertrain Dynamics». In: *SAE International Journal of Vehicle Dynamics, Stability, and NVH* 2 1 (2018), pp. 41–54 (cit. on p. 48).
- [14] Kim Sungmin. «Moment of Inertia and Friction Torque Coefficient Identification in a Servo Drive System». In: *IEEE Transactions on Industrial Electronics* 66.1 (2019), pp. 60–70 (cit. on pp. 48–50, 54).
- [15] Shengping Fu, Luo Ning, Huang Hanlin, Zhou Yuhang, and Ming Wei. «Torsional Vibration Attenuation Characteristics and Stiffness Identification of Flexible Coupling in Vehicle Power Train». In: *Shock and Vibration* (2020), pp. 1–13 (cit. on p. 60).